The Application of Raman Spectroscopy for Analysis of Multi-Component Systems

Hansen, Susanne Brunsgaard; Berg, Rolf W.; Stenby, Erling Halfdan

Publication date:
2000

Document Version
Publisher's PDF, also known as Version of record

The Application of Raman Spectroscopy for Analysis of Multi-Component Systems

Susanne Brunsgaard Hansen

Department of Chemistry

and

Department of Chemical Engineering, IVC-SEP,

Technical University of Denmark

DK-2800 Lyngby, Denmark

Contents

Appendices **a**- 1

Preface

The present thesis "The Application of Raman Spectroscopy for Analysis of Multi-Component Systems" is submitted in partial fulfilment of the requirements for the Ph.D. degree in Chemistry at the Technical University of Denmark (DTU, Danmarks Tekniske Universitet). The Ph.D. work has been carried out at Department of Chemisty, DTU, Department of Chemical Engineering, Engineering Research Centre IVC-SEP, DTU, Department of Chemistry, University of Bergen, Norway and Chemical Institute, H. C. Ørsted Institute, University of Copenhagen from July 1997 to July 2000.

Numerous people have contributed valuable help and support during the last three years. I would first of all like to thank my supervisor Dr. Rolf W. Berg and co-supervisor Dr. Erling H. Stenby for consistent and inspirational guidance. Especially it has been a pleasure to work with and learn from Rolf about the Raman technique.

Dr. Daniel H. Christensen and Dr. Ole Faurskov Nielsen are thanked for stimulating discussions and for giving me access to the FT-Raman instrument at the H. C. Ørsted Institute. Lykke Ryelund is acknowledged for technical assistance.

Dr. Simon I. Andersen, IVC-SEP, Dr. Søren Dalsager and M.Sc. Chemical Engineer Tine Lindgren, DONG A/S (the National Oil and Gas Company of Denmark) are thanked for their participation in several meetings and for many fruitful discussions. Dong A/S is thanked for delivering natural gas samples. Jørgen Klemmensen, Nybro Gas Treatment Plant, is thanked for technical assistance.

Dr. Harald Kallevik and Dr. Johan Sjöblom are thanked for scientific guidance at my stay at the University of Bergen during the autumn of 1998. A special thank to Harald for introducing me to chemometrics. All members of the FLUCHA group are thanked for stimulating discussions.

Dr. Ib Laursen, Department of Automation, DTU, is acknowledged for providing the microwave instrumentation used in the attempts to find a method to reduce fluorescence problems in Raman spectroscopy. It was a pleasure to learn from him and discuss the issue with him.

In the summer 1998 Rolf and I visited Dr. Philippe Marteau, Université Paris Nord, France. Philippe Marteau is thanked for fruitful discussions with respect to the titanium cell and for help and discussions thereafter.

During the last three years I have been surrounded by a friendly atmosphere. I would like to thank the scientific and technical staff at the Department of Chemistry. Special thanks to the members of the Structural Chemistry group. I would also like to thank all members in the IVC-SEP group. Especially I acknowledge Dr. Abhijit Dandekar, Povl V. Andersen and Tran T. Dang for invaluable technical support. This also applies to the technical staff at the workshop at Department of Chemistry, and to Troels Langhoff and Susanne Helmark, Department of Chemistry.

Finally I would like to express my gratitude to IVC-SEP, DONG A/S, The Nordic Energy Research Program and The Danish Technical Research Council for financial support during the Ph.D. study.

The Ph.D. work has resulted in the following publications:

1. S. Brunsgaard Hansen, R. W. Berg and E. H. Stenby, "Determination of methyl tertiary butyl ether (MTBE) in gasoline by Raman spectroscopy", Asian Chem. Letters **4**, 65 (2000).
2. H. Kallevik, S. Brunsgaard Hansen, Ø. Saether, O. M. Kvalheim and J. Sjöblomm, "Crude oil model emulsions characterized by means of near infrared spectroscopy and multivariate techniques", J. Dispersion Sci. Technol. **21**, 245 (2000).
3. S. Brunsgaard Hansen, R. W. Berg and E. H. Stenby, "High pressure measuring cell for Raman spectroscopic studies of natural gas", Appl. Spectrosc. **55(1)**, xx (2001).
4. S. Brunsgaard Hansen, R. W. Berg and E. H. Stenby, "Raman spectroscopic studies of methane-ethane mixtures as a function of pressure", appear in Appl. Spectrosc.

Susanne Brunsgaard Hansen
Hvalsø, Denmark
December 2000

Dansk Resumé

Foreliggende afhandling "Anvendelse af Ramanspektroskopi til Analyse af Multi-Komponent Systemer" omfatter resultater fra min forskning som ph.d.-studerende ved DTU (Danmarks Tekniske Universitet). Den røde tråd gennem afhandlingen er Raman spektroskopiens anvendelse indenfor petrokemi.

Efter en kort introduktion i Kap. 1, beskrives i Kap. 2 det anvendte udstyr i projektet. Afsnittet falder i to dele: Første del, Kap. 2.1, omhandler Ramanudstyret og anden del, Kap. 2.2 omhandler de anvendte celler (beholdere).

En del af Ramanspektrene i afhandlingen er optaget på et dispersivt Ramanspektrometer på Institut for Kemi, DTU. Mange af spektrene optaget på dette apparat var, som det vil blive set, vellykkede og informative. Et tilbagevendende problem var dog, at nogle af prøverne fluorescerede ved eksitation med synligt laserlys resulterende i en baggrund i Raman-spektrene. Denne baggrund var i nogle tilfælde så bred og intens at få (eller slet ingen) Ramanbånd blev observeret. Heldigvis var der i projektet mulighed for at anvende et NIR-FT-Ramanapparat på H. C. Ørsted Instituttet, Københavns Universitet. Dette apparat anvender en Nd-YAG laser (1064 nm) som ekcitationskilde. Den længere ekciationsbølgelængde resulterede i mindre fluorescens og mange af spektrene blev optaget uden baggrund. Begge apparater beskrives kort i Kap. 2.1.

En stor del af projektet omhandlede Ramanmålinger på gasser under højt tryk. Det var bl.a. fra starten af projektet planen at måle på naturgasprøver taget direkte under højt tryk. Når en gasprøve under højt tryk fyldes i en celle ekspanderer gassen i første omgang, hvilket medfører et temperaturfald. Temperaturfaldet forårsager, at de tungere komponenter i naturgassen kondenserer. En del af ph.d.-projektet gik ud på at designe og få opbygget en celle, i hvilket denne kondensering undgås. Dette arbejde er beskrevet i Kap. 2.2. Udover denne "hjemmelavede" celle har vi en kommerciel såkaldt "titancelle" til rådighed. Med denne celle forsynet med et stempel er det ved drejning muligt at øge trykket i en gasprøve manuelt. Denne celle er ligeledes beskrevet i Kap. 2.2. Begge celler har vist sig meget

velegnede til gasprøver og til Ramanspektroskopiske optagelser af disse. I Kap. 3 beskrives detaljeret, hvordan man på en simpel måde kan bestemme dødvolumen og totalvolumen af sådanne celler.

Kap. 4 omhandler arbejdet vedr. naturgasmålinger. Afsnittet falder i tre dele: Første del, Kap. 4.2, beskriver de Ramanspektroskopiske undersøgelser af en naturgasprøve taget fra Nybro Gasbehandlingsanlæg (Vest Jylland). Prøven blev analyseret med henblik på at undersøge, om det var muligt at detektere mikrodråber af kondensat. Mikrodråberne forekommer ikke naturligt i naturgassen, men stammer fra triethylenglycol og kompressorolie. Anden del, Kap. 4.3, beskriver de Ramanspektroskopiske undersøgelser af en naturgasprøve fra Ll. Torup Naturgaslager (Nord Jylland). Denne prøve blev analyseret med henblik på at undersøge, om det var muligt at detektere mikrodråber af Oppanol i gassen. Oppanol anvendes som tildækningsfilm i bunden af lageret for at undgå at vand evaporerer ind i gassen. Det blev konkluderet, at det ikke er muligt at detektere mikrodråber af hverken triethylenglycol, kompressorolie eller Oppanol. Tredje del, Kap. 4.4, beskriver en grundig kvalitativ analyse af tre forskellige naturgasprøver ved forskellige tryk. Det mest overraskende resultat var, at det er muligt at detektere hydrogensulfid. I Kap. 4.4 beskrives ligeledes et interessant forsøg på at lave en kvantitativ analyse af naturgas.

Kap. 5 beskriver studierne vedr. skift i bølgetal som funktion af tryk. ν_1 methanbåndet (det symmetriske C-H strækningsbånd) falder i bølgetal med stigende tryk. Undersøgelserne vedr. dette fald i ν_1 methanbåndets bølgetal som funktion af trykket beskrives for både ren methan og methan / ethan blandinger. Det blev konkluderet, at positionen af dette bånd afhænger af, i hvilke omgivelser methanmolekylet vibrerer, dvs. hvilke andre type molekyler der er til stede. Bølgetalsfaldet som funktion af trykket er ligeledes beskrevet for ν_1 ethanbåndet med samme konklusion til følge. Overordnet blev det konkluderet, at ν_1 bølgetalspositioner kan anvendes til at bestemme tryk i methanblandinger, hvis komponenter og kompositionen i blandingen er kendt.

I Kap. 6 beskrives arbejdet vedr. en interessant observation, som givetvis kan anvendes til at bestemme tryk i methanblandinger, hvori komponenter og komposition er ukendt. Intensitetsforholdet mellem to methanbånd, ν_3 (asymmetrisk C-H stræk) og $2\nu_2$ (overtone-

båndet af methanbøjningsbåndet), som funktion af trykket for ren methan, to forskellige methan / ethan blandinger og en methan / nitrogen blanding er beskrevet i kapitlet. Det ses tydeligt i de præsenterede spektre, at $?_3$ båndet falder i intensitet relativt til $2?_2$ båndet, når trykket øges. Plot af intensitetsforholdet mellem de to bånd som funktion af trykket er vist for ren methan og alle methanblandingerne. Plottene viser, at intensitetsforholdet, $I?_3 / I2?_2$, ved et givet tryk er uafhængigt af methanblandingens indhold og sammensætning. Det blev overordnet konkluderet, at intensitetsforhold-metoden kan anvendes til at bestemme tryk i methanblandinger i hvilket sammensætningen ikke er kendt. Denne opdagelse kan vise sig nyttig til at bestemme tryk i f.eks. fluidinklusioner.

I Kap. 7 beskrives nogle Ramanspektroskopiske analyser af benzin. Afsnittet falder i to dele: Første del, Kap. 7.2, omhandler bestemmelse af indholdet af additivet MTBE (methyl tertiary butyl ether) i oktan 98 benzin. MTBE tilsættes til benzin for at hindre bankning og øge oktantallet. "Kunstige" (MTBE / heptan blandinger) er ligeledes undersøgt. Karakteristiske MTBE-bånd blev fundet i spektret af ren MTBE. På grund af fluorescens var det ikke muligt at observere disse MTBE-Ramanbånd i benzin, og detektionsgrænsen for stoffet i de "kunstige" benzinprøver var relativt høj, ~30 vol. %. Amerikanske (og danske) undersøgelser har vist, at MTBE kan forurene grundvandet. MTBE detektionsgrænsen for MTBE i drikkevand blev derfor checket med henblik på at undersøge om Ramanmetoden kunne være anvendelig som testmetode. Detektionsgrænsen blev fundet til 0.3-0.4 vol. %, hvilket sandsynligvis er en højere værdi end MTBE indholdet i forurenet grundvand. Anden del, Kap. 7.3, omhandler dels overvejelser om, hvorvidt hydrogensulfider kan observeres i Ramanspektret af benzin, dels overvejelser om aromatindhold. Benzenindholdet i benzin er forsøgt bestemt ved hjælp af arealforholdsmetoden. Overvejelser omkring toluen, ethylbenzen og ortho-, meta- og para-xylen indhold i benzin er ligeledes gennemgået.

Kap. 8 beskriver foreløbige studier vedr. det ternære system vand-methanol-dekan (som funktion af tryk). Kapitlet beskriver først og fremmest vanskelighederne forbundet med systemet, især mht. fluorescens. Ren methanol fluorescerede ikke, hvorimod methanolfaserne i blandinger med dekan og / eller vand fluorescerede. FT-Ramanspektrene af systemet gav også høj baggrund i methanolfasespektrene og overraskende nok også i

dekanfasespektrene. Det blev konkluderet, at baggrunden skyldtes væskebeholderens materiale, dvs. glas. Bedre Ramanspektre (uden fluorescensbagggrund) er ønskelige, hvis det ternære system skal kunne undersøges i detaljer vha. Ramanspektroskopi. En mulighed kunne f.eks. være at bruge rent, syntetisk kvarts som cellemateriale i stedet for glas og dermed måske undgå baggrund i FT-Ramanspektrene. I kapitlet er ligeledes beskrevet overvejelser vedr. titancelle og dens egnethed som højtrykscelle for det ternære system. Overvejelserne er baseret på målene i cellen og om der er begrænsninger mht. blandingssammensætning. Overordnet konkluderes, at der er begrænsninger, men at de kan reduceres ved at reducere dødvolumenet i cellen.

Abstract

The present thesis "The Application of Raman Spectroscopy for Analysis of Multi-Component Systems" contains results from my research as a Ph.D. student at DTU (the Technical University of Denmark). The common dominator through out this thesis is the application of Raman spectroscopy in petro chemistry.

After a brief introduction in Chap. 1 the applied equipment is described in Chap. 2. The chapter consists of two parts: The first part, Chap. 2.1, concerns the Raman equipment and the second part, Chap. 2.2, concerns the high pressure measuring cells.

Many of the Raman spectra presented in this thesis are obtained by use of a dispersive Raman spectrometer (Department of Chemistry, DTU). Most of the spectra obtained on that instrument were, as it will be seen, fine and very informative. In some cases however problems arose due to fluorescence. The fluorescence resulted in a background in the spectra, which sometimes was so broad and intense that it obscured the Raman signals. However, we had access to an NIR-FT-Raman instrument. The excitation source in this instrument was a Nd-YAG laser (1064 nm). Due to excitation with light of a longer wavelength it was possible to obtain spectra without fluorescence. Both of the Raman instruments are described shortly in Chap. 2.1.

A considerable part of the work concerned Raman spectroscopic studies of high pressure gases. It was from the start the intention to obtain Raman spectra of natural gas, which were totally representative. When a natural gas sample at high pressure is sampled into a cell the gas will expand during transfer, resulting in a drop in temperature. Thus some of the heavier hydrocarbons will condense and the gas is thereby not representative. The design and construction of a cell to avoid the temperature drop is described in Chap. 2.2. A so-called "titanium cell" made from titanium metal and with flat sapphire windows has also been used. With this titanium cell it is possible to increase the pressure of a gas by manually moving a piston in the cell chamber. This cell is described in Chap. 2.3. In Chap.

3 a simple method to determine the dead volume and the total volume of a cell chamber is described.

Chap. 4 describes the work concerning Raman spectroscopic studies of natural gas. The chapter consists of three parts: Part one, Chap. 4.1, concerns the studies of a natural gas sample from Nybro Gas Treatment Plant (at the west coast of Jutland). The purpose was to investigate the feasibility of Raman spectroscopy to characterise natural gas samples from Nybro with respect to micro droplets of condensate (triethylene glycol and compressor oil). The second part, Chap. 4.2 describes Raman spectroscopic studies of a natural gas sample from Ll. Torup Gas Storage Facility (North of Jutland). The purpose of this work was to investigate if it was possible to detect micro drops of oppanol in natural gas samples from Ll. Torup by means of Raman spectroscopy. It was concluded that it was not possible to detect micro drops at all. In the third part, Chap. 4.3, is given a detailed qualitative analysis of three different natural gas samples at different pressures. The most surprising observation was that it was possible to detect hydrogen sulfide even though it should only be present in Danish natural gas at very low concentrations (according to DONG A/S 1-3 mg / Nm^3). In Chap. 4.3 are also described interesting attempts to make quantitative analysis of natural gas.

In Chap. 5 some studies of wavenumber shifts as a function of pressure are described. The ν_1 methane band (symmetric C-H stretching) decreases in wavenumber position as a function of pressure. Investigations with respect to the wavenumber shifts as a function of pressure is described for pure methane and two methane / ethane mixtures. It was concluded that the position of the methane ν_1 band at a given pressure is dependent on the surroundings in which the methane molecule is vibrating. In fact the decreasing effect is enhanced if ethane molecules surround the methane molecules. The wavenumber position of the ν_1 ethane band as a function of pressure is also described. The overall conclusion was that ν_1 band positions could be used to determine the pressure in methane containing mixtures, e.g. fluid inclusions, provided the components in the mixture and the composition of the mixture are known.

Chap. 6 describes a very interesting observation, which probably can be used to determine pressures in methane containing mixtures, in which the components and composition are unknown. The intensity ratio between two methane bands, ν_3 (asymmetric C-H stretching) and $2\nu_2$ (the overtone band of the methane deformation band), as a function of pressure for a pure methane sample, two different methane / ethane mixtures and a methane / nitrogen mixture is described in the chapter. It is clearly seen in the spectra that the intensity of the ν_3 band decreases relatively to the intensity of the $2\nu_2$ band as the pressure is increased. Plots of the intensity ratio between the two bands, $I\nu_3$ / $I2\nu_2$, are presented for the pure methane sample and the methane mixtures. The plots show that the intensity ratio at a given pressure is independent of the composition. The overall conclusion was that the presented intensity ratio method could be used to determine the pressure in methane mixtures in which the components and the composition are not known. This observation might turn out to be very useful e.g. in determining the pressure in fluid inclusions.

Chap. 7 describes some Raman spectroscopic studies of gasoline. The chapter contains two parts: Part one, Chap. 7.2, concerns the determination of the content of the anti-knocking additive MTBE (methyl tertiary butyl ether) in octane 98 gasoline and in artificial gasoline samples, i.e. MTBE / heptane mixtures. Characteristic MTBE bands were found in the Raman spectrum of a pure MTBE sample. Due to fluorescence it was not possible to observe these bands at all in the Raman spectra of gasoline, and the detection limit was relatively high in the artificial gasoline samples, ~30 vol. %. It is known from USA (and Denmark) that MTBE can penetrate soil and thereby pollute drinking water reserves. Thus it was found of interest to determine the detection limit of MBE in drinking water. The purpose was to investigate the feasibility of Raman spectroscopy as a tool to measure the MTBE content in the water reserves. The detection limit was found to 0.3-0.4 vol. % MTBE. The second part of the chapter, section 7.3, concerns considerations with respect to hydrogen sulphides and the aromatic content in gasoline. Because of the fluorescence it was decided to apply the FT-Raman instrument. Attempts to determine the benzene content by the area ratio method are described. Considerations on toluene, ethyl benzene and ortho-, meta- and para-xylene are also described. An overall conclusion was that Raman spectroscopy might be a useful method to detect benzene (separately) and / or aromatics and perhaps sulphides in gasoline.

Chap. 8 concerns some preliminary studies of the ternary water-methanol-decane system. The chapter mainly describes the difficulties encountered so far, especially with respect to fluorescence. First of all the Raman spectrum of pure methanol gave no observable fluorescence background. When mixed with decane and / or water however fluorescence was to be observed in the spectra of the methanol phase (especially when mixed with decane). In fact the background was so intense and broad in most of the spectra that the use of the FT-Raman technique was indispensable. A high background also dominated the FT-Raman spectra of the methanol phase and surprisingly also the decane phase. It was concluded that the background was due to the container material of the liquid cell, i.e. the glass. If the Raman technique should be used in an informative way with respect to the ternary system better Raman spectra have to be obtained. One possibility could for instance be to use liquid cells of pure, synthetic quartz and thereby perhaps acquire FT-Raman spectra with a low background. Some considerations on the titanium cell with respect to its suitability as a high pressure mixture container for the ternary system are also given in the chapter.

1. Introduction

1.1. The Ph.D. Project

Raman spectroscopy is an analytical method based on measurements of radiation scattered from a given sample. The method is named after the Indian physicist Sir Chandrasekhara V. Raman (1888-1970), who was the first to observe the effect experimentally (in 1928)[1]. The technique is widely used today, due to a lot of advantages, e.g. it is a non-destructive method, the spectra are usually obtained without touching the sample, spectra can be obtained through transparent containers such as glass and only small amounts of samples are necessary for the measurements. The main objective of the Ph.D. project has been to use the Raman technique to analyse multi-component systems related to the petro chemistry.

When a well has been drilled down to a reservoir and the production of oil or natural gas begins, we are provided with raw materials for fuel for transportation, heating houses etc. Before the fuel products can be used, however, the reservoir fluids have to pass many processes in the production phase. For instance some compounds already are added to the fluids in the well, that is e.g. to enhance the recovery or to prevent production problems, and some compounds are removed for the sake of health and environmental reasons. Some of these aspects will be described later in connection with some of the Raman spectra obtained during the Ph.D. project.

An interesting feature of the project was the observation that wavenumber positions, bandwidths etc. depend on the pressure. Thus many Raman spectra of natural gas, methane and methane mixtures as a function of pressure have been obtained in the course of the project. Based on analysis of these observations there are prospects of using Raman spectroscopy in determination of pressure in methane containing mixtures e.g. fluid inclusions.

1.2. The Thesis

The thesis is organised such that the first two chapters deal with equipment. Short descriptions of the two Raman instruments and a detailed description of two high pressure

measuring cells are given. The following three chapters are concerned with Raman spectroscopic studies of high pressure gases and the two last chapters are concerned with Raman spectroscopic studies of liquids. The purposes of the works presented are given in introductions to each chapter.

Theories describing the scattering processes responsible for Raman spectroscopy have been omitted in the thesis. The Raman effect has been described thoroughly in the literature, in publications and in textbooks, e.g. ref. 2. All information derived from the spectra are however described in details. Thus the author is convinced that even readers with no knowledge on Raman spectroscopy should have a good chance of informative reading.

1.3. References

1. C. V. Raman and K. S. Krishnan, "A new type of secondary radiation", Nature **121**, 501 (1928).
2. N. B. Colthup, S. E. Wiberley and L. H. Daly, *Introduction to Infrared and Raman Spectroscopy*" (Academic, New York, 1975), 2. ed.

2. Equipment

2.1 Raman Instrumentation

Most of the Raman spectra in the present thesis have been obtained by use of a dispersive DILOR Raman instrument using visible light as the exciting source. One strong feature in this instrument is a liquid nitrogen cooled CCD (charge coupled device) detector with a high sensitivity. The Raman spectra obtained were generally very informative, especially the spectra of the high pressure gases, including natural gas samples. In some few cases however difficulties arose in obtaining the spectra because of a phenomenon called fluorescence. This is some sort of strong absorption and reemission in the visible region. It arises typically when working with coloured samples or samples with impurities. The fluorescence phenomenon results in a spectral background, which is sometimes so intense and broad that it masks the Raman spectrum. Attempts to reduce fluorescence backgrounds have been done in the project i) by data manipulation of Raman spectra of gasoline and ii) by obtaining spectra of fluorescent liquids simultaneously with the exposure to microwaves. The latter procedure was unsuccessful in the way that the decrease in fluorescence background observed at first turned out to be a decrease in intensity over the whole spectrum due to a thermal effect. Methods for reducing fluorescence backgrounds have been described in the literature, e.g. a method based on exposure of laser light for a long time to burn out the fluorescence (called photobleaching)[1]. The best way to reduce the fluorescence is without doubt to use an excitation wavelength, which does not excite the fluorescence of the sample. Photons of a high wavelength typically does not contain enough energy to excite a molecule up to an electronic state, for which reason NIR lasers (λ: 780-1064 nm) now widely are used for Raman measurements on fluorescent samples. So called FT-Raman spectra obtained by using NIR excitation and a Michelson interferometer were firstly described by Gebbie *et al*. (1964)[2] and thereafter by Chase and Hirschly (1986)[3]. Since then this FT (Fourier transformation) technique has been thoroughly treated in the literature. Using a longer wavelength causes a decrease in sensitivity because the intensity is proportional to ν^4. However, the advantage of using a FT-Raman instrument is that it is still useful for samples, which would otherwise exhibit fluorescence. The advantage of the dispersive DILOR Raman instrument is that it is highly sensitive, but its drawback is its

sensitivity to fluorescence. It ought to be mentioned that NIR lasers can be used in combination with the dispersive DILOR instrument. This was tried in the project (Chap. 4.2.2 and Chap. 4.3.4) but with moderate success.

2.1.1 The Dispersive Raman Instrument

The dispersive Raman instrument is shown schematically in Fig. 2.1. It is a confocal DILOR-XY instrument from France. With this instrument it is possible to obtain Raman spectra in a microscopic or macroscopic way. When using the microscopic technique the collection geometry is 180° (back scattering). In the macroscopic position it is possible to choose between 90° and 180° collection geometry. Selection between the three different setups is done manually with mirrors. The choices are indicated by "↕" in the figure. The Rayleigh filtration is done either by use of the foremonochromator or by a super plus holographic notch filter from Kaiser Optics. It is possible to choose between two spectrographs named as 1st spectrograph, with a grating of 1800 grooves per mm, and 2nd monochromator, with gratings of 150 or 600 grooves per mm. The selection between the gratings is done by two mirrors indicated by M_8 and M_{11}. Finally the light is detected by a liquid-nitrogen-cooled CCD detector (1024 x 256 pixels). For excitation four different lasers are available: an Argon-ion laser, a He-Ne laser and two diode lasers (exciting wavelengths, λ_{air}: 488, 514.5, 632, 785 and 833 nm). All dispersive Raman spectra presented in this thesis have been obtained at room temperature, excited with vertically polarized light, in the direct pass mode and by use of the notch filter, i.e. not using the foremonochromator. The number of accumulations were mostly three, i.e. the presented spectra are the average of three accumulations to exclude cosmic events. Polarized spectra, I_{VV} and I_{Vh} configurations (V: vertical, H: horizontal), were obtained by use of a polarizer in the scattered beam. In the following the dispersive Raman spectra will be referred to as "Raman spectra".

Raman data obtained with the DILOR instrument are acquired and plotted in such a way that wavenumber shifts increase from left to right. Since IUPAC (The International Union of Pure of Applied Spectroscopy) recommends that Raman spectra are presented with wavenumber shift increasing from right to left[4] wavenumber axes have been reversed by

use of extra software. All the spectra presented here have been processed and designed by use of the Microcal Origin program[5].

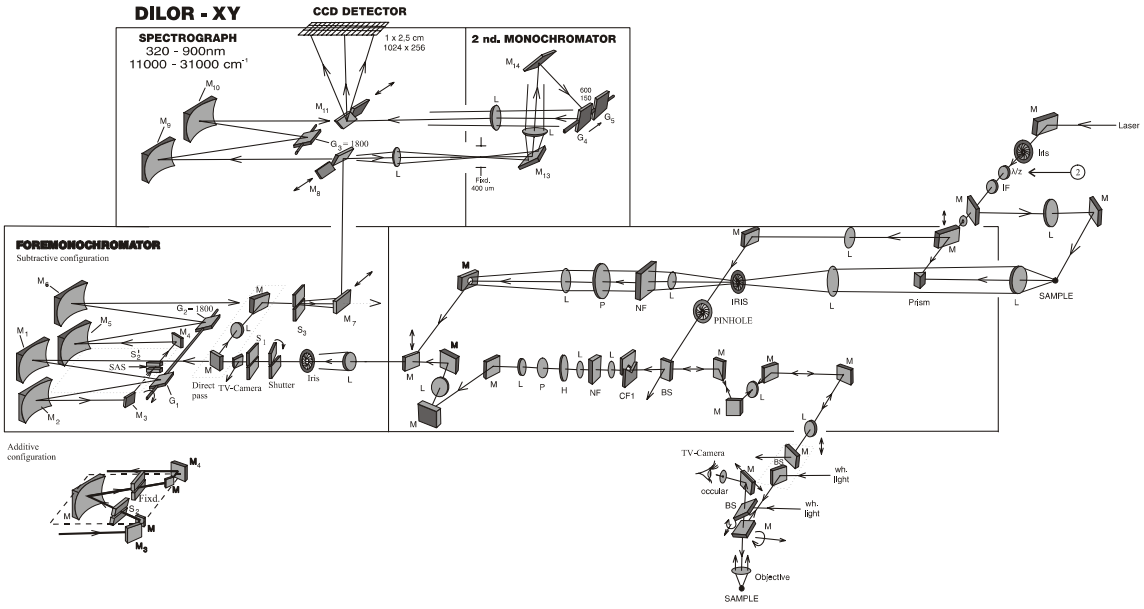

Fig. 2.1. A schematic illustration of the DILOR Raman instrument. (M = mirror, G = grating, L = lens, IF = interference filter, BS = beam splitter, NF = notch filter, P = polarizer, S = slit, SAS = Stokes / Anti-Stokes needle). Figure courtesy R. W. Berg and S. Helmark.

2.1.2 The NIR-FT-Raman Instrument

The NIR-FT-Raman spectra have been obtained on a BRUKER model IFS66 FT (Fourier transform) spectrometer equipped with a FRA-106 module. This instrument uses a NIR Nd:YAG laser as the exciting source (λ_{air} = 1064 nm). The detector is a Ge-detector cooled to liquid nitrogen temperature. All the NIR-FT-Raman spectra presented were obtained at room temperature in the 180° scattering configuration. The spectral resolutions were 4-6 cm^{-1} and laser power was 200-300 mW. None of the spectra were calibrated for instrumental response. The NIR-FT-Raman spectra presented have also been processed and designed by the Microcal Origin program[5].

2.2. The High Pressure Cells

2.2.1 Introduction

When working with gases at high pressures it is important to operate with sample cells, which are perfectly tight. To get this tightness is perhaps the greatest challenge when constructing high pressure cells for measurements. To obtain a Raman spectrum it is a necessity that the sample cell has at least one section, which is transparent for the exciting light source and the scattered light. Problems can occur e.g. with sealing of transparent materials or with leaks in the valves. Two different high pressure cells have been used during this Ph.D. project: a home built "sapphire tube cell" and a "titanium cell" with sapphire windows. Both of the cells have shown to be very suitable for obtaining Raman spectra of high pressure gases. The sapphire tube cell was primarily developed with the purpose to obtain Raman spectra of natural gas. It has however also been used with success in Raman spectroscopic studies of other gases. With the sapphire tube cell it is possible to reduce the pressure by letting gas out of a valve and with the titanium cell it is possible to increase the pressure by manually moving a piston in the cell chamber. In these ways it has been possible to study Raman spectra of different gases as a function of pressure. The next Chap. 2.2.2 concerns the sapphire tube cell and Chap. 2.2.3 the titanium cell. The design and construction of the cells have been presented separately in published papers: the sapphire tube cell in ref. 6 and the titanium cell in ref. 7.

2.2.2. The Sapphire Tube Cell

High pressure optical cells have been thoroughly described in the literature, e.g. in refs. 8-14. The main idea with the development of our sapphire tube cell was to be able to obtain Raman of natural gas samples, which should be totally representative. When a natural gas sample at high pressure is sampled into a measuring cell at ambient pressure the gas will expand resulting in a drop in temperature (Joule-Thomson effect). Due to this temperature drop some of the heavier hydrocarbons in the natural gas might condense and the gas sample may thereby not be representative. Considerations with respect to the design and construction of a system to avoid this temperature drop within the cell are described in the following:

To avoid condensation it was decided that the cell should be constructed in such a way that it could be transported to the natural gas plants, connected to the sampling loops, flushed at a low flow and thereafter gradually (at a speed which didn't lead to condensation) filled with gas for Raman measurements. At the natural gas plants, the natural gas sampling loops connects by means of stainless steel Swagelok fittings. Therefore it was decided to use such fittings as the basic construction parts of the cell.

The greatest hurdle in manufacturing the cell was without doubt the providing of the transparent material component. One possibility was the use of flat circular windows. A circular tube was chosen instead because it can be connected to standard high pressure fittings and sealed by means of **O**-rings. Due to the fittings the outer diameter was constrained to 6.35 mm. Tubes of quartz were provided (Buch & Holm A/S) but they showed to vary considerably in dimensions (±0.4 mm). In the first version a little tube with an outer diameter of 6.3 mm, an inner diameter of 3.7 mm and a length of 39.5 mm was inserted and used as the transparent part of the cell (quartz tube cell). The tube and the tube connection to the fittings (adapter) are shown in Fig. 2.2.

Fig. 2.2. Photograph showing the quartz tube inserted in the tube connectors (Cajon ultra torr adapter). Photo: S. Helmark.

According to a formula given by Lux[15], Formula 2.1 (which "nur ungefähr gilt"), the allowed working pressure of a quartz tube, with the dimensions given above, can be calculates to a high value: 195 $kgcm^{-2}$ (19.1 MPa). To avoid any risk the cell was only tested up to a pressure at 15.0 MPa (without any explosion of the tube). Because of the

variation in the diameter of the tube, however, the cell based on it was found to leak when the pressure was raised.

(2.1) $P = \sigma \frac{r_a^{\,2} - r_i^{\,2}}{r_a^{\,2} + r_i^{\,2}}$, r_a: outer radius (cm), r_i: inner radius (cm), σ: tensile strength of quartz, 400 $kgcm^{-2}$

A tube of sapphire was the next choice, first of all because it can be ordered in precise dimensions but also because the allowed working pressure is considerably higher than for quartz. In Fig. 2.3 the Raman spectrum of methane is shown, obtained in the tube cell equipped with a sapphire tube from Saphikon, Milford. As it is seen there is a broad fluorescence background in the red end of the spectrum (high cm^{-1} values) due to impurities in the sapphire. The impurities are traces of transition metal ions, here mostly Cr^{3+}. In fact the term sapphire is misleading: Pure α-Al_2O_3 is called corundum; sapphire is α-Al_2O_3 incorporated with Fe^{2+}, Fe^{3+} and Ti^{4+}; when Cr^{3+} is incorporated the name is ruby[16]. Although the fluorescence is most dominating at higher wavenumber shifts it is so broad that it even overwhelms signals near the methane band around 2900 cm^{-1}.

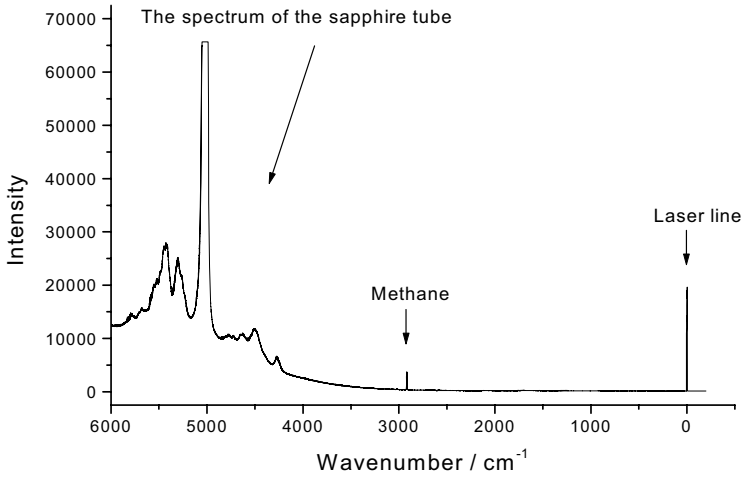

Fig. 2.3. The Raman spectrum of methane and the sapphire tube delivered by Saphikon, Milford. The sapphire tube cell was filled with methane of purity N45 (99.995 %), from Hede Nielsen A/S. The pressure was 4.0 MPa_A. The spectrum was obtained by use of the 1st spectrograph. The 514.53 nm_{air} of the Ar-ion laser was used as the excitation source (~200 mW) and the collection geometry was 90°.

It was therefore decided to get a better tube. After trying several materials the cell was finally equipped with a tube of sapphire with a very high purity (and to a much higher price). The tube was a special order from ST Sanchez Technologies, France. The quality of spectra obtainable with this tube is shown in Fig. 2.4. It is seen that it was almost without fluorescence (the fluorescence was higher when the tube was new). Two small peaks arising from the Cr^{3+} (ruby) are seen at ~5030 cm^{-1} and ~5004 cm^{-1}.

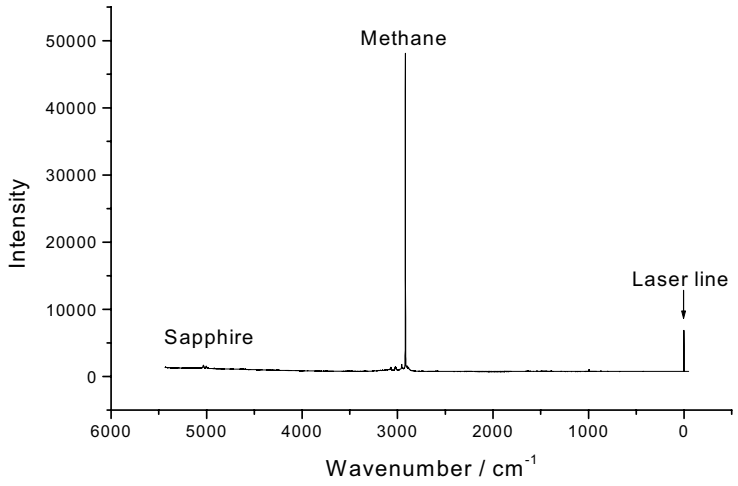

Fig. 2.4. Typical Raman spectrum obtained with an aged specially ordered tube from ST Sanchez Technologies, France. The cell was filled with natural gas from the Ll. Torup Gas Storage Facility (~88 vol% methane). The pressure was 6.4 MPa_A. For experimental details see legends to Fig. 2.3.

The dimensions of the ordered sapphire tube were 39.5 ± 0.2 mm length, 6.35 ± 0.01 mm outer diameter and 4.32 ± 0.5 mm inner diameter. According to Saphikon the allowed working pressure for a sapphire tube with the given diameters, 6.4 mm and 4.3 mm, is 51 MPa[17] (the safety factor at room temperature is set to 3). Note: the allowed working pressure for a quartz tube with the same dimensions is given to 6 MPa (safety factor 3). According to the formula by Lux[15] the working pressure for a quartz tube of the same dimensions can be calculated to ~14.7 MPa).

The final layout of the cell, equipped with that sapphire tube of high quality and modified to obtain mechanical stability etc., is shown schematically in Fig. 2.5. In Appendix A are listed all of the components from which the cell was built, including catalogue numbers and pressure limits. The Danish Swagelok Company has supplied all Swagelok fittings, including the two packless valves (2a) and (2b). With respect to **O**-rings the original ones in (4), (8) and (12) have been replaced by **O**-rings of nitrile rubber because even small amounts of CO_2 in natural gas were found to spoil the viton. The parts (5) and (8) were connected through a hole in the metal disc (7) and welded together. The metal discs were stabilised by rods around the tube (11), and surrounded by a safety metal net (9). To mechanically stabilise the whole cell a brass plate was provided (16), and through the holes (18a) and (18b) in the rack it was screwed on to an aluminium block socket. Finally the cell was equipped with a pressure gauge (15), a Wika bourdon manometer (measure range: 0-25.0 MPa_R).

The sapphire tube cell was leaking tested up to 15.0 MPa, at first with water and thereafter with methane, and it was found to be perfectly tight. The total volume of the cell was determined to 10.0 ± 0.5 cm^3, by a method described in Chap. 3.

Filling of the cell: The cell was transported to the gas plants, either to The Nybro Gas Treatment Plant or The Ll. Torup Gas Storage Facility. At the plant the fitting (1) (at the valve (2a)) was connected to the DONG A/S sampling loop. Both valves (2a) and (2b) were opened and the cell was flushed with gas at a low flow and at a low pressure. After flushing, the valve (2b) was gradually closed, and the cell was filled with natural gas to the full maximum pressure, very slowly to avoid any explosion of the sapphire tube. After filling, valve (2a) was closed, the cell disconnected and the blind plugs were put on. Hereafter the cell was transported to the Raman Laboratory for Raman measurements.

In Fig. 2.6 a photograph of the sapphire tube cell is shown.

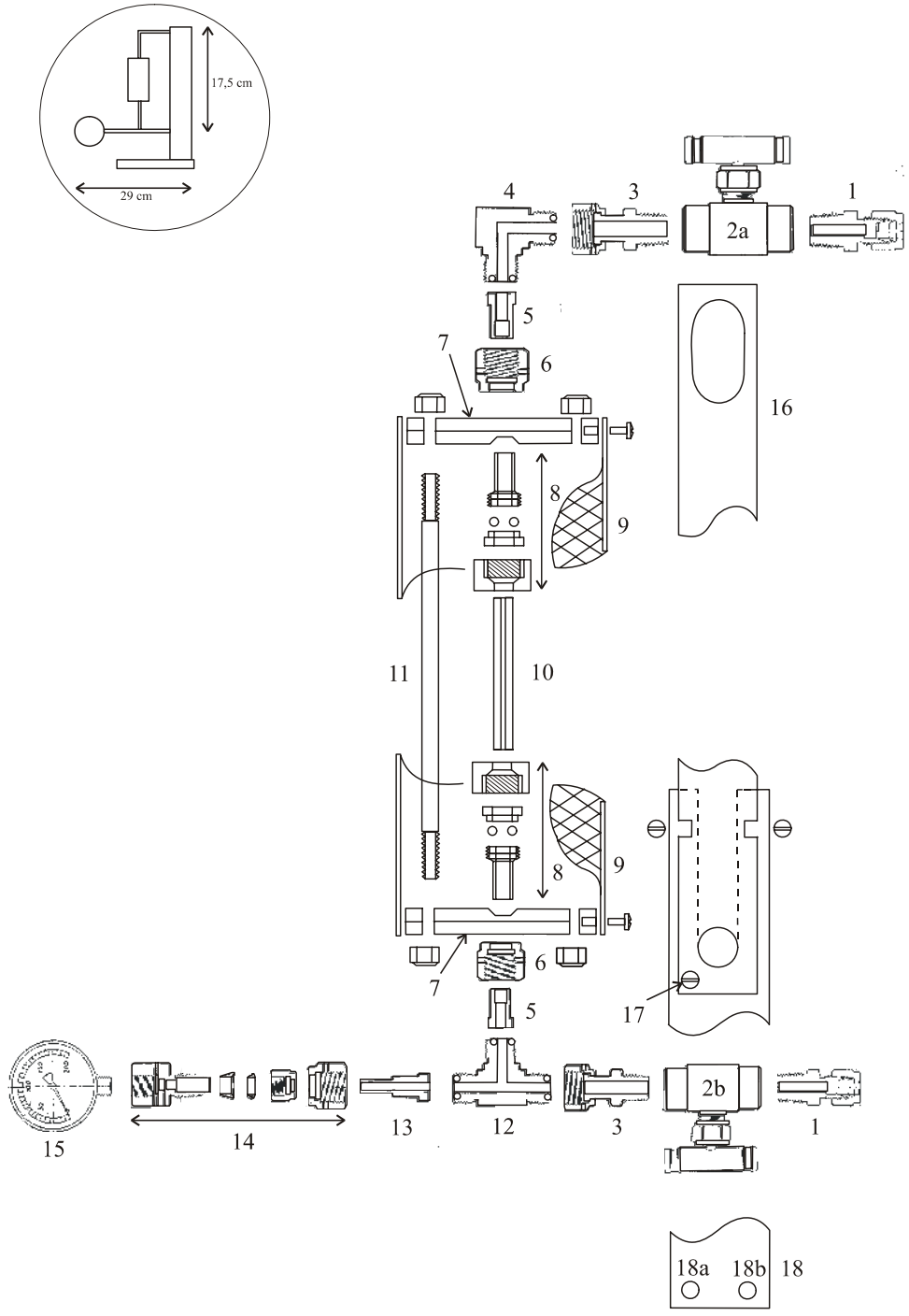

Fig. 2.5. Schematic illustration of the sapphire tube cell. The overall dimensions of the assembled cell are indicated in the circle. (1) Male connector (NPT) including blind plug; (2) Packless valve; (3) Male connector, including two **O**-rings; (5) Socket weld gland; (6) Female nut; (7) Metal disc; (8) Cajon ultra torr adapter, including two **O**-rings; (9) Safety metal net; (10) Sapphire tube (dimensions: 39.5 ± 0.2 mm length, an outer diameter of 6.35 ± 0.01 mm, an inner diameter of 4.32 ± 0.5 mm); (11) Connector rod; (12) Tee, including three **O**-rings; (13) Tube adapter gland; (14) Female connector; (15) WIKA pressure gauge (measure range: 0-25.0 MPa_R); (16) Stabilising brass plate; (17) Screw for grounding to earth; (18) Rack (the cell was screwed on a aluminium block socket through 18a and 18b).

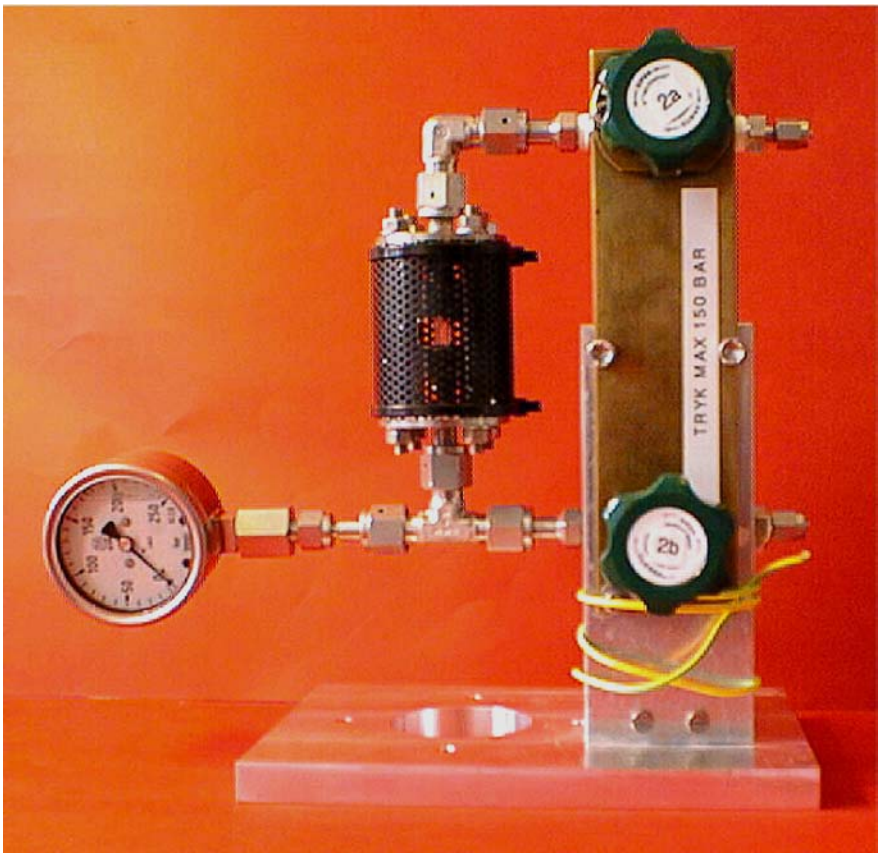

Fig. 2.6. Photograph showing the sapphire tube cell. Photo: S. Helmark.

2.2.3 The Titanium Cell

The construction of the titanium cell is based on the two cells described in refs. 11-13. The cell has been designed and machined by the French company ROP, which does not exist any more. In September 1998 the cell was modified by ST Sanchez Technologies, Viarmes, France, a successor of ROP. In Fig. 2.7 the titanium cell is schematically shown, seen from the front and from the side.

The transparent section in the cell consists of two flat sapphire windows sealed to the metal with viton gaskets. The diameter of the sapphire windows is 10 mm and the thickness is 7 mm. Allowed working pressures for sapphire windows with different sizes have been given by Saphikon[17]. The allowed working pressure is however not given for a window in the dimensions that the sapphire windows in the titanium cell have. In Appendix B are listed the allowed working pressures (referred to as "burst pressures" in the table) with the different sizes (diameter D and plate thickness PT), including the D/PT values. In the Appendix B is also included a plot of the allowed working pressure as a function of D/PT. From the plot it can be concluded that the allowed working pressure for the sapphire windows in the titanium cell (D/PT~1.4) definitely must be higher than 120 MPa.

The cell has been equipped with a pressure transmitter with digital display (FlexBar HRT 81-611-311-3118) obtained from Kamstrup A/S, Århus, Denmark. According to the company the pressure range is from –0.1 to 40.0 MPa_R and the accuracy is better than 0.25 % f.s. (full scale), i.e. better than 0.1 MPa. A certificate of calibration, delivered by Kamstrup A/S, provides traceability of measurements to recognised national and international standards.

When the cell has been filled with gas it was possible to change the pressure by changing the internal volume. The volume is changed by a hand driven wrench, which moves the piston in the cell (cf. Fig. 2.7). When the pressure once has been increased it is possible to move the piston in both directions and thereby achieve a wanted pressure very precisely, e.g. 6.0 ± 0.1 MPa_A. The piston was originally designed to be surrounded with seven gasket seals to ensure complete tightness of the cell. The whole cell has been pressure tested and

leak tested with methane up to a pressure of 40.0 MPa_A (not higher because of the upper pressure limit of the pressure transmitter) and it was found to be perfectly tight.

The dead volume (net cell volume) and the total volume of the cell chamber (dead volume plus maximum piston volume) has been determined to be 5.2 cm^3 and 11.9 ± 0.1 cm^3, respectively, by the method described in Chap. 3. A photograph of the titanium cell ready for Raman measurements is shown in Fig. 2.8.

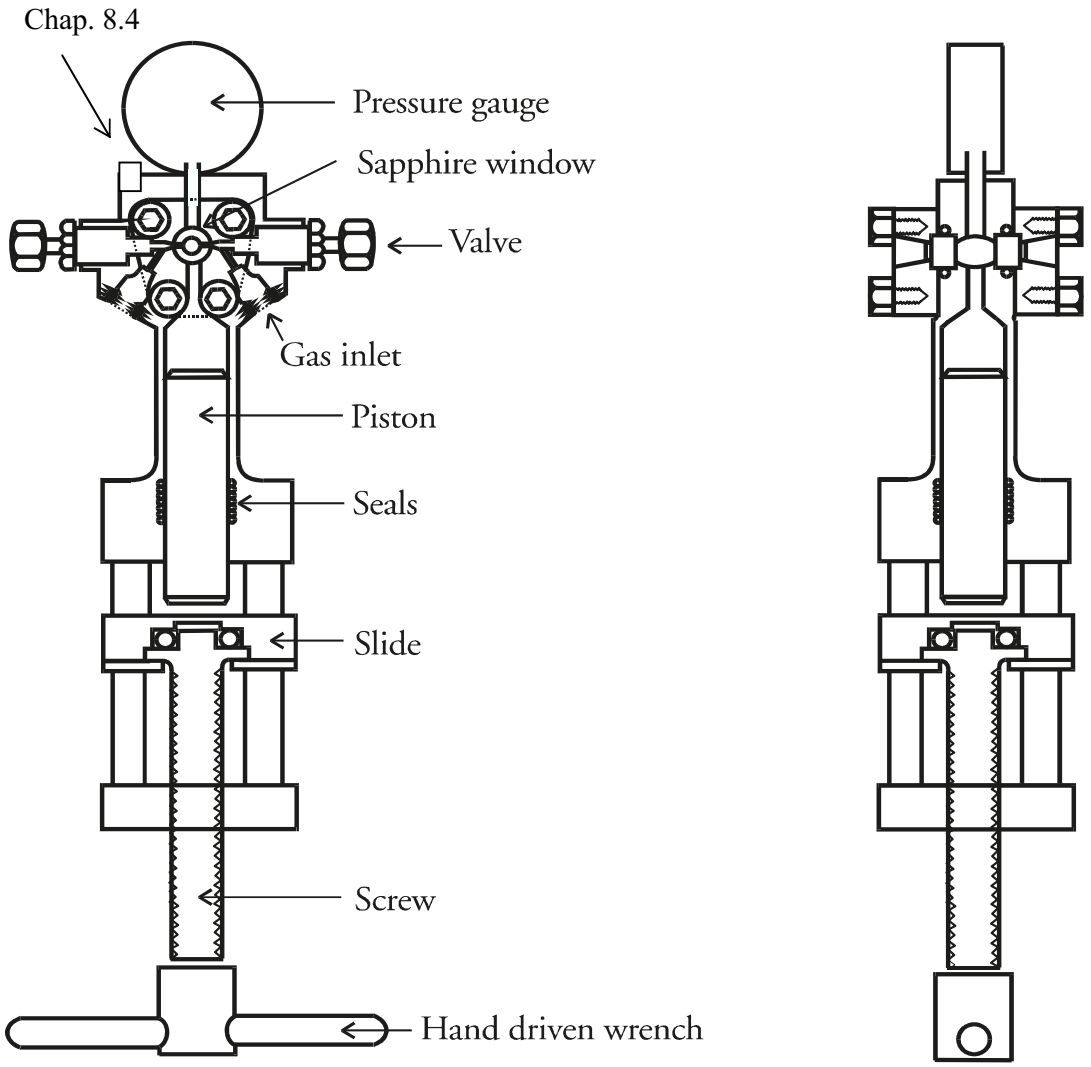

Fig. 2.7. Schematic illustration of the titanium cell, seen from the front and from the side.

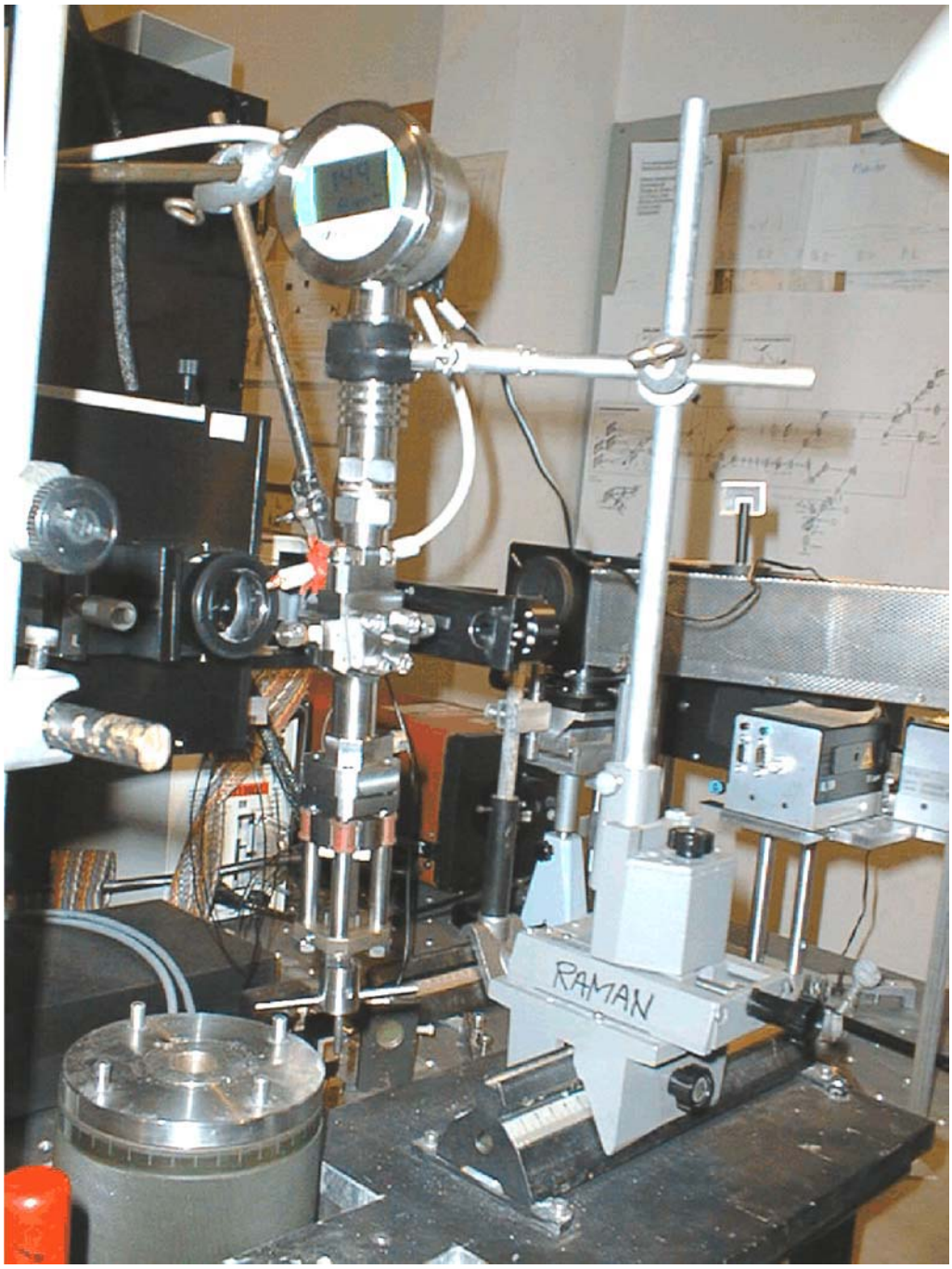

Fig. 2.8. Photograph showing the titanium cell, ready for Raman measurements. The pressure is read on the transmitter to 149 bar_R (14.9 MPa_R). The little red lamp just in front of the entrance to the spectrometer is a Neon lamp. If a spectrum of a sample is obtained simultaneously with lines from this Neon lamp it is possible to accurately calibrate the spectrum with respect to wavenumber position, as will discussed in Chap. 5. Photo: S. Helmark.

2.3 References

1. H. J. Sloane and R. Bramston-Cook, " Raman spectroscopy of some polymers and copolymers of styrene, butadiene and methylmethacrylate", Appl. Spectrosc. **27**, 217 (1973)
2. G. W. Chantry, H. A. Gebbie and C. Hilsum, "Interferometric Raman spectroscopy using infra-red excitation", Nature **203**, 1052 (1964).
3. T. Hirschfeld and B. Chase, "FT-Raman spectroscopy: development and justification" Appl. Spectrosc. **40**, 133 (1986).
4. E. D. Becker, J. R. Durig, W. C. Harris and G. J. Rosasco, "Presentation of Raman spectra in data collections", Pure Appl. Chem. **53**, 1879 (1981).
5. Microcal Origin program packet, version 6 (Microcal Software Inc., Northampton, U.S.A., 1999).
6. S. Brunsgaard Hansen, R. W. Berg and E. H. Stenby, "High pressure measuring cell for Raman spectroscopic studies of natural gas", Appl. Spectrosc. **55(1)**, xx (2001).
7. S. Brunsgaard Hansen, R. W. Berg and E. H. Stenby, "Raman spectroscopic studies of methane-ethane mixtures as a function of pressure", appear in Appl. Spectrosc.
8. J. C. Stryland and A. D. May, "Optical cell for the observation of Raman scattering in gases at high pressures", Rev. Sci. Instrum. **31**, 414 (1960).
9. A. D. May and J. C. Stryland, "Optical cells for the observation of Raman scattering in gases at medium pressures", Rev. Sci. Instrum. **34**, 992 (1963).
10. A. J. Rest, R. G. Scurlock and M. F. Wu, "Design of a variable pressure infrared absorption cell, "J. Phys. E: Sci. Instrum. **21**, 1102 (1988).
11. Ph. Marteau, J. Obriot and R. Tufeu, "Experimental determination of vapor-liquid equilibria of CO_2 + limonene and CO_2 + citral mixtures", J. Supercrit. Fluids **8**, 20 (1995).
12. Ph. Marteau, P. Tobaly, V. Ruffier-Meray and A. Barreau, "In situ determination of high pressures phase diagrams of methane-heavy hydrocarbon mixtures using an infrared absorption method", Fluid Phase Equilibria **119**, 213 (1996).
13. Ph. Marteau, J. Obriot, A. Barreau, V. Ruffier-Meray and E. Behar, "Experimental determination of the phase behaviour of binary mixtures: methane-hexane and methane-benzene", Fluid Phase Equilibria **129**, 285 (1997).

14. I.-M. Chou, J. D. Pasteris and J. C. Seitz, "High-density volatiles in the system C-O-H-N for the calibration of a laser Raman microprobe", Geochim. Cosmochim. Acta. **54**, 535 (1990).
15. H. Lux, "Arbeiten bei höherem Druck" in *Anorganische Chemie.* (Barth. Leipzieg, 1954) chap. 16, p. 547-550.
16. A. G. Sharpe, *Inorganic Chemistry* (Longman Inc., New York, 1986), Chap. 12, p. 278.
17. www.saphikon.com/tubebrst.ht.

3. Determination of Dead Volume and Total Volume of a Cell Chamber.

3.1 Introduction

When working with high pressures it is very important to know the exact total volume and the dead volume in the experimental cell for many reasons, e.g. safety approvals and prediction of pressure range. In the following a simple method to determine such volumes is described. The method is demonstrated by reference to a so-called syringe experiment, Chap. 3.2 and the titanium cell experiment, Chap. 3.3. It is based on the movement of a piston in the cell chamber and the reading of the thereby caused changes in readable pressure. When the total volume and dead volume in the titanium cell once has been determined, the cell can be used to find total volumes of other cell chambers. The titanium cell experiment is also presented in ref. 1, in a condensed version.

3.2 The Syringe Experiment

The instrumentation used in this experiment was an acetylene Bourdon manometer, with a range up to 4 MPa_A (Clutogena, A/S Danilbo), connected either to a 5 ml plastic syringe (Imacillin Mikstur, Astra) or a 20 ml plastic syringe (Terumo, Syringe). A home-made paper ruler was pasted on both of the syringes to achieve a more precise reading. The gas "filled" in the syringes was air.

The method is based on the following equations:

$$
\begin{aligned}
& V \cdot \rho = m \\
& V = m\rho^{-1} \\
& V = V_{dead} + V_h \\
& V_{dead} + V_h = m\rho^{-1} \\
& V_h = m\rho^{-1} - V_{dead}
\end{aligned}
\qquad (3.1)
$$

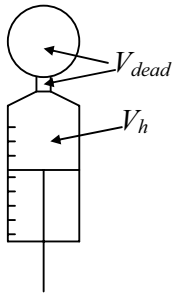

Fig. 3.1.

V: volume (cm^3), ρ: density (gcm^{-3}), m: mass (g). V_{dead} and V_h are illustrated in Fig. 3.1.

From the last equation, numbered (3.1), it is seen that if V_h is plotted as a function of ρ^{-1}, a straight line will be obtained. The slope of the line is the mass of air in the syringe and manometer, and the point of intersection with the y-axis is $-V_{dead}$. The inverse density, ρ^{-1}, of the air, can be calculated from the gas equation.

$$pV = ZnRT \Leftrightarrow \frac{V}{n} = \frac{ZRT}{p}$$

$$\rho = \frac{nM}{V} \Leftrightarrow \rho^{-1} = \frac{V}{n} \cdot \frac{1}{M}$$

$$\rho^{-1} = \frac{ZRT}{pM} \qquad (3.2)$$

p: the pressure, Z: the compression factor, n: the amount of substance, T: the temperature, R (the gas constant) = 8.31441 $JK^{-1}mol^{-1}$ and M (the molar mass of air) = 28.959 $gmol^{-1}$ [2].

In equation (2a) the reciprocal density is expressed, including the units.

$$\rho^{-1}[m^3 g^{-1}] = \frac{Z \cdot R[JK^{-1}mol^{-1}] \cdot T[K]}{M[gmol^{-1}] \cdot p[Pa]} \qquad (3.2a)$$

The procedure for the syringe experiments is schematically shown in Fig. 3.2.

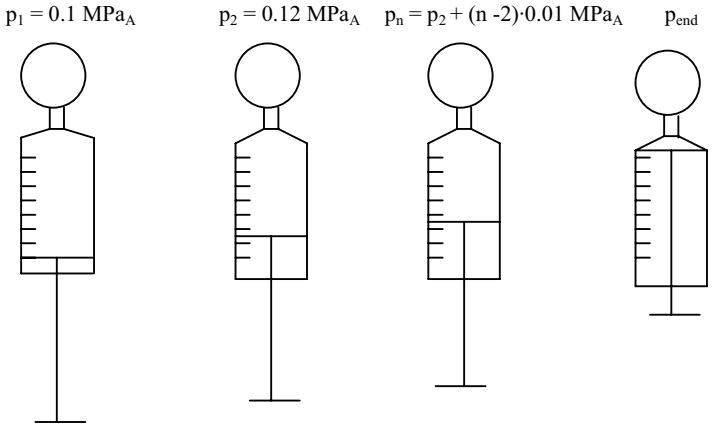

Fig. 3.2. The procedure for the syringe experiment.

1. The piston was placed at the lowest mark. This position corresponds to the largest volume, V_{total}. The syringe was then connected tightly to the Bourdon manometer and the pressure was read to 0.1 MPa_A.
2. The piston was then pushed until a pressure at 0.12 MPa_A was reached. The volume at this pressure was read and noted.
3. Step 2 was repeated a number of times, each time at a pressure that was 0.01 MPa_A higher.
4. The last measurement. For the 5 ml syringe it was at $V_h = 0$; for the 20 ml syringe it was at a V_h corresponding to a pressure of 0.24 MPa_A.

The temperature was read and noted for all the steps.

ρ^{-1} was calculated for all the positions by means of equation 3.2. The pressure range in the syringe experiments was 0.1-0.24 MPa_A. At such low pressures it is reasonable to consider air as an ideal gas. In fact, tables reveal that Z at 300 K and 0.1, 0.2 and 0.4 MPa_A is 1.000, 0.9996 and 0.9989, respectively[2]. Thus, the Z factor does not influence the calculations.

In Fig. 3.3 the plot of the volume as a function of ρ^{-1} is shown. The data from the 5 ml syringe were based on 6 different measurement series, in which the points of intersection ($-V_{dead}$) were in the range -3.2625 → -3.3552. The data from the 20 ml syringe were based on 3 different measurements in the range -3.2250 → -3.3495. The measurements with the 5 ml syringe showed a better reproducibility compared to the 20 ml syringe. Thus the following results are delivered:

$V_{dead} = \underline{(3.3 \pm 0.1)\ cm^3}$.

V_{total} (5 ml syringe) = (5.0 + 3.3) cm^3 = (8.3 ± 0.1) cm^3

V_{total} (20 ml syringe) = (20.0 + 3.3) cm^3 = (23.3 ± 0.1) cm^3

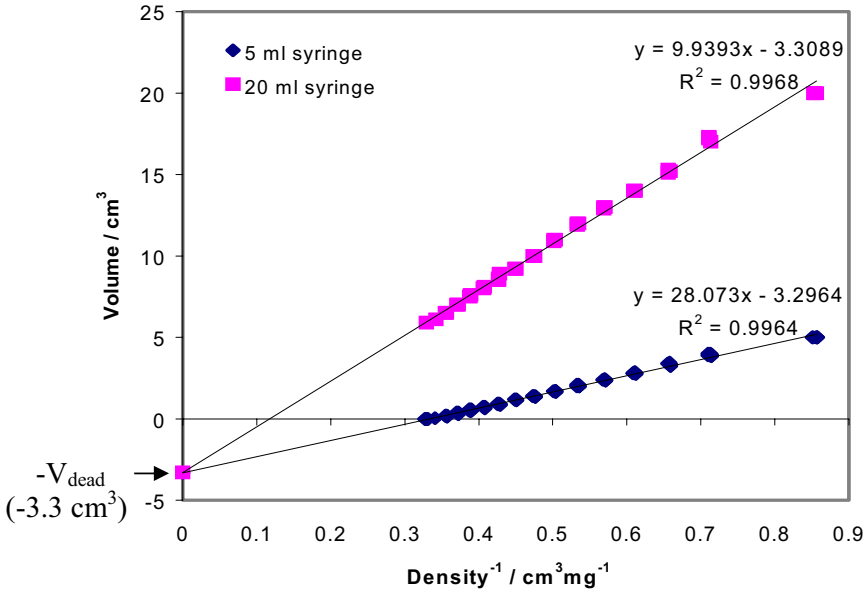

Fig. 3.3. Piston movement in the two syringes as a function of density^{-1}.

When looking carefully at the points in Fig. 3.3 it seems like they don't follow perfect straight lines. In fact it looks like they have a tendency to follow S-shaped curves. The tendency is however so small, that it in this work was ignored.

It is worth to give a remark about the Bourdon manometer. An illustration of such a manometer is shown in Fig. 3.4. The principle is that when the pressure is raised, then the elliptically tube will expand and thereby move the hinge which moves the needle for the pressure reading. This means, in fact, that the higher the pressure is, the higher the dead volume will be. However, in this work it was assumed that the expansion is small compared to the total volume, especially with the low pressures applied in this experiment. Therefore this expansion was not taken into account.

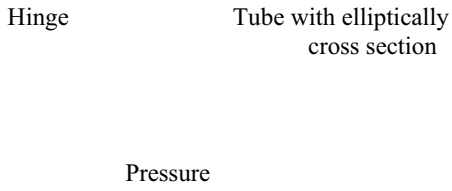

Fig. 3.4. An illustration of the Bourdon manometer.

3.3. The Titanium Cell Experiment

The instrumentation used in this experiment was a Vernier gauge and the titanium cell equipped with the pressure transmitter, FlexBar HRT (Kamstrup). The gases used were nitrogen (purity N45, i.e. 99.995 %, Hede Nielsen A/S) and methane (purity N45, Hede Nielsen A/S).

The method is based on equation (3.1) as in the previous experiment. This time however it was the hight, h, of the piston movement, which was measured. From equation (3.3) it is seen, that if $h\pi r^2$ is plotted as a function of ρ^{-1}, then a straight line will be observed, with $-V_{dead}$ as the intersection with the y-axis.

$$V_h = m\rho^{-1} - V_{dead}$$

$$(h\pi r^2) = m\rho^{-1} - V_{dead} \qquad (3.3)$$

h: measured hight, r: radius of the piston.

The pressures in this experiment were high, so it is not correct to consider the two gases, CH_4 and N_2, as ideal. Thus it was necessary either to find Z as a function of pressure in the literature or to find experimental data for ρ. In this work the latter has been done.

The experimental data for ρ versus p and T were found in ref. 2. In Fig. 3.5a the density for methane as a function of temperature at 6.0 MPa_A is shown. A straight line connected the points and the same behavior is seen for plots at other temperautures. Therefore an interpolation has been made to get the densities at the temperature, i.e. the temperature measured under the experiment (between 290 and 300 K).

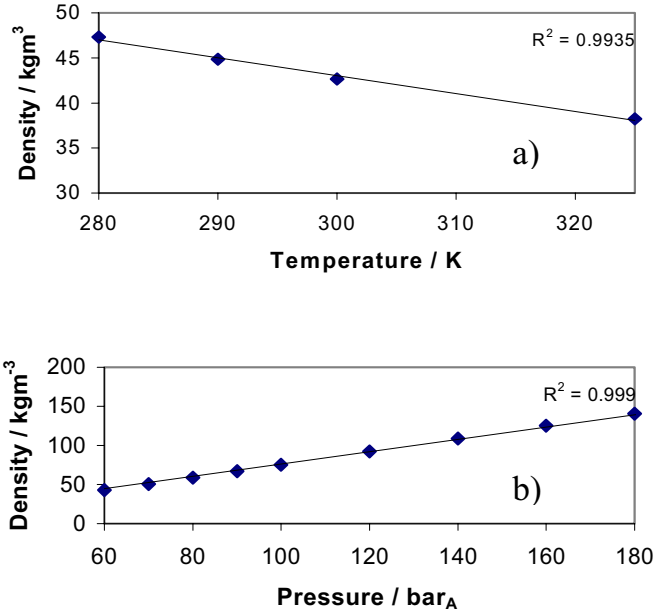

Fig. 3.5. Density (methane) as a function of a) temperature at 6.0 MPa_A and b) pressure at 300 K (note: the pressures are given in bar_A). The points were acquired from ref. 2.

The reported density for methane as a function of pressure is shown in Fig. 3.5b. Also here points following a straight line were obtained, so interpolation can be made for values that are not included in the table of ref. 2. However, with the wrench it was possible to screw the piston in the titanium cell in both directions and thereby achieve a wanted pressure very precise, e.g. (6.0 ±0.1) MPa_A. Thus interpolation was only necessary at the starting pressure and at the final pressure.

The experimental procedure for the experiment was the same as described previously, but because of the much higher pressures the height of the piston position was only measured (with the Vernier gauge) for every 1.0 MPa_A. Three measuring series were done. Measurements were repeated 3 times with renewed sample gas. At first the titanium cell was filled with nitrogen at a pressure of 5.7 MPa_A and the measurements done and repeated. Then the cell was filled with methane at 7.0 MPa_A and measurements done, and at last it was filled with methane again but this time at a pressure at 8.2 MPa_A. Values for $h\pi r^2$ (the diameter of the piston was measured to 15.95 mm, i.e. r = 0.7975 cm) were plotted as a function of ρ^{-1}. The result of the work is shown in Fig. 3.6. All data points are listed in Appendix C. It is seen that the 3 series of measurements are in very good agreement with respect to extrapolation to the measured $h\pi r^2$ at zero reciprocal density. The found intersections with the y-axis were -5.1429, -5.1508 and -5.2018 cm^3. Thus the rounded value for V_{dead} must be 5.2 cm^3.

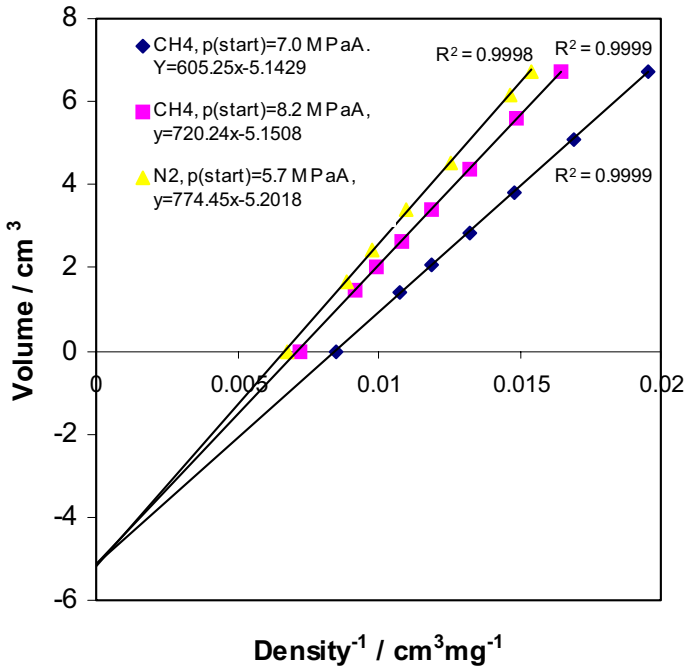

Fig. 3.6. Piston movement in the titanium cell as a function of density^{-1}. Each experiment was repeated three times. Rhombs: the cell filled with methane at a starting pressure at 7.0 MPa_A (t = 25.7 °C), squares: the cell filled with methane at a starting pressure at 8.2 MPa_A (t = 26.4 °C) and triangles: the cell filled with nitrogen at a starting pressure at 5.7 MPa_A (t = 24.4 °C).

The height of the piston was measured to 3.36 cm and the radius to 0.7795 cm. Thus the piston volume, V_{piston}, was easily found. The total volume of the titanium cell is the sum of the dead volume and the piston volume.

$V_{dead} = \underline{(5.2 \pm 0.1)\ \text{cm}^3}$

$V_{piston} = \pi \cdot (0.7975\ \text{cm})^2 \cdot 3.36\ \text{cm} = 6.7\ \text{cm}^3$

$V_{total} = V_{dead} + V_{piston} = \underline{(11.9 \pm 0.1)\ \text{cm}^3}$

Finally the titanium cell was filled with water (in vacuum to reduce the amounts of bubbles) and weighed to 2058.7 g. The titanium cell without water was weighted to 2047.1 g, i.e. the amount of water in the cell was 11.6 cm^3. This result is in fair accordance with the above given total volume of the titanium cell.

As in the previous section, dealing with the syringe experiments, it is also here worth while to give a remark on the pressure gauge. The titanium cell was equipped with a FlexBar pressure transmitter from Kamstrup A/S, as mentioned in Chap. 2.2.3. The pressure in the titanium cell affects a sensitive isolating diaphragm in the transmitter. The higher the pressure is the more this diaphragm is expanded. Thus the higher the pressure is, the higher the volume in the transmitter will be. It is however presumed that this expansion is negligible and therefore it has not been taken into account. This assumption seems to be justified.

3.4. Final Remarks

The described method to determine volumes of cell chambers by this simple method based on the piston movement has shown to be suitable for its purpose. It is in fact also possible, by the described method, to determine total volumes of another cell chamber simply by connecting it to the titanium cell (cf. ref.1). In that way the total volume of the sapphire tube cell has been determined to $(10.0 \pm 0.5)\ \text{cm}^3$. The uncertainty was a little larger than for the piston itself due to the larger dead volume. The volume of the sapphire tube cell was also determined by weighing the cell filled with water and without, 10.0 ml. A third method requiring relatively large equipment, with a pump, can also be used to determine volumes. This method is again based on piston movement and pressure volume relations. By such a

pump (ISCO Syring pump, model 260D) the total volume of the sapphire tube cell was determined to 10.48 cm^3.

3.5. References

1. S. Brunsgaard Hansen, R. W. Berg and E. H. Stenby, “Raman spectroscopic studies of methane-ethane mixtures as a function of pressure”, appear in Appl. Spectrosc.
2. Gaz encyclopedie des l’air liquide, Elsevier, 1976.

4. Raman Spectroscopic Studies of Natural Gas

4.1. Brief Introduction

The present work concerns Raman spectroscopic studies of natural gas. The chapter consists of three parts: The first part, Chap. 4.2, concerns the analysis of a natural gas sample from Nybro Gas Treatment Plant with respect to micro droplets of condensate (triethylene glycol and compressor oil). The second part, Chap. 4.3, is on the analysis of a natural gas sample from Ll. Torup Natural Gas Storage Facility, with respect to micro droplets of Oppanol. The third part, Chap. 4.4 concerns the analysis of three different natural gas samples at different pressures. A detailed qualitative analysis and an attempt of a quantitative analysis are presented.

Detailed introductions with respect to the purposes of each of the three parts are given separately.

4.2. Natural Gas Sample from The Nybro Gas Treatment Plant

4.2.1 Introduction

Natural gas is produced in the Danish sector of the North Sea. The gas is transmitted via a pipeline from the Tyra field (since 1999 also from the South Arne field) in the North Sea to The Nybro Gas Treatment Plant at the west coast of Jutland (commissioned in 1982). At The Nybro Gas Treatment Plant (in the following just referred to as Nybro) the quality of the natural gas is continuously beeing measured, e.g. by gas chromatography. Already at the platforms in the North Sea the natural gas undergoes separation and scrubbing processes, e.g. removal of sulphur compounds, water vapour and heavy hydrocarbons. The desulphurisation brings the sulphur content in the natural gas down to typically 1-3 mg / Nm^3, which is in agreement with the requirements set by the authorities in Denmark. If water vapour is present in the gas it can lead to the formation of solid gas hydrates (clathrates). Therefore it is important to remove the water before transmission to the shore. The gas industry traditionally uses a method based on the absorption of water to triethylene glycol in an absorber column. When the natural gas passes the absorber column some of the triethylene glycol will be carried with the gas as small droplets. These droplets are trapped in a so-called demister (mist eliminator). Triethylene glycol will however also be in the gas as vapour. This triethylene glycol in the gaseous phase might condense to micro droplets (diameter 20-50 nm) when the gas is transmitted to Nybro. Heavy hydrocarbons are also removed from the natural gas at the platforms – this is primarily to avoid condensation problems. When the natural gas arrives to Nybro at pressures up to 12 MPa, the pressure is reduced to 8 MPa, after which the gas is filtered and measured. At Nybro and in downstream systems liquids are regularly drained from drain pots. These liquids have shown to be triethylene glycol and lubricating oil from platform compressor systems.

This chapter concerns Raman spectroscopic studies of a liquid collected at Nybro, hereafter called condensate, Chap. 4.2.2. It also concerns Raman spectroscopic studies of a natural gas sample from Nybro, Chap. 4.2.3. The main objective of the present study was to investigate the feasibility of the Raman technique to characterise natural gas samples from Nybro with respect to micro droplets of triethylene glycol and lubricating oil. Assignment of the Raman spectrum of the natural gas will be treated in Chap. 4.4.

4.2.2 Raman Spectroscopic Studies of a Condensate from Natural Gas

Oils can cause difficulties in obtaining Raman spectra by use of visible light excitation, especially if the oils are coloured. The difficulties arise because of strong absorption in the visible region resulting in a broad fluorescence background in the Raman spectrum as described in Chap. 2.1. A sample of condensate from Nybro, delivered by DONG A/S (condensate Varde N-E, 10.07.97), had an intensive yellow colour, so fluorescence was expected when using the 514.53 nm_{air} line of an Ar-ion laser as the exciting source. Therefore it was decided to try with longer excitation wavelengths. In Fig. 4.1 the Raman spectrum of the condensate obtained by use of 784 nm_{air} excitation is shown. As it is seen there is fluorescence in spite of the NIR excitation, especially at lower wavenumbers. Two small peaks are however observable at ~1440 and ~1297 cm^{-1}, arising from CH_2 bending and $-(CH_2)_n-$ in phase twist[1], respectively. The spectrum is flattening off at higher wavenumbers as a combined result of lower fluorescence and lack of detector sensitivity. This phenomenon will be discussed again in Chap. 4.3.4. In Fig. 4.1 is also included the NIR-FT-Raman spectrum (excitation wavelength, λ_{air}: 1064 nm) of the condensate. As it is seen this spectrum is almost without fluorescence, so it is obvious that NIR-FT-Raman spectroscopy is a good choice when studying oils.

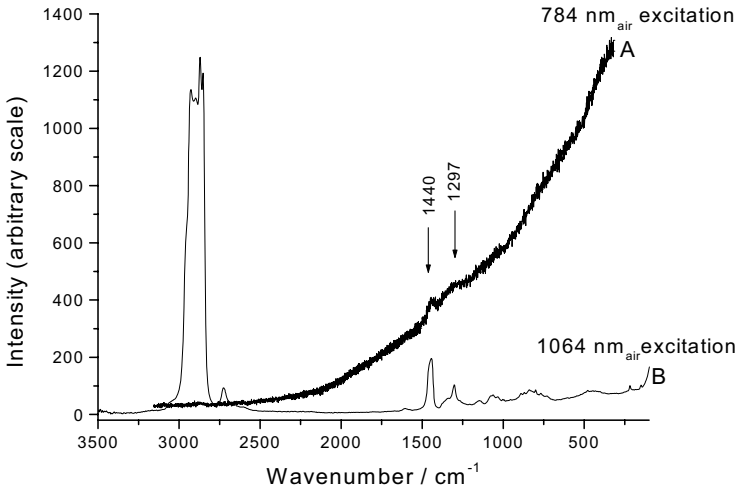

Fig. 4.1. Raman spectra of a sample of condensate from Nybro, A: obtained by use of the 2nd monochromator with a grating of 600 grooves per mm. The exciting source was a diode laser, (λ_{air}= 784 nm). The sample was placed directly under the microscope, i.e. 180° scattering, on a little plate of quartz. B: obtained by use of a FT-Raman spectrometer. The sample was placed in a small tube of quartz. Experimental details as described in Chap. 2.1.2. The FT-Raman spectrum has been multiplied by a factor 700.

Two samples of lubricating oil were examined, a compressor oil delivered by Hahnemann Technology, Denmark (labelled Shell Corena Oil P 150) and a compressor oil delivered by the Physical Plant, Mechanical Division, DTU (not labelled). The NIR-FT-Raman spectra of these two oils are shown in Fig. 4.2 (black and blue curve). To make a comparison easy the NIR-FT-Raman spectrum of the condensate from Nybro is also included in the figure (red curve). As it is seen, the three spectra are almost identical. The best fit is between the condensate and the Corena compressor oil, except for a little more fluorescence at lower wavenumbers for the latter. Based on Fig. 4.2 it was concluded that the condensate from Nybro was lubricating oil from the platforms. This conclusion was in accordance with other analyses on the condensate performed by DONG A/S.

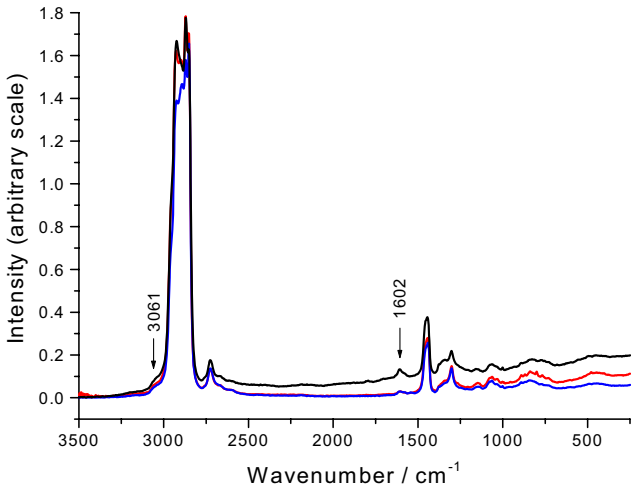

Fig. 4.2. NIR-FT-Raman spectra of the condensate from Nybro (red curve), a compressor oil delivered by the Physical Plant, Mechanical Division, DTU (blue curve) and a compressor oil delivered by Hahnemann Technology, Denmark (black curve). The samples were placed in small tubes of quartz. Experimental details as described in Chap. 2.1.2.

Most of the bands in the spectrum are due to C-H and C-C vibrations. These bands will therefore not be sorted out in the spectrum of a natural gas sample. Two bands at ~3061 cm^{-1} and ~1602 cm^{-1} in Fig. 4.2 gave rise to considerations. One possibility is that the bands are alkene bands, even though the band at ~1602 cm^{-1} is quite low for typical C=C stretching wavenumbers[2]. Another possibility is that they are aromatic bands, but because

of the absence of a band at ~1000 cm^{-1} or ~800 cm^{-1} (in the case of para substitution) this is doubtful. The band at 1602 cm^{-1} could be a candidate as a characteristic band to search for the lubrication oil in natural gas samples, but since it is very weak it is however unrealistic.

4.2.3 Analysis of a Natural Gas Sample from Nybro with respect to Micro Droplets of Triethylene Glycol and Lubricating Oil

The sapphire tube cell was transported to Nybro and filled with natural gas from the plant inlet, before downstream of pressure regulation and filtration. The pressure was 10.2 MPa_A. The Raman spectrum of the sample is shown in Fig. 4.3. It was very gratifying to see that there was no fluorescence at all.

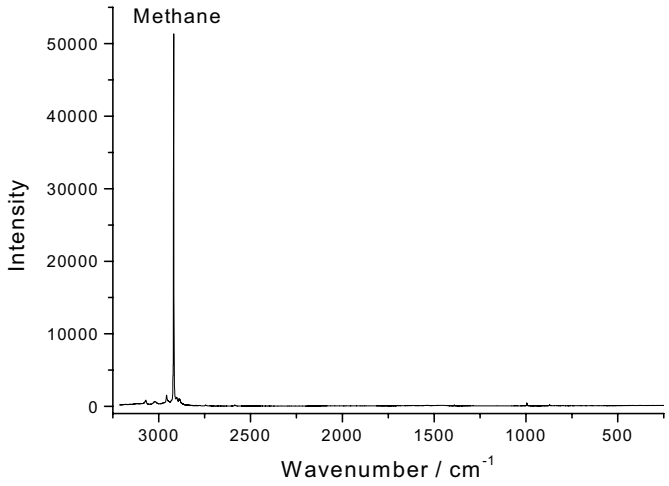

Fig. 4.3. The Raman spectrum of a natural gas sample from Nybro (10.2 MPa_A) contained in the sapphire tube cell. The spectrum was obtained by use of 1st spectrograph. The exciting source was the 514.53 nm_{air} line of the Ar-ion laser (~200 mW). The sample was placed in the macroscopic sampling position and the collection geometry was 90°.

The spectrum of triethylene glycol* was found in the literature[3]. Several intense (s,m) Raman bands were given ~2875, 1467, 1278, 1246, 1120, 1060, 883, 830 cm^{-1} (there is also a broad band ~3400 cm^{-1}, which is very strong in IR spectra, but weak in Raman spectra). Most of these bands are C-H vibration bands. The first six are due to C-H stretching, C-H

* $HO\text{-}CH_2\text{-}CH_2\text{-}O\text{-}CH_2\text{-}CH_2\text{-}O\text{-}CH_2\text{-}CH_2\text{-}OH$

bending, CH_2 twisting, CH_2 twisting, CH_2 rocking and CH_2 rocking respectively. The assignments are in accordance with the literature[1,4,5] (in ref. 5 are given calculated wavenumbers for a very similar compound, triethylene glycol dimethyl ether). For aliphatic ethers in-phase C-O-C stretching occur at 890-820 cm^{-1} [5]. The two bands at 883 and 830 cm^{-1} are therefore assigned as C-O-C stretching bands, which is in accordance with ref. 4. Since virgin-natural gas contains no compound with C-O-C bonds, those two bands can be used as characteristic bands to search for triethylene glycol in the gas. Fig. 4.4 depicts the Raman spectrum also shown in Fig. 4.3 in an expanded way. Wavenumber positions of the two characteristic bands are indicated with arrows. No such bands can be seen. From the figure it is concluded that it is not possible to detect triethylene glycol. Small peaks are seen in the region, but it looks more like noise. Also a condensate band at ~1602 cm^{-1} is not observed in the spectrum

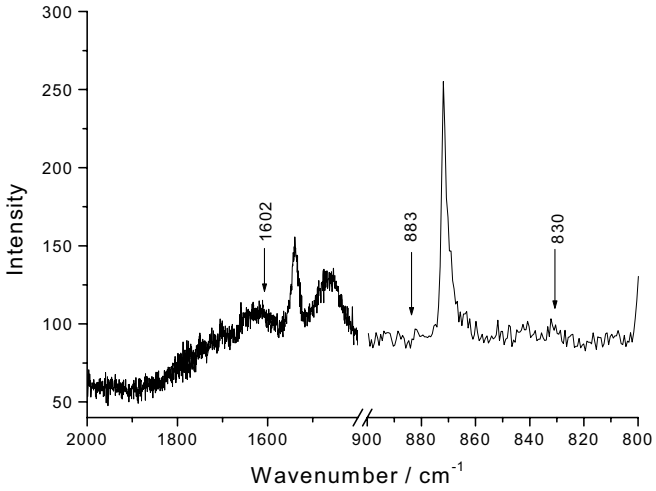

Fig. 4.4. Fractions of the Raman spectrum also showed in Fig. 4.3. Positions where the two characteristic triethylene glycol wavenumbers should occur are indicated with arrows (883 and 830 cm^{-1}), and so is the position of the weak characteristic signal observed in the NIR-FT-Raman spectrum of condensate from Nybro (1602 cm^{-1}).

4.2.4 Conclusion

By comparing the NIR-FT-Raman spectra of the condensate from Nybro with those of the two compressor oils, it was seen that the spectra were almost identical. It was therefore concluded that the condensate originated from the compressor systems at the platform. It was not possible to detect micro droplets of compressor oil in the Raman spectra of the natural gas sample sampled at Nybro.

The water absorbing compound triethylene glycol was found (in the literature) to have two characteristic Raman bands at 883 and 830 cm^{-1}. These two bands were searched for in the Raman spectrum of the natural gas sample, but with a negative result. It can be concluded that the Raman method in the present version is not a feasible technique to detect micro droplets (20-50 nm) of lubricating oil and triethylene glycol in natural gas.

On the other hand it was a pleasure to discover that the cell was very suitable for obtaining high quality Raman spectra of the natural gas without fluorescence.

4.3. Natural Gas Sample from Ll. Torup Gas Storage Facility

4.3.1 Introduction

Natural gas is transmitted from Nybro to the market. In order to compensate for changes in the seasonal demand of gas Dong A/S operates two natural gas storage facilities, Stenlille at mid Zealand (commissioned in 1994) and Ll. Torup Gas Storage Facility in the North of Jutland (commissioned in 1986). Some experiences from the latter (in the following just referred to as Ll. Torup), will be discussed in this chapter. The storage at Ll. Torup is established as caverns (chambers) in a salt dome. The natural gas is stored at temperatures ~40-50°C and under high pressure, 16-23 MPa, depending of the depth of each individual cavern[6]. Each cavern can be operated down to 8 MPa. The overall storage facility consists of seven caverns at a depth of 1200-1500 m. The caverns are cylinder shaped and they are typically 200-300 m high with a diameter of 50-65 m. The caverns were constructed by a leaching process, flushing sweet water into the structure in a controlled manner and disposing salt brine elsewhere in the ocean environment. As a consequence some residual water remains at the bottom of the caverns. A problem is that the water might evaporate into the natural gas. As a measure to reduce this water evaporation DONG A/S decided to cover the bottom and the residual water in the caverns by a thin film. For this purpose various polymerised olefinic hydrocarbons products have been used by other gas companies. Oppanol was the material selected by DONG A/S and was used as described above in two of the caverns at Ll. Torup. Small amounts of the Oppanol however evaporated into the gas. Hence, when the natural gas from the caverns was brought to ambient temperature conditions, Oppanol condensed from the gaseous phase forming condense micro droplets with a size 20-50 nm. The objective of this part of the project was to investigate the feasibility of the Raman technique to characterise natural gas samples from Ll. Torup with respect to such Oppanol micro droplets.

This chapter concerns Raman spectroscopic studies of both a natural gas sample from Ll. Torup and of pure Oppanol. The purpose of the Raman spectroscopic studies of pure Oppanol was to identify some characteristic bands, which are not seen in the spectra of "pure" natural gas, Chap. 4.3.2-4.3.5. These chapters also serve as a presentation of the possibilities in the Raman instrument, and considerations in which way to obtain the best

Raman spectrum. The characteristic bands in the spectrum of pure Oppanol were searched in the Raman spectrum of the natural gas sample from Ll. Thorup Chap. 4.3.6 and finally in a Oppanol / methane mixture with a high content of Oppanol, Chap. 4.3.7.

4.3.2 The Raman Spectrum of Oppanol

The Oppanol sample from Ll. Torup (sample 80617-9, delivered by DONG A/S) was a colourless viscous liquid. It was a homopolymer synthesised from the monomer 2-methyl-1-propen[7] (isobuten). The structural formula is shown in Fig. 4.5. The extent of polymerisation, *n*, is between 4 and 25, i.e. it is a lowmolecular polymer belonging to class B3 according to the patent[8].

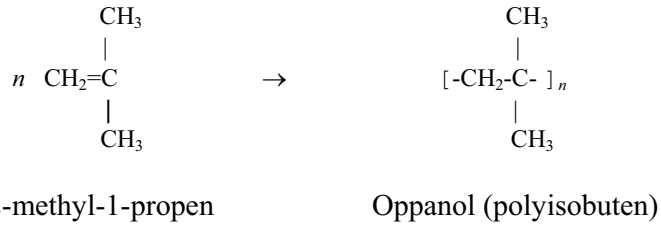

Fig. 4.5. The structural formula of Oppanol, the monomer and the polymerised product.

The Raman spectrum of the Oppanol sample from Ll. Torup is shown in Fig. 4.6. The most intense bands in the spectrum occur in the C-H stretching region. CH_3 bending bands are seen near 1443 cm^{-1}. A weak band at ~1662 cm^{-1} is assigned as C=C stretching in the CH_2=C< group. It was therefore concluded that the Oppanol sample contained residuals of the monomer 2-methyl-1-propen. This is confirmed by the fact that there are also weak bands at ~3073 and ~1390 cm^{-1} arising from respectively asymmetric CH_2 stretching and CH_2 deformation in the CH_2=C< group (literature values are 3090-3075 cm^{-1} (w) and 1420-1390 cm^{-1} (vs)[9]).

Characteristic features in the Raman spectrum of Oppanol: For molecules with methyl groups, a symmetric CH_3 umbrella deformation at ~1375 cm^{-1} is seen in IR spectra but normally not in Raman spectra. The overtone (2ν) of that vibration on the other hand is

seen in the Raman spectra. In tert-butyl compounds the symmetric CH_3 umbrella deformation splits up in two bands (1400-1395 cm^{-1} and 1374-1366 cm^{-1}) with different intensity[1]. Normally the band with lowest wavenumber is the most intense. In the Raman spectra of Oppanol, Fig. 4.6, a similar splitting is also seen for the two overtones at 2768 cm^{-1} and 2913 cm^{-1} but with almost the same intensity. The Raman spectrum of MTBE (methyl tertiary butyl ether) is described in details in Appendix F. It also revealed two overtone bands and the one with the lowest wawenumber was most intense.

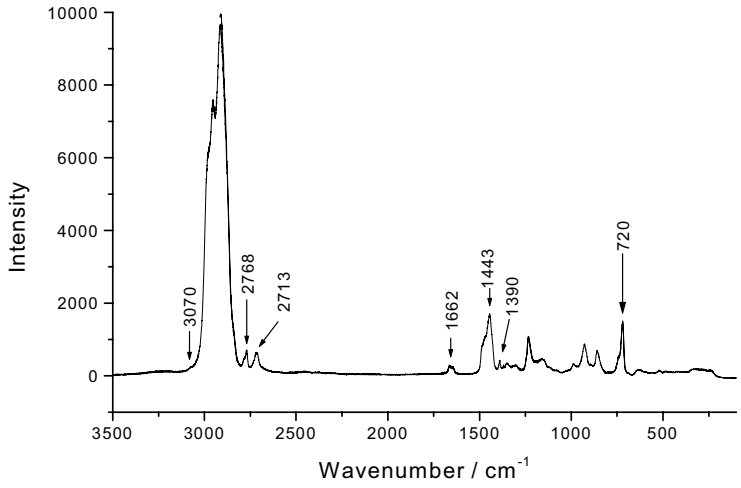

Fig. 4.6. The Raman spectra of Oppanol obtained by use of the 1st spectrograph with a grating of 1800 grooves per mm. A little piece of platinum foil shaped to a cup was cleaned, made red-hot and cooled to ensure the absence of impurities. The Oppanol sample was placed in this cup under the microscope, i.e. 180° scattering. The 514.53 nm_{air} line of the Ar-ion laser was used as the exciting source.

Another characteristics in the Raman spectrum of MTBE was the band at ~720 cm^{-1}. This band was assigned in Appendix F to the symmetric C-C stretching involving the tertiary carbon in the tert-butyl group[9-11]. The structure of Oppanol is rather similar to the butyl group, Fig. 4.7, so it is not surprising that an analogous band is observed in Fig. 4.6 at ~720 cm^{-1}. By means of this characteristic band it should be possible to detect Oppanol in natural gas from Ll. Torup, provided that components with tert-butyl groups, e.g. neo-pentane, are only present in the natural gas at low concentrations.

The tert-butyl group Oppanol

Fig. 4.7. Comparison between the tert-butyl group and Oppanol.

4.3.3 The Raman Spectrum of Oppanol Obtained with the 2nd Monochromator

In Fig. 4.8 the Raman spectrum of Oppanol is presented, obtained with the 2nd monochromator. By comparing this spectrum with the spectrum shown in Fig. 4.6 two things are worth noticing: i) a difference with respect to peak wavenumber position and ii) a inferior resolution in the spectrum obtained with the 2nd spectrograph. The 2nd monochromator is equipped with a sinus drive controlled grating which probably has an inaccurate spindle[12]. There is, as it is seen about 23 cm^{-1} in difference between the spectrum obtained with 1st spectrograph and 2nd monochromator. Normally the wavenumber calibration error is rather constant, corresponding approximately to the difference of the laser line from zero, as seen in Fig. 4.8. The 2nd monochromator is as expected not so precise. A spectrograph with a cosine bar driven grating with 1800 grooves per mm and a focal length at 800 mm ("the first spectrograph) has a better resolution than a sinus bar spectrograph with a grating of 600 mm and a focal length at 300 mm ("the second monochromator"). But, the better resolution with the 1st spectrograph gives a smaller spectral window per measurement and the spectrum has to be combined piece by piece from several segment measurements. Therefore it takes longer time to obtain the spectrum. Thus the advantage of using the 2nd monochromator is that it has a higher sensitivity and it is quicker to obtain a spectrum. The advantage of using the 1st spectrograph is a better resolution and a higher wavenumber precision. The very infrared range can only be measured with the 2nd monochromator.

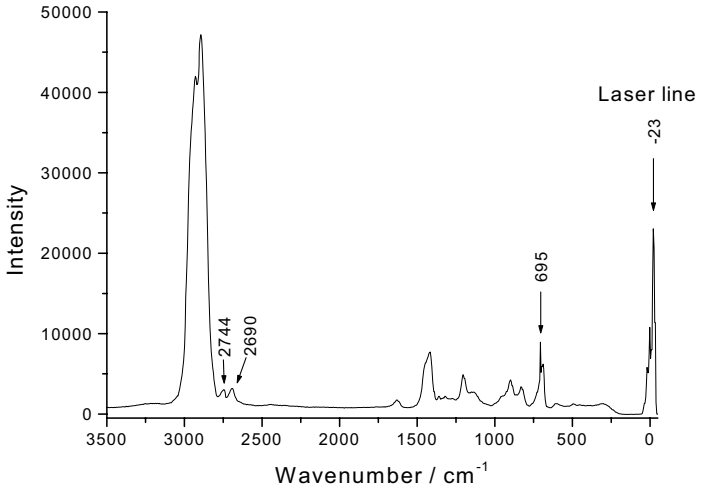

Fig. 4.8. The Raman spectrum of Oppanol obtained by use of the 2nd monochromator with a grating of 600 grooves per mm. Exciting source and sample treatment was the same as described in Fig. 4.6.

4.3.4 The Raman Spectra of Oppanol Obtained with three Different Lasers

In Fig. 4.9 the Raman spectra of Oppanol are shown, obtained with the 2nd monochromator and three different lasers: the Ar-ion laser, 514.53 nm_{air} (spectrum A) and two diode lasers with exciting wavelengths 785 nm_{air} and 833 nm_{air} (spectrum B and C respectively). The same bands appear in them, but there is an unexplained anomaly in the region round 1500 cm^{-1}. It is seen that spectra B and C flatten off in the left (red) end of the spectrum, i.e. at higher wavenumber shifts. This observation is in accordance with studies of quantum efficiency curves of typical silicon based CCD detectors[13]. Such curve shows that a CCD detector is most insensitive at ~3000 cm^{-1} when using 785 nm_{air} and 830 nm_{air} as the exciting source and most sensitive in the same spectral region when using the Ar-ion laser, 514.53 nm_{air}.

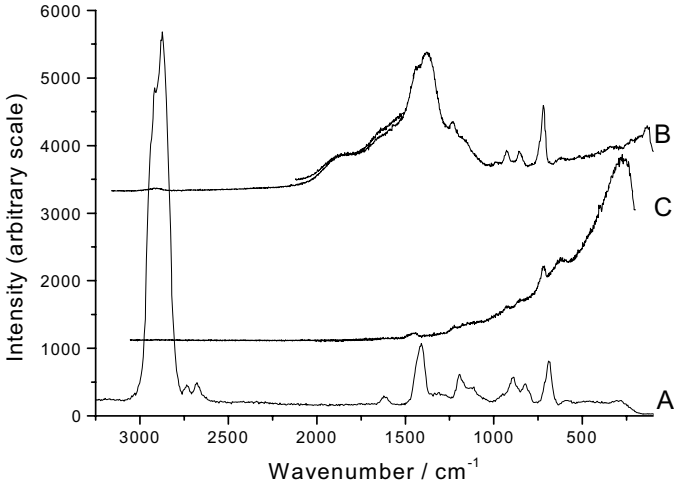

Fig. 4.9. Raman spectra of Oppanol obtained by use of the 2nd monochromator with a grating of 600 grooves per mm. Three different lasers were used, A: Ar-ion laser, $\lambda = 514.53\ nm_{air}$, B: diode laser, $\lambda = 785\ nm_{air}$ and C: diode laser, $\lambda = 833\ nm_{air}$. Sample treatment was the same as described in the legend to Fig. 4.6.

4.3.5 Conclusion (so far)

Raman spectra of Oppanol have been obtained with two different resolutions and three different lasers. To get higher resolution (more details) in the spectra, the 1st spectrograph is the best choice. The diode lasers were not good exciting sources, especially if the spectral range up to higher wavenumbers is considered.

Oppanol has a spectrum with three characteristic bands similar to what was found for MTBE, which we have studied in detail previously. The two overtone bands at ~2768 cm^{-1} and ~2713 cm^{-1} are relatively weak, so it is not expected that they can be detected in spectra of natural gas samples containing droplets of micro Oppanol. The band at ~720 cm^{-1} are however relatively intense and sharp. With this band there should be a possibility to characterise natural gas samples from Ll. Torup with respect to a content of droplets of Oppanol.

4.3.6 The Raman Spectrum of a Natural Gas Sample from Ll. Torup

The sapphire tube cell was transported to Ll. Torup and filled with natural gas from TO7, one of the sump sealed caverns at a pressure of 6.4 MPa_A. The Raman spectrum of this sample was recorded and is shown in Fig. 4.10 (the whole spectrum in a wider range, including the sapphire bands, was shown in Fig. 2.4).

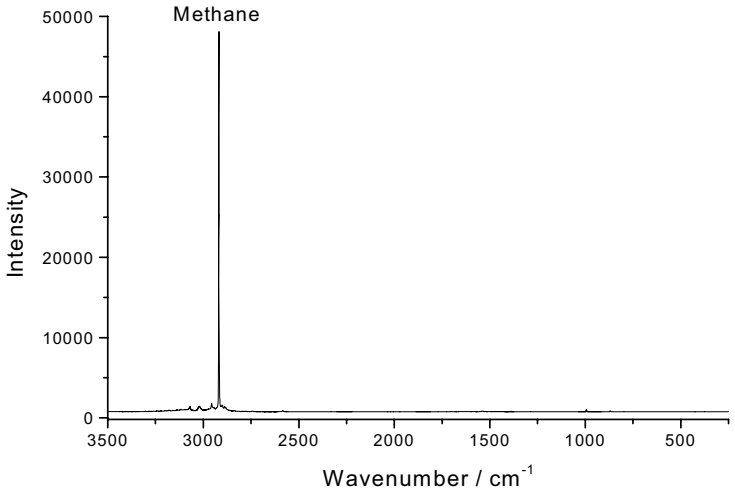

Fig. 4.10. The Raman spectrum of a natural gas sample from Ll. Torup, 6.4 MPa_A, contained in the sapphire tube cell. The spectrum was acquired by use of the 1st spectrograph (1800 grooves per mm). The sample was placed in the macroscopic entrance position and the collection geometry was 90°. The 514.53 nm_{air} line of a Ar-ion laser was used as the exciting source (~200 mW, vertically polarised).

The spectrum was almost identical with the spectrum of the natural gas sample from Nybro presented in Fig. 4.3. There are however small differences, which will be discussed later. Also in this spectrum, the methane ν_1 stretching band at ~2920 cm^{-1} is so intense that it overwhelms other bands in the spectrum. Therefore it has been expanded in Fig. 4.11, curve A. In the figure the spectrum of the pure Oppanol is also included, curve B. As expected the two overtone bands (indicated with arrows in the 3100-2300 cm^{-1} region) cannot be observed in the spectrum of the Ll. Torup natural gas sample. Also the band at ~720 cm^{-1} is not observable (position indicated with an arrow in the 1700-400 cm^{-1} region of the figure). Apparently the amount of Oppanol in the natural gas is too low to be detected with the limited sensitivity available in the Raman spectrometer.

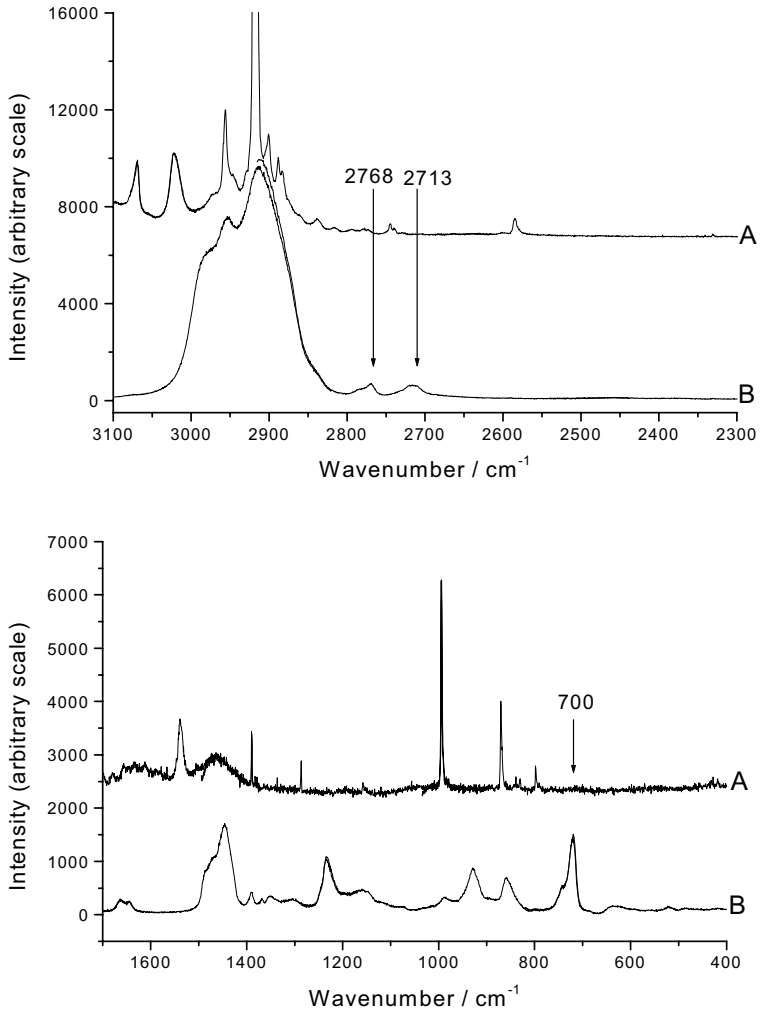

Fig. 4.11. The blown up Raman spectra of the gas sample from Ll. Torup (A) [also shown in Fig. 4.10] and the spectrum of pure Oppanol (B) [also shown in Fig. 4.8]. The positions of the two overtones (from the symmetric umbrella deformation) and the C-C stretching involving the tertiary carbon in the tert-butyl group are indicated with arrows.

4.3.7 The Raman Spectrum of an Oppanol / Methane Mixture Prepared in a "Home-made Cavern"

This study was undertaken in order to investigate the possibility of detecting micro droplets of Oppanol in an Oppanol / methane mixture with a *high* content of Oppanol. A 400 ml metallic cylinder with valves at the bottom and the top was used as a miniature cavern. A plate smeared with 10.42 g Oppanol was placed in it (since the density of Oppanol is 0.889

gcm^{-3} at 20°C [8] this amount correspond to 11.72 cm^3). Then the cylinder was filled with methane at a pressure of > 8.6 MPa_A and left for 24 days to make sure that the Oppanol has evaporated into the gaseous methane. The Raman spectrum of this mixture, obtained in the sapphire tube cell is shown in Fig. 4.12.

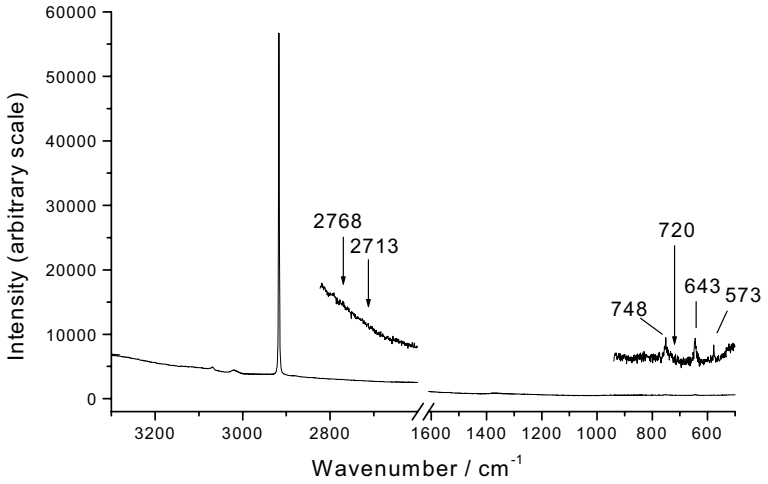

Fig. 4.12. The Raman spectrum of the Oppanol / methane mixture contained in the sapphire tube cell at 8.6 MPa_A. Fractions of the spectrum have been blown up by a factor of 20. For experimental conditions see legend to Fig. 4.10.

None of the three characteristic Oppanol bands (indicated with arrows in the figure) are observed in the spectrum. So, even at a high Oppanol concentration it is not possible to detect the micro droplets. In return, three bands were seen at ~748, ~643 and ~573 cm^{-1}. So far it has not been possible to identify these bands. They can not arise from vibrations in the methane molecule or in the Oppanol. They are neither plasma lines from the Ar-ion laser. Probably they are due to impurities in the cylinder. This explanation is supported by the fact that there was a fluorescence background in the red end of the spectrum.

4.3.8 Conclusion

The characteristic Oppanol bands found in Chap. 4.3.2 have been searched in the Raman spectrum of a natural gas sample from Ll. Torup. It was not possible at all to detect Oppanol. It is therefore concluded that the Raman technique in the present version is not suitable to characterise natural gas samples with respect to Oppanol micro droplets. The characteristic Oppanol bands have also been searched for in the Raman spectrum of an Oppanol / methane mixture with high content of Oppanol. Even in this mixture it was not possible to detect any presence of micro droplets.

4.4. Analysis of Three Different Natural Gas Samples

4.4.1 Introduction

In the previous chapters Raman spectroscopic studies of natural gas with respect to traces of micro droplets (unwanted compounds) have been described. This chapter is concerned with the analysis of natural gas with respect to "natural" (reservoir) gas components. Three different natural gas samples have been studied aiming at a qualitative analysis. This work is presented in Chap. 4.4.2. Attempts to make a quantitative analysis have also been done in the project. This work is presented in Chap. 4.4.3. Most of the results in the present work have been presented in ref. 14.

4.4.2 Qualitative Analysis of Three Different Natural Gas Samples

Three different natural gas samples at high pressures were delivered by DONG A/S. The samples were taken i) from Nybro gas inlet, raw (10.2 MPa_A), ii) from the same plant downstream of pressure regulation and filtration (8.0 MPa_A), and iii) from the Ll. Torup, stock (6.4 MPa_A). Each sample was successively contained in the sapphire tube cell. The Raman spectra of the former and latter were presented in full scale in Chap. 4.3.3 (Fig. 4.3) and Chap. 4.3.5 (Fig.4.10), respectively. As seen in these two spectra, the band at ~2920 cm^{-1} arising from C-H stretching in methane, was by far the most intense one in the spectra. To make bands from other components discernible in the natural gas spectra we have therefore expanded and divided them in four sections, to obtain a better separation between the bands. The spectra are shown in Fig. 4.13 (Fig. 4.13.a: 3150-2850 and 2850-2450 cm^{-1}, Fig. 4.13.b: 2450-1300 and 1300-300 cm^{-1}). In addition to the Raman spectra A, which are the spectra of the natural gas sample from Ll. Torup, polarized Raman spectra of the sample were also obtained. These spectra are included in Fig. 4.13 below spectra A, indicated as pol VV and pol VH (vertical and horizontal polarization, respectively). The polarized spectra were obtained to help interpreting the bands. Curves B are the spectra of the filtered natural gas sample from Nybro and curves C are the spectra of the raw natural gas sample from Nybro. In Fig. 4.13 the spectra of the latter sample at a lower pressure, 1.1 MPa_A, are also included, because it was found of interest to investigate, if there were observable

differences between natural gas samples at high and low pressure. The low pressure was achieved by letting gas out of the valve 2b, as described in Chap. 2.2.1.

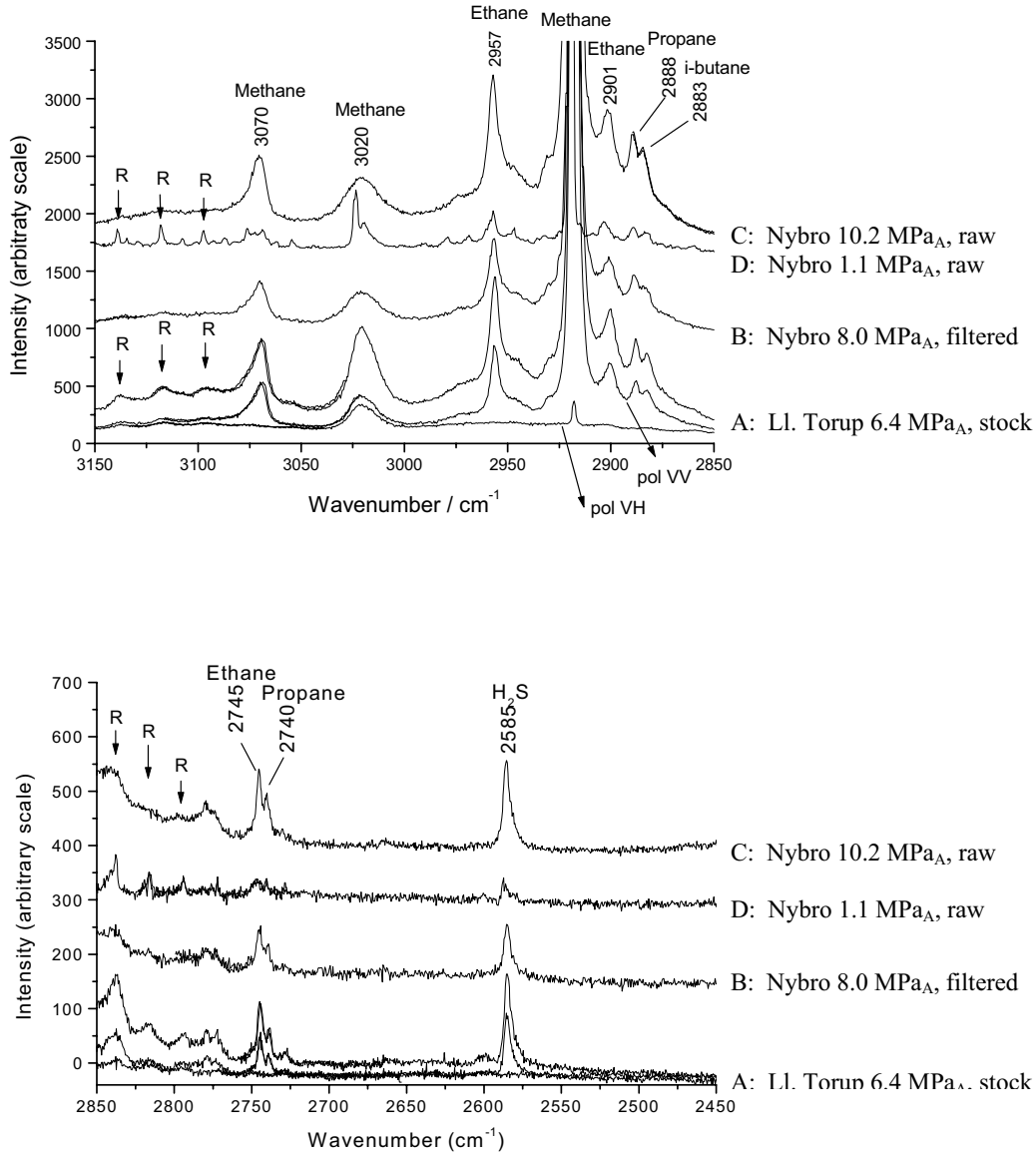

Fig. 4.13.a. The Raman spectra of three natural gas samples (contained in the sapphire tube cell) from A: Ll. Torup (6.4 MPa_A), upper curve: no polarizer, lower curves: VV and VH polarization; B: Nybro, downstream of pressure regulation and filtration (8.0 MPa_A); C: Nybro, raw (10.2 MPa_A) and D: same as C, but at a lower pressure (1.1 MPa_A). All spectra were obtained by use of the 1st spectrograph and with the 514.53 nm_{air} line of the Ar-ion laser as the exciting source (~200 mW). The collection geometry was 90°.

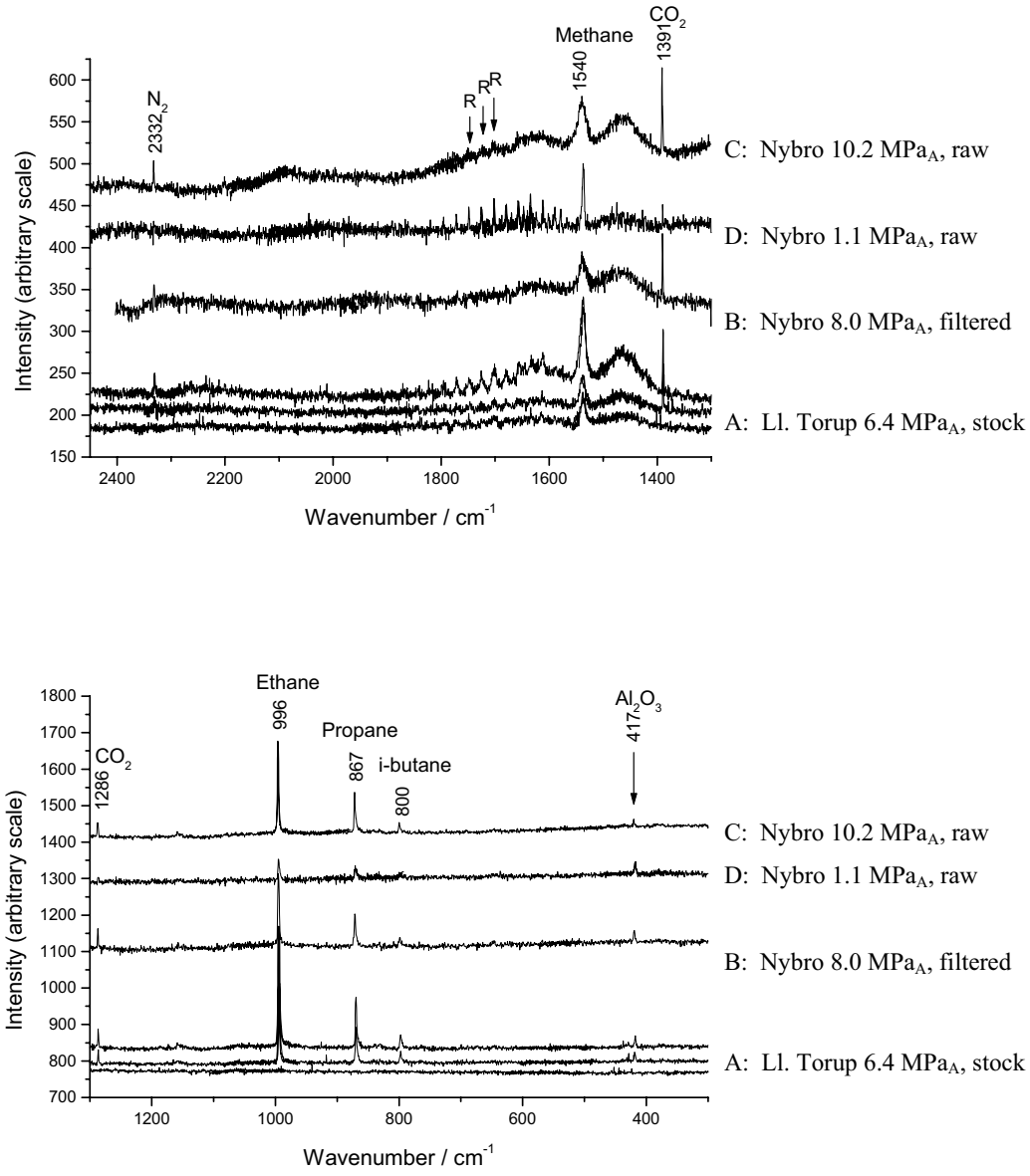

Fig. 4.13.b. The Raman spectra of three natural gas samples.
Experimental details as described in legend to Fig. 4.13.a.

By comparing spectra D and C it can be seen that the intensity of the peaks increase with increasing pressure (due to higher gas concentration). In fact there is also a shift of band position towards lower wavenumbers with increasing pressure. Such wavenumber shifts will be discussed in detail in Chap. 5.

By comparing all of the spectra in Fig. 4.13 it can be concluded that the same components are to be seen in all of them. After some consideration it was possible to identify all bands. Some of these considerations will be discussed in the following. In Table 4.1 is shown the composition in a typical Danish natural gas sample, measured by gas chromatography. These components were searched for in the natural gas Raman spectra, first the organic compounds and thereafter the inorganic components.

Table 4.1. Composition of a typical Danish natural gas sample measured by gas chromatography at the Nybro Gas Treatment Plant.

Component	Concentration
methane	87.77 mol%
ethane	6.45 mol%
propane	2.92 mol%
n-butane	0.58 mol%
i-butane	0.44 mol%
n-pentane	0.084 mol%
i-pentane	0.12 mol%
hexane and higher	0.068 mol%
CO_2	1.12 mol%
N_2	0.34 mol%
H_2S	1-3 mg/Nm^3

The organic compounds: The band at ~2918 cm^{-1} is, as already mentioned, the methane ν_1 (C-H symmetric stretching) band. The methane ν_3 (C-H asymmetric stretching) band is observed at ~2920 cm^{-1} and the methane ν_2 (asymmetric bending) at ~1540 cm^{-1}. Both of these two bands are depolarized (I_{VH} / Ivv = 0.75), as they should be when the vibrations involved are not total symmetric. In addition to the pure vibrational transitions it is also possible to observe rotational-vibrational transitions (P and R branches) for these two

depolarized bands. Some of the rotational-vibrational transitions are indicated with arrows in Fig. 4.13. In addition to methane molecule other alkanes like ethane, propane and i-butane were detected in the natural gas (cf. Table 4.2 p. 4-27 in which all of the bands in the spectra are listed and assigned).

The band at ~3070 cm^{-1} has previously been observed in Raman spectra from CH_4 rich inclusions, and here it was assigned as due to higher hydrocarbons[15] and to C-H stretching in olefinic hydrocarbons[16]. In the high pressure studies of *pure* methane samples (which will be treated in Chap. 5 and Chap. 6) the band was however still observed. The correct assignment therefore must be that it belongs to methane itself. The most reasonable explanation is then that it is the overtone of the methane ν_2 band at ~1534 cm^{-1}. The ν_2 has E symmetry and tables for group theory reveals that the direct product E x E for the T_d (tetrahedron) point group involves the totally symmetry species A_1 corresponding to ν_1. This is in accordance with the fact that the band at ~3070 cm^{-1} is polarized. Aromatic molecules also have polarized bands in this spectral region arising from the symmetric C-H stretching in the benzene ring. In Fig. 4.14 spectra are presented for natural gas samples obtained at 6.4 MPa_A (thin curve A) in the 3120-2980 cm^{-1} region, together with the spectrum obtained of a pure methane sample (thick curve B), successively contained in the sapphire tube cell.

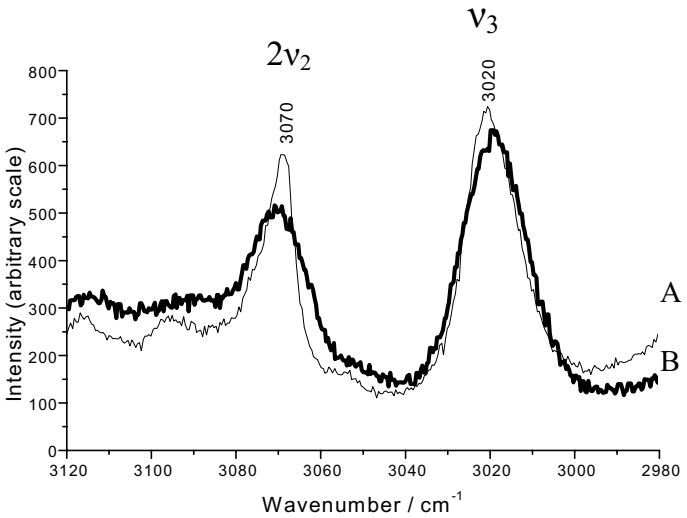

Fig. 4.14. A comparison between the methane bands at ~3070 cm^{-1} ($2\nu_2$) and ~3020 cm^{-1} (ν_3). A: The Ll. Torup natural gas sample (6.4 MPa_A) (the spectrum also shown in Fig. 4.13.a). B: Methane sample (6.2 MPa_A) of purity N45 (99.995 %), Hede Nielsen A/S. Experimental details for both samples are given in Fig. 4.13.a.

By comparing the spectra of the natural gas sample to the methane sample (with almost the same pressure) it seems like the area ratio between the band at ~3070 cm^{-1} and the band at ~3020 cm^{-1} is the same for the two samples. In fact the area ratios determined by use of the Microcal Origin peak fitting software module[17] (Gaussian function as the fitting function) were found to be almost the same. It is therefore concluded that the band at ~3020 cm^{-1} is not due to aromatics present in the natural gas. This is in agreement with the information that aromatics (benzene, toluene and xylene isomers) are only present in the Danish natural gas at very low concentrations (according to DONG A/S on a level of 20-50 ppm_v).

The inorganic compounds: According to the literature the wavenumbers of the normal modes of vibration in CO_2 are ~1340 cm^{-1} (ν_1, symmetric stretching), 667 cm^{-1} (ν_2, bending) and 2350 cm^{-1} (ν_3, asymmetric stretching)[18]. ν_1 is Raman active whereas ν_2 and ν_3 are IR active. The overtone $2\nu_2$ (~1334 cm^{-1}) is however Raman active and has same symmetry and almost the same wavenumber as the ν_1, resulting in Fermi resonance[19]. Due to this Fermi resonance wavenumbers have been shifted, intensities altered and both bands are mixed into each other. The Fermi CO_2 diad is clearly seen in Fig. 4.13.b at ~1391 (ν_1) cm^{-1} and ~1286 cm^{-1} ($2\nu_2$). According to the literature the intensity ratio of ν_1 and $2\nu_2$ is a function of density in a pure CO_2 fluid[20]. The same tendency is faintly seen in the Raman spectrum of the natural gas samples in Fig. 4.13.b (ν_1 increases relatively to $2\nu_2$ with increasing pressure). In ref. 16, CO_2 is also detected in the Raman spectrum of a CH_4 inclusion, but it seems that only the ν_1 band is observed.

N_2 was also detected at ~2332 cm^{-1} in the Raman spectra of the natural gas samples. Most surprisingly it was that it is possible to detect H_2S at ~2585 cm^{-1}, even though it should only be present in Danish natural gas in quite low concentrations. The H_2S content should typically be 1-3 mg / Nm^3, because of the desulphurisation done off shore, as mentioned in Chap. 4.2.1. According to the literature, the ν_1 (symmetric S-H stretching) for gaseous H_2S occurs at 2611 cm^{-1} [21-24], and ν_3 (asymmetric S-H stretching) band occurs at 2627 cm^{-1} [22,23]. With a phase change from gaseous to liquid state, the bands of H_2S shift towards lower wavenumbers, ~2574 cm^{-1} [25,26]. In Fig. 4.13.a the H_2S band was found at ~2585 cm^{-1}. From this it seems that the H_2S molecules are in a state near the liquid state in natural gas at high pressure. H_2S has three fundamental vibrations and all of them are Raman permitted according to standard selection rules. According to the literature the ν_2 (S-H bending) band

should be at 1183 cm^{-1} [22,23,27] and this vibration has in fact been observed in a Raman spectrum at ~0.13 MPa[22,23] [the same H_2S Raman spectrum are presented in both ref.]. In the same Raman spectrum the ν_3 band was seen at ~2627 cm^{-1} as a weak signal among rotational-vibrational bands. It was found of interest to reproduce the H_2S Raman spectrum and investigate if it was possible to observe the ν_3 band in a more conclusive way.

A H_2S gas sample was made from 5 mg CaS (one piece) and sulphuric acid. The gas was collected in a bent squared ampoule replacing water. The Raman spectrum of the gas sample is shown in Fig. 4.15. Besides the H_2S ν_1 band at ~2617 cm^{-1} it is also possible to see the N_2 and O_2 ν_1 bands at ~2333 cm^{-1} and ~1559 cm^{-1}, respectively. One might wonder why we see N_2 and O_2, but probably they are due to N_2 and O_2 from the air adsorbed to the CaS piece.

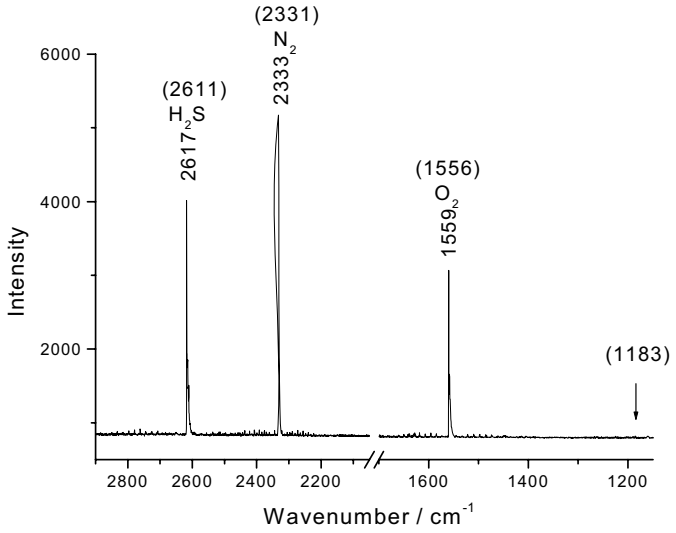

Fig. 4.15. The Raman spectrum of a homemade H_2S sample, contained in a bent (squared) ampoule. In the spectrum N_2 and O_2 signals were to be seen. The spectrum was acquired by use of the 1st spectrograph and with the 514.53 nm_{air} line of the Ar-ion laser as the excitation source (~200 mW). The sample was placed in the macroscopic position and the collection geometry was 90°.

In Fig. 4.16 the same spectrum of H_2S and N_2 is shown in an expanded condition to get the possibility to search for the H_2S ν_3 band at ~2627 cm^{-1}. As it is seen the band is not observable (the wavenumber position is indicated with an arrow). Band shapes of the ν_1 bands for both H_2S and N_2 are almost identical with the band shapes shown in the literature[22, 23], so the absence of ν_3 seems to be a property of the H_2S molecule.

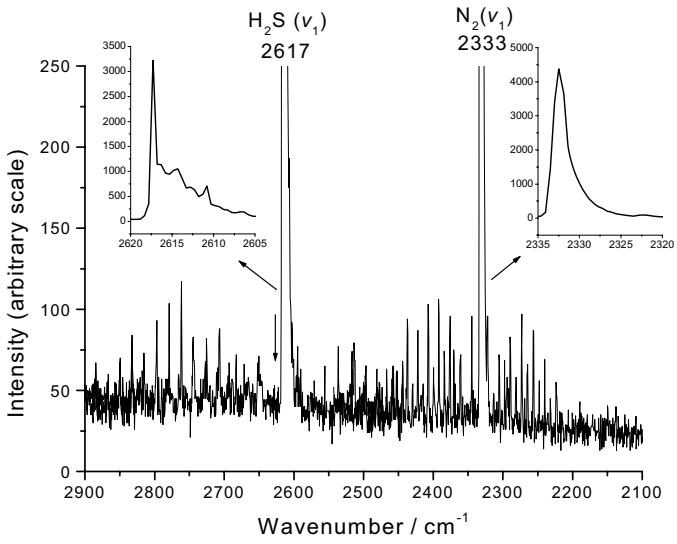

Fig. 4.16. Section of the Raman spectra of H_2S and N_2 shown in Fig. 4.15. Also shown are inserts with band shapes for the H_2S ν_1 band and the N_2 ν_1 band.

In the Raman spectra of natural gas, Fig. 4.13 there remains up to this point only one peak to be interpreted, i.e. the band at ~417 cm^{-1}. According to DONG A/S also carbonoxysulphide, COS, molecules are present in their natural gas. Since both CO_2 and H_2S are present the COS may originate from the chemical equilibrium[28],

$$CO_2 + H_2S \Leftrightarrow COS + H_2O$$

The COS molecule has three Raman active fundamentals ~524 cm^{-1}, ~859 cm^{-1} and ~2055 cm^{-1} [29,30]. None of these bands is seen in the expanded Raman spectra of the natural gas samples (Fig. 4.13b). Thus it is concluded that COS cannot be detected in the natural gas,

probably because of low concentration. COS has been identified in a fluid inclusion, by means of the 859 cm^{-1} Raman line (and also by IR spectroscopy by the 2051 cm^{-1} line)[28].

With respect to the band at ~417 cm^{-1}, it was observed that the band also occurred in the Raman spectrum of a high pressure nitrogen sample contained in the sapphire tube cell and later from the empty sapphire cell. Therefore it was concluded that the band did not arise due to vibrations of molecules in the natural gas. The band at ~417 cm^{-1} was instead assigned as a lattice vibration in sapphire. This is in accordance with the literature[31] and the observation that the peak did not increase in intensity with increasing pressure.

In Table 4.2 all the vibrational bands observed in the Raman spectra of the natural gas samples, shown in Fig. 4.13, are listed and assigned.

Table 4.2. Wavenumbers (cm^{-1}) and assignments of bands seen in the Raman spectra of natural gas, Fig. 4.13. Wavenumbers in parentheses are from the literature.

Wavenumber / cm^{-1}	Assignment / component	Tentative assignment / vibration based on e.g. refs. 26, 32
3070	methane ($2 \cdot 1534 = 3068$)[33]	overtone ($2\nu_2$) / pol.
3020	methane (3020)[33]	antisym. C-H str. / depol.
2957	ethane (2954)[33]	overtone ($2\nu_{11}$) / pol. ← Fermi resonance
2918	methane (2917)[33]	sym. C-H str. / pol.
2901	ethane (2896)[33]	sym. C-H str. / pol. ← Fermi resonance
2887	propane (2887)[33]	sym. C-H_3 str. / pol.
2883	i-butane (2880)[33]	sym. C-H_3 str. / pol.
2745	ethane (2742)[33]	overtone ($2\nu_2$) / pol.
2740	propane (2739)[33]	overtone ($2\nu_2$) / pol.
2585	H_2S (g:2611, l:2574)[21-26]	sym. S-H str. / pol.
2332	N_2 (2331)[34] *	N-N str. / pol.
1540	methane (1534)[33]	antisym. bend. / depol.
1391	CO_2 (1388)[19]	sym. C-O str. / pol. ← Fermi resonance
1286	CO_2 (1285)[19]	overtone ($2\nu_2$) / pol. ← Fermi resonance
996	ethane (988)[33]	C-C str. / pol.
867	propane (867)[33]	sym. C-C str. / pol.
800	i-butane (794)[33]	sym. C-C str. / pol.
417	Al_2O_3 (418)[31]	Al-O (lattice)

* from ref. 34. Harmonic frequency: $\omega_e = 2359.6$ cm^{-1}. Anharmonicity constant: $\chi_e\omega_e = 14.46$ cm^{-1}

4.4.3. Quantitative Analysis of Natural Gas

The parameter underlying quantitative Raman spectroscopy is the scattering cross section. The present quantitative analysis is based on such cross sections applied in a so-called "ratio method". The method is described in e.g. ref. 35 for the case of two component inclusions. In natural gas however there are many components so the method must be used on the assumption that the concentration of one component, here methane, is known. The irradiance, the scattering volume, the angle of collection of light and other experimental details are the same for all present species. By Formula (4.1), which is a modified Placzek relation[36], it is seen that it is possible to determine the mole fraction of any component in the natural gas if i) the component shows a band in the Raman spectrum and ii) the RNDRS (relative normalised differential Raman scattering)[37] cross section for the component is known.

$$\frac{C_x}{C_{methane}} = \frac{A_{x(\upsilon_x)} \cdot \Sigma_{methane(\upsilon_1)}}{A_{methane(\upsilon_1)} \cdot \Sigma_{x(\upsilon_x)}} \qquad (4.1)$$

C_x: Mole fraction of component x in the natural gas.

$\Sigma_{x(\nu x)}$: RNDRS, relative to N_2, cross section for component x vibrating at wavenumber ν_x. (referred to as $\sigma_{r,A(\nu 4)}$ in ref. 35).

$\Sigma_{methane(\nu 1)}$: $\nu_1 = 2917$ cm^{-1} was used having literature values 9.1, 8.7 and 9.3 [37]; in the present the average (i.e. 9.03) was used in the calculations.

$A_{x(\nu x)}$: Area of the band at wavenumber ν_x for component x.

The RNDRS cross sections, determined relative to N_2, are listed in ref. 37. Since the cross sections have been normalised they should be independent of the wavelength of the exciting source. There are however relatively large variations between the observed values given in different references. The values listed for the 515 Ar-ion nm_{air} exciting wavelength were consistently used here, and in the cases where there are more than one value given the average value was used.

Areas of the bands were determined by use of the Microcal Origin peak fitting software[17]. As previously a Gaussian function was fitted to each band and the area between the curve and an estimated base line determined. The determined area ratios $A_x/A_{methane}$ are listed in Table 4.3. The band areas were reproducible with a relative uncertainty ~5-10% (for the $A_{methane}$ areas the likely accuracy was better than 5%). The main source of uncertainty was without doubt the estimation of the position of the base line. In Table 4.3 are also listed the concentrations (C_x) for propane, CO_2 and N_2 calculated by Formula (4.1). By comparing these values with the concentrations found by gas chromatography (measured by DONG A/S, also included in the Table) it is seen that there is a very good agreement with respect to magnitude. Keeping in mind the uncertainty in the area ratios and the problems of precision with respect to the RNDRS cross sections, one should not expect more precise results. Furthermore, all the RNDRS cross sections used in the calculations are for gases at low pressure. It is known that the RNDRS values depend somewhat on pressure[38]. For gases up to 10% larger cross sections have been found of high pressures.

Determination of the H_2S concentration was also tried by the "ratio method", but the results were very questionable. The calculations gave the values 9600 mg / Nm^3 for the Nybro filtered sample (8.0 MPa_A) and 13100 mg / Nm^3 for Nybro raw sample (10.2 MPa_A). According to DONG A/S, as mentioned before, the concentration typically is 1-3 mg / Nm^3. An explanation could be that because of the two lone-pairs of electrons on sulphur, the H_2S molecule scattering cross section could be much more pressure dependent than the other molecules in the natural gas and thereby giving a relatively much more intense band in the Raman spectrum at high pressures. Another (speculative) explanation might be the absorption of H_2S to the walls during filling of the cell, followed by later evaporation. It seems that an investigation of this effect in the Raman spectra of H_2S and H_2S mixtures as a function of pressure needs to be done.

The RNDRS cross-sections for i-butane are not given in ref. 37 (and as far as the author knows they have not been reported elsewhere). For ethane (993 cm^{-1}) it has not been given for the 514.5 nm_{air} exciting wavelength. Since the concentrations of these two components in the natural gas samples are known it is possible to calculate, and in this way determine the cross sections by formula (4.2).

Table 4.3. Determination of i) mole fraction of gas components in natural gas (first part of the table) and ii) RNDRS cross sections for ethane and i-butane (second part of the table).

Component *x* Analysed		Band ν_x / cm^{-1}	$\Sigma_{x(\nu_x)}$	$A_x/A_{methane(\nu_1)}$	C_x/mol% calcd[c].	C_x/mol% measd., GC[d]
Propane	A[a]	867	1.7[b]	0.003054	-	-
	B[a]	867	1.7[b]	0.003674	1.71	2.84
	C[a]	867	1.7[b]	0.003647	1.71	2.99
CO_2	A[a]	1285	0.78[b]	0.005734	-	-
	B[a]	1285	0.78[b]	0.001097	1.12	1.36
	C[a]	1285	0.78[b]	0.001283	1.31	0.92
CO_2	A[a]	1388	1.21[b]	0.000978	-	-
	B[a]	1388	1.21[b]	0.001496	0.98	1.36
	C[a]	1388	1.21[b]	0.001021	0.67	0.92
N_2	A[a]	2331	1[b]	0.000407	-	-
	B[a]	2331	1[b]	0.000566	0.45	0.33
	C[a]	2331	1[b]	0.000456	0.36	0.34
Ethane	A[a]	993	-	0.005938		-
	B[a]	993	0.85[c,e]	0.006783		6.34
	C[a]	993	0.88[c,f]	0.006870		6.23
i-butane	A[a]	794	-	0.001002		-
	B[a]	794	2.02[c,e]	0.001122		0.44
	C[a]	794	1.60[c,f]	0.001005		0.50

[a] Gas samples from A: Ll. Torup, stock, B: Nybro, filtered and C: Nybro, raw.

[b] Values from literature[37]. [c] Values calculated in this work. [d] Gas chromatographic analysis done by DONG A/S (gas chromatography (GC) data for the Ll. Torup sample were not available). $C_{methane}$ for the Nybro filtered and Nybro raw natural gas samples were 87.85% and 88.16% respectively. [e] 8.0 MPa_A. [f] 10.2 MPa_A.

$$(4.2) \quad \Sigma_{x(\upsilon_x)} = \frac{C_{methane}}{C_x} \cdot \frac{A_{x(\upsilon_x)} \cdot \Sigma_{methane(\upsilon_1)}}{A_{methane(\upsilon_1)}}$$

The 993 cm^{-1} band of ethane and the 794 cm^{-1} band of i-butane were used. Area ratios are listed in Table 4.3 (second part of the table) and so are the gas concentrations measured by gas chromatography. The RNDRS cross section for i-butane (794 cm^{-1}) (relative to N_2) at 8.0 MPa_A was found to be 2.02. At 10.2 MPa_A it was found to be 1.60. The RNDRS cross section for ethane (993 cm^{-1}) at 8.0 MPa_A (relative to N_2) was found to be 0.85, and at 10.2 MPa_A it was 0.88. The values given in ref. 37 were 1.24 (488 nm exciting wavelength) and 2.2 (364 nm exciting wavelength).

4.4.4 Conclusion

The Raman spectra of samples of natural gas from Nybro and Ll. Torup have been presented and interpreted. It was possible to assign all of the bands in the spectra. The heaviest alkane to be detected was i-butane. The band at ~3070 cm^{-1} was reassigned as the overtone of the ν_2 vibration in methane in contrast to previously. It was possible to detect N_2, CO_2 and (surprisingly) also H_2S.

Attempts to make a quantitative analysis of the natural gas by the so-called “ratio method” have also been described. There was agreement (with respect to magnitude) between this analysis and analysis done by gas chromatography, except for H_2S. Further Raman studies of H_2S and H_2S mixtures need to be done, both with respect to band positions and relative ν_1 band area as a function of pressure. Finally the RNDRS cross sections have been determined for ethane at 8.0 MPa_A and 10.2 MPa_A (0.85 and 0.88 respectively) and for i-butane at the same pressures (2.02 and 1.6).

4.5 Analysis of a "Ready for Use" Natural Gas Sample

It was found of interest to obtain the Raman spectrum of a natural gas sample after distribution to the market. Thus a tube was connected to a natural gas tap at the Technical University of Denmark. A separating funnel was flushed with the gas and after some time closed and placed in the macroscopic sampling position for Raman measurements. The Raman spectrum of the natural gas sample is shown in Fig. 4.17. A fluorescence background was observed, probably due to the glass material. Only three distinct peaks were observable. The band at ~2919 cm^{-1} as previously mentioned can be assigned to the methane ν_1 (C-H symmetric stretching). The bands observed at ~3472 cm^{-1} and ~3220 cm^{-1} have given rise to some considerations.

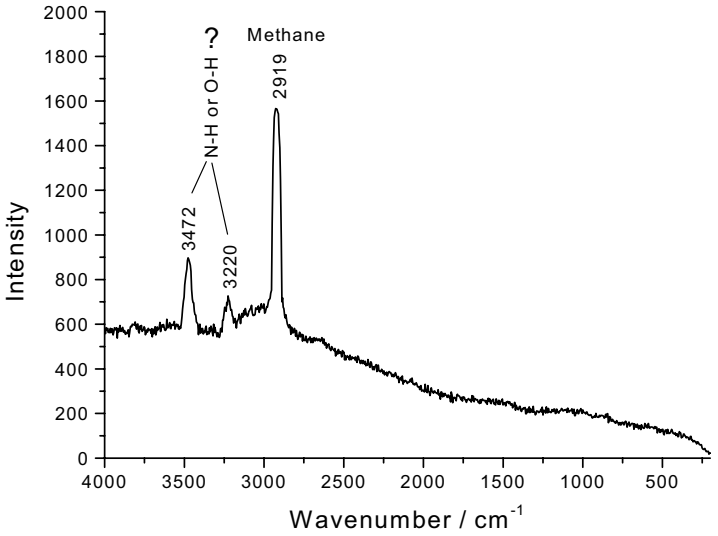

Fig. 4.17. Raman spectrum of a natural gas sample sampled at the Technical University of Denmark. The sample was a thin gas (~0.1 MPa_A). The spectrum was acquired by use of the 2nd monochromator and the 514.53 nm_{air} line of the Ar-ion laser was used as the excitation source (~200 mW). The collection geometry was 90 °.

The bands are relatively intense and they were reproducible. They have not been observed in any of the Raman spectra of the natural samples obtained so far (cf. for instance the spectrum shown in Chap. 2, Fig. 2.4). Thus, it is concluded that the bands do not arise due to the "natural" components in natural gas.

Pure natural gas is odourless. Therefore before distribution a tracer is added so that the gas can be smelled in the case of leaks. When the natural gas was sampled the applied tracer was the sulphur compound THT (tetrahydrothiopen). Structural formula is shown in Fig. 4.18. The amount of THT added in the natural gas corresponded to a sulphur content of 4-7 mg / Nm^3 [39].

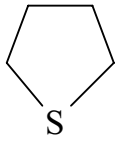

Fig. 4.18. THT (tetrahydrothiophen)

It was considered if the band at ~3472 cm^{-1} and ~3220 cm^{-1} could arise from vibrations in this molecule. Thus the Raman spectrum of THT was found in the literature[40]. In this spectrum, however, no such bands were to be observed.

Since the band ~3472 cm^{-1} and ~3220 cm^{-1} do not arise from the THT molecule, it is concluded that the bands in all probability arise from vibrations in molecules containing N-H or O-H groups.

4.6. References

1. D. Lin-Vien, N. B. Cholthup, W. G. Fately and J. G. Grasselli, *The Handbook of Infrared and Raman frequencies of Organic Molecules* (Academic Press, Boston, 1991), Chap. 2.
2. Ref. 1, Chap. 6.
3. *Raman / IR Atlas of Organic Compounds*, B. Schrader and W. Meier (Verlag Chemie, Weinheim, 1977), A 4-13.
4. Ref. 1, Chap. 5.
5. K. Fukushima and K. Sakurada, "Conformational Adaptation of triethylene glycol dimethyl ether in cation capture as studied by Raman spectroscopy", J. Mol. Struc. **248**, 227 (1991).
6. www.dong.dk/uk/publications, "The Natural Gas Storage Facilities in Ll. Torup and Stenlille".
7. B. Werner Christensen, Internal Rapport, Department of Organic Chemistry, Technical University of Denmark (1995).
8. Deutsche Patent Schrift 25 49 313, Wolfram Kleinitz (inventor).
9. D. Lien-Vien, N. B. Cholthup, W. G. Fately and J. G. Grasselli, *The Handbook of Infrared and Raman Frequencies of Organic Molecules* (Academic Press, Boston, 1991).
10. J. B. Cooper, K. L. Wise, W. T. Welch, R. R. Bledsoe and M. B. Summer, "Determination of weight percent oxygen in commercial gasoline: A comparison between FT-Raman, FT-IR and dispersive near-IR spectroscopies", Appl. Spectrosc. **50**, 917 (1996).
11. J. A. Dean, *Handbook of Organic Chemistry* (McGraw-Hill, New York, 1987).
12. T. Nørbygaard and R. W. Berg, "Calibration procedure for a DILOR Raman spectrometer with sinus drive controlled grating and CCD detector", in preparation.
13. R. L. McCreery, "Instrumentation for dispersive Raman spectroscopy" in *Modern Techniques in Raman Spectroscopy*, J. J. Laserna, ed. (John Wiley & Sons Ltd., New York, 1996). Chap. 2, p. 41.
14. S. Brunsgaard Hansen, R. W. Berg and E. H. Stenby, "High pressure measuring cell for Raman spectroscopic studies of natural gas", Appl. Spectrosc. **55(1)**, xx (2001).

15. H. J. Kish and A. M. van den Kerkhof, "CH_4-rich inclusions from quartz veins in the Valley-and-Ridge province and the anthracite fields of the Pennsylvania Appalachians", Amer. Mineral. **76**, 230 (1991).
16. B. Wopenka, J. D. Pasteris and J. J. Freeman, "Analysis of individual fluid inclusions by Fourier transform infrared and Raman microspectroscopy", Geochim. Cosmochim. Acta. **54**, 519 (1990).
17. Microcal Origin version 6 and The Peak Fitting Module version 6 (Microcal Software Inc., 1999).
18. K. Nakamoto, *Infrared and Raman Spectra of Inorganic and Coordination Compounds* (John Wiley and Sons. Inc., New York, 1997), 5 th. ed., p. 31.
19. E. Fermi, Z. Physik, "Über den Ramaneffekt des Kohlendioxydes", **71**, 250 (1931).
20. Y. Garrabos, R. Tufeu, B. Le Neindre, G. Zalczer and D. Beysens, "Rayleigh and Raman scattering near the critical point of carbon dioxide", J. Chem. Phys. **72**, 4637 (1980).
21. W. R. Fenner, H. A. Hyatt, J. M. Kellam and S. P. S. Porto, "Raman cross section of some simple gases", J. Opt. Soc. Am. **63**, 73 (1973).
22. J. G. Hochenbleicher, W. Klöckner and H. W. Schrötter, *Laser-Tag. Beitr. Vortragsveranst.* (Essen, FRG, 1974), p. 191.
23. H. W. Schrötter and H. W. Klöckner, "Raman scattering cross sections in gases and liquids" in *Topics in Current Physics, Raman Spectroscopy of Gases and Liquids,* A. Weber, Ed. (Springer-Verlag, New York, 1979), Chap. 4, p. 123.
24. H. C. Allen, Jr., L. R. Blaine and E. K. Plyer, "Infrared spectrum of hydrogen sulfide from 2200 to 2800 cm^{-1}", J. Chem. Phys. **24**, 35 (1956).
25. G. M. Murphy and J. E. Vance, "Raman spectra of hydrogen and deuterium sulfides in the gas, liquid and solid states", J. Chem. Phys. **6**, 426 (1938).
26. G. Hertzberg, *Molecular Spectra and Molecular Structure* (D. Van Nostrand, New York, 1964).
27. H. C. Allen, Jr. and E. K. Plyler, "Infrared spectrum of hydrogen sulfide", J. Chem. Phys. **25**, 1132 (1956).
28. S. Grishina, J. Dubessy, A. Kontorovich and J. Pironon, "Inclusions in salt beds resulting from thermal metamorphism by dolerite sills (eastern Siberia, Russia), Eur. J. Mineral. **4**, 1187 (1992).

29. W. G. Penney and G. B. B. M. Sutherland, "On the relation between the form, force constants, and vibration frequencies of triatomic systems", Proc. Roy. Soc. London, **156**, 654 (1936).
30. J. Wagner, "Studium zum Raman-Effekt. Mitteilung 126: Kohlenoxysulfid und Cyanchlorid" in *Zeitschrift für Physicalische Chemie*, (Akademische Verlagsgesellschaft, Becker & Erler kom.-Ges., Leipzig, 1941), p. 309.
31. C. Coupry and D. Brissaud, "Application in art jewelry and forensic science" in *Raman Microscopy Developments and Applications*, G. Turell and J. Corset, Eds. (Academic Press Inc., San Diego, 1996), Chap. 10, p. 420.
32. D. Lien-Vien, N. B. Cholthup, W. G. Fately and J. G. Grasselli, *The Handbook of Infrared and Raman Frequencies of Organic Molecules* (Academic Press, Boston, 1991).
33. *Raman / IR Atlas of Organic Compounds,* B. Schrader and W. Meier (Verlag Chemie, Weinheim, 1974 and 1977), group A.
34. K. Nakamoto, *Infrared and Raman Spectra of Inorganic and Coordination Compounds* (John Wiley and Sons, Inc., New York, 1997), 5th ed., Part A, p. 156.
35. B. Wopenka and J. D. Pasteris, "Limitations to quantitative analysis of fluid inclusions in geological samples by laser Raman microprobe spectroscopy", Appl. Spectrosc. **40**, 144 (1986).
36. G. Placzek, "Rayleigh-Streuung und Raman-Effekt" in *Handbuch der Radiologie*, E. Marx, ed. (Akademische-Verlag, Leipzig, 1934), vol. VI.2, p.205.
37. Ref. 23, p. 137.
38. D. Fabre and B. Oksengorn, "Pressure and density dependence of the CH_4 and N_2 Raman lines in an equimolar CH_4/N_2 Gas Mixture", Appl. Spectrosc. **46**, 468 (1992).
39. www.dong.dk/dk/naturgas/gaskvalitet.
40. *Raman / IR Atlas of Organic Compounds,* B. Schrader and W. Meier (Verlag Chemie, Weinheim, 1977), J6-08.

5. ν_1 Wavenumber Shifts as a Function of Pressure in Methane and Methane Mixtures

5.1. Introduction

In the study of the Raman spectra of natural gas obtained at different pressures, described in the previous chapter, interesting observations arose. The appearance of the natural gas Raman spectra showed to be dependent on the pressure in various ways. This chapter mainly concerns wavenumber shifts as a function of pressure. Some general remarks with respect to the Raman spectrum of pure methane is given in Chap. 5.2. Chap. 5.3 concerns calibration of the pressure gauges (Chap. 5.3.1), and how to calibrate Raman spectra with respect to wavenumber position (5.3.2). The ν_1 (C-H symmetric stretching) band shift as a function of pressure in pure methane is treated in Chap. 5.4. These shifts are compared with values given in the literature. Wavenumber shifts for methane / ethane mixtures have not previously been studied in the literature. These wavenumber shifts are given and discussed in Chap. 5.5. The main goal of the present work was to investigate if it could be possible to determine the total pressure or component partial pressures in a mixture containing methane and ethane by means of the wavenumber shifts. Most of the results in the present work have also been presented in ref. 1.

From this point and through out the thesis the C-H symmetric stretching, the C-H bending and the C-H asymmetric stretching in methane will just be referred as to ν_1, ν_2 and ν_3 respectively.

5.2. Raman Spectra of a Pure Methane Sample

The Raman spectrum of a pure methane sample at 8.1 MPa_A contained in the sapphire tube cell was obtained. The C-H stretching region (3200-2800 cm^{-1}) of this spectrum is shown in Fig. 5.1. Like in the spectra of natural gas the ν_1 methane band at ~2918 cm^{-1} is by far the most intense one in the spectrum. A part of the spectrum is shown in an expanded condition, so that two other much weaker bands become obvious. The band at ~3020 cm^{-1}

is the methane ν_3 band and the band at ~3070 cm^{-1} is the overtone $2\nu_2$ from the ν_2 methane vibration as concluded in Chap. 4.4.2. It is also possible to observe some of the rotational-vibrational transitions belonging to the ν_3 at ~3137 cm^{-1} and ~3115 cm^{-1}, indicated with arrows (note that only a part of the R branch can be observed in the spectrum).

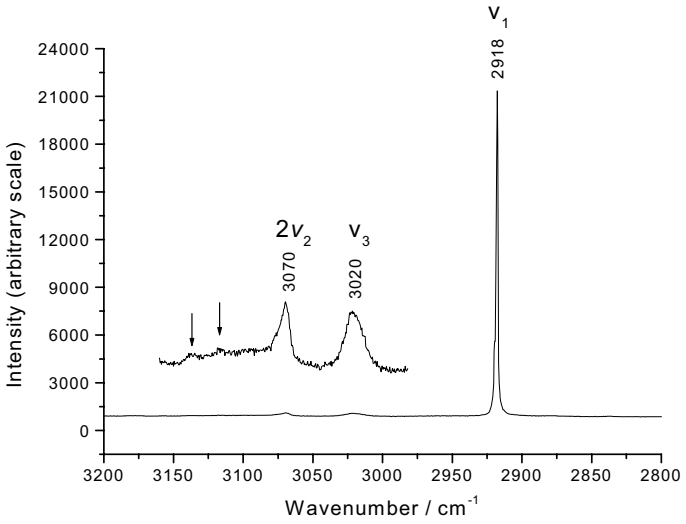

Fig. 5.1. The Raman spectrum (3200-2800 cm^{-1}) of a pure methane sample (N45, 99.995%, Hede Nielsen A/S) contained in the sapphire tube cell at 8.1 MP_A. The spectrum was obtained by use of the 1st spectrograph and the 514.53 nm_{air} line of the Ar-ion laser as the exciting source (~200 mW). The collection geometry was 90°.

In Fig. 5.2 examples of Raman spectra of the methane ν_1 band obtained in the titanium cell at four different pressures are represented. Three things are worth noticing in the figure as the pressure is raised: the intensity increases, the wavenumber position of the ν_1 band decreases and the line width broadens. The first observation is, as mentioned previously, due to higher concentration of gas molecules with increasing pressure. The wavenumber shifts of the ν_1 band as a function of pressure are relatively small (within 1-2 cm^{-1}). Before discussing these wavenumber shifts it is therefore important to verify the calibration of the spectra and the pressure gauges.

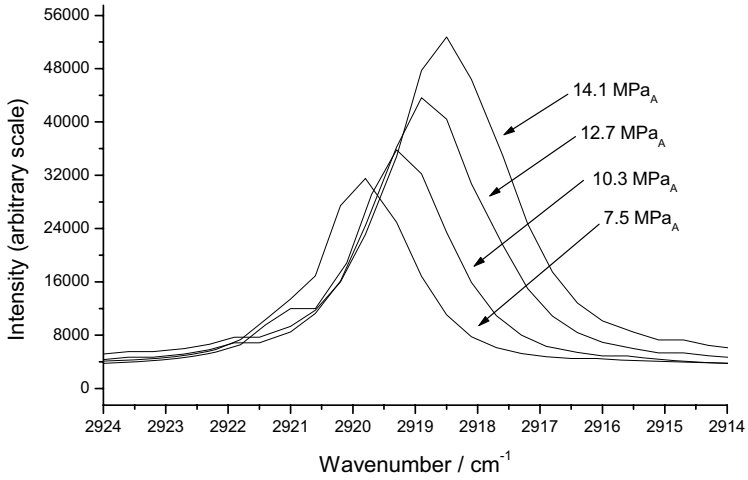

Fig. 5.2. The Raman spectra of pure methane in the ν_1 region obtained in the titanium cell at four different pressures. The collection geometry was 180°. For other experimental details see legend to Fig. 5.1.

5.3. Calibrations

5.3.1 Calibration of the Pressure Gauges

To achieve the most accurate pressure results the pressure gauges were calibrated. As mentioned in Chap. 2.2 the pressure gauge connected to the sapphire tube cell is a Bourdon manometer and the pressure gauge connected to the titanium cell is a pressure transmitter with digital display. The calibration was done with a dead weight tester. In the dead weight tester a piston moved with little friction in a cylinder pushed by the pressure. By the connection to a precision weight machine the pressure was measured by weight (1 $kgcm^{-2}$ corresponds to 0.981 bar, i.e. 0.0981 MPa_A). The applied weight tester was a Desgrandes et Huot 26000 (the weight) and Desgrandes et Huot 410 (piston and cylinder).

5.3.2 Calibration of Wavenumber Positions

The methane ν_1 wavenumber shifts as a function of pressure are, as it is seen from Fig. 5.2, relatively small (within 1-2 cm^{-1}). Thus it is very important to calibrate the spectra.

The application of emission lines from the noble gases is probably the most common way to calibrate a Raman spectrum with respect to wavenumber position. These lines are accurately known and they are listed extensively in the literature, e.g. in ref. 2. A Neon lamp is often used[3] or the plasma lines from an Ar-ion laser[4]. Normally a filter is inserted in the Ar-ion laser beam to isolate the desired laser line, e.g. the 514.53 nm_{air} line. If this filter is removed a high number of plasma emission lines will be obtained in the "Raman" spectrum. (In Chap. 2.1.1, Fig. 2.1, the filter is indicated by IF, interference filter). Emission lines are mostly given in wavelength units (nm) in the literature, which means that one has to do the conversion to Raman shifts in a way depending on which laser beeing used. To avoid this conversion Raman shifts standards are also used in the literature. Raman spectra of any known compound can in principle be used as a Raman shift standard as long as they exhibit enough well defined sharp peaks. In ref. 2 17 well defined indene Raman shifts are given as an example of such a wavenumber calibration. In this work wavenumber calibration was done by use of a small low pressure Neon lamp (included in the photograph of the titanium cell, Chap. 2.2, Fig. 2.8).

In Fig. 5.3 is shown the Raman spectrum of a methane sample contained in the titanium cell at 9.1 MPa_A, A. (Compared to the methane spectrum shown in Fig. 5.1 there is a weak fluorescence background in the left end of the spectrum arising from the sapphire windows in the titanium cell. This is most probably due to small impurities; the windows are relatively thick). In Fig. 5.3 the spectrum of the same methane sample is also included, obtained simultaneously with the light from a Neon lamp, B. Four Neon emission lines, indicated with arrows, are observed in the spectrum. These four lines were searched for in the literature[2].

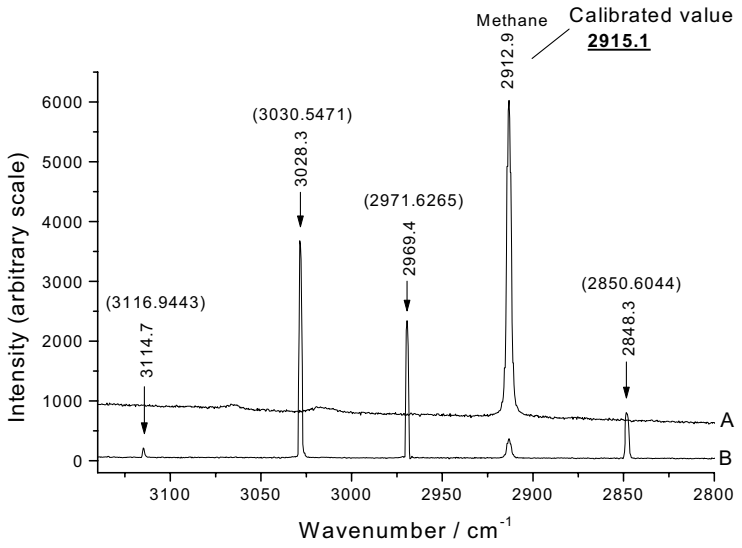

Fig. 5.3. The Raman spectrum of a pure methane sample contained in the titanium cell at a pressure of 9.1 MPa_A, A, and the same sample obtained simultaneously with the light from a Neon lamp, B. The collection geometry was 180°. For other experimental details see legends to Fig. 5.1.

Ref. 2 reports lists of observed wavelength in air, λ_{air}, as well as calculated wavelengths in vacuum, λ_{vac}, of the Neon emission lines ($\lambda_{vac} = n \cdot \lambda_{air}$, n: refractive index). In this work the following values in vacuum have been used. λ_{vac}: 613.01462, 609.78503, 607.60198 and 603.16670 nm_{vac} corresponding to 3116.9443, 3030.5471, 2971.6265 and 2850.6044 $cm^{-1}{}_{vac}$, respectively, when using the Ar-ion laser (514.5310 nm_{air}[4], 514.67417 nm_{vac}[2]) as the exciting source. These values are given in parentheses in Fig. 5.3. The averaged difference between the observed Neon lines and the literature values was calculated to 2.2 cm^{-1}. The final calibrated methane ν_1 band position was found to be 2915.1 cm^{-1}.

All spectra in the present work were calibrated by means of the same four Neon lines in the same manner as just described.

5.4. ν_1 Wavenumber Shifts in Pure Methane as a Function of Pressure

By combined use of the sapphire tube cell and the titanium cell it was possible to obtain Raman spectra of methane in the pressure range from 0.1 to 15.3 MPa_A. One measurement at 39.6 MPa_A was also performed. The cells were filled with pure methane (N45, 99.995%, Hede Nielsen A/S). After calibration the methane ν_1 band position was plotted as a function of the total pressure. This work is represented in Fig. 5.4. In the plots are also included values from the literature[5] (wavenumber calibration done by use of the spectral line at 2912.8 cm^{-1} of an Argon lamp). In the upper Plot I the total pressure range is shown. To be able to see some details at lower pressures an expansion of Plot I is given in Plot II. Measured values are listed in Table 5.1.

Table 5.1. Measured ν_1 wavenumber position for pure methane as a function of pressure.

P MPa_A	ν_1 CH_4 cm^{-1}_{vac}	P MPa_A	ν_1 CH_4 cm^{-1}_{vac}
0.1	2917.2	7.5	2915.3
1.1	2916.9	9.1	2915.1
2.1	2916.7	10.3	2914.7
2.9	2916.5	11.1	2914.5
3.5	2916.4	12.7	2914.2
4.2	2916.2	14.1	2913.7
5.1	2915.9	15.3	2913.5
6.4	2915.7	39.6	2910.6

In Fig. 5.4 series C and series D (squares and triangles) indicate the values obtained from the methane sample in the sapphire tube cell and the titanium cell, respectively. As it is seen these values are in very good agreement.

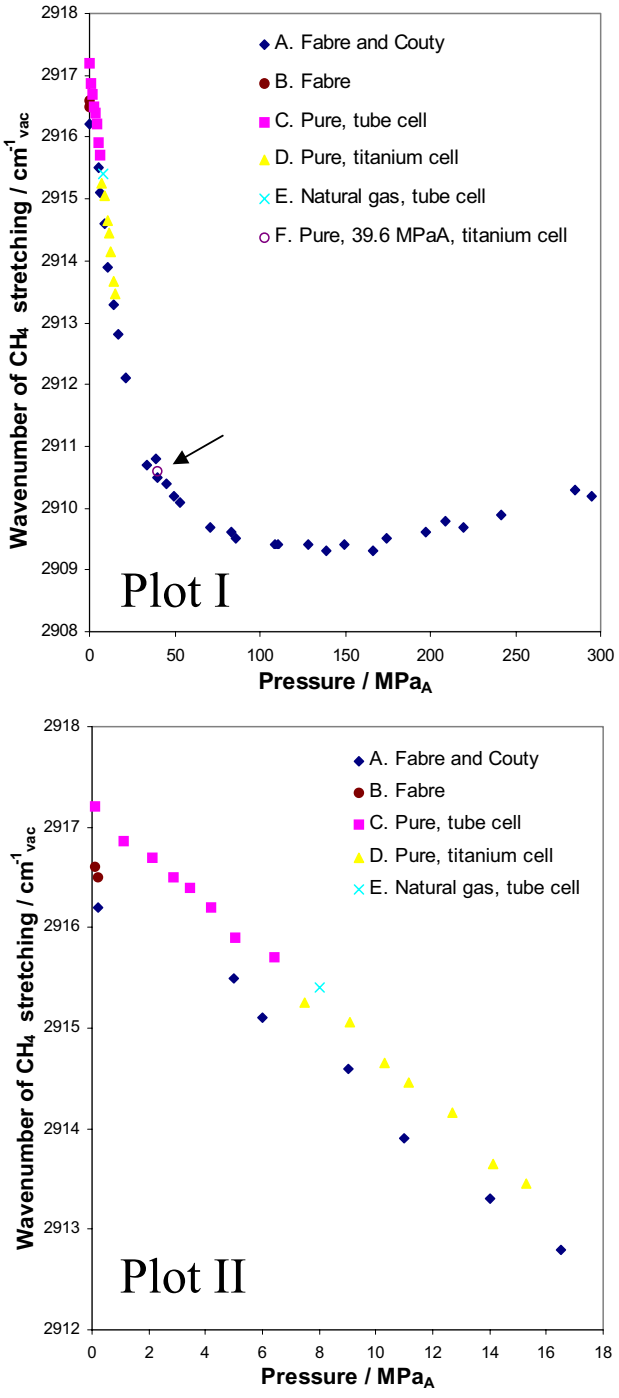

Fig. 5.4. The methane ν_1 band position as a function of pressure. Plot I) total range and Plot II) expansion at lower pressures. A: ref. 5, B: ref. 6, C: pure methane sample obtained in the sapphire tube cell, D: pure methane sample measured in the titanium cell, E: natural gas sample from Nybro, 8.0 MPa_A, measured in the sapphire tube cell and F: pure methane, 39.6 MPa_A, measured in the titanium cell.

It is also seen in Fig. 5.4 that the measured methane ν_1 band positions are in quite close agreement with the literature except for one value – the ν_1 band at the wavenumber position at 2916.2 cm^{-1}_{vac} for a pressure ~2 bar (0.2 MPa). Private communication with Philippe Marteau gave the information that the first three values in the table of ref. 5 were in error[6]. The values corrected by Denise Fabre[6] are listed in our Table 5.2 and two values are also included in the plot in Fig. 5.4 (series B). As it is seen the corrected values are in more agreement with our results. The slopes of the tendency lines are almost the same, but our values are about 0.5 cm^{-1} higher. Other relevant data from the literature can be given: The methane ν_1 band position was found to 2917 cm^{-1}_{vac} (at 2 atm) in ref. 7 and 2917.0 cm^{-1}_{vac} ref. 8 (measured in a plot). Our high pressure measurement at 39.6 MPa_A is also included in Fig. 5.4, Plot I, and as it is seen this value is in very good agreement with the literature (an arrow is inserted to guide the eyes).

Table 5.2. Corrected methane ν_1 wavenumbers as a function of pressure, given by D. Fabre[6].

P MPa	ν_1 CH_4 cm^{-1}_{vac}
$0.1<P<0.2^{I}$	2916.6
0.2	2916.5
$<1.0^{II}$	2916.4

[I] Inserted in Fig. 5.4 as 0.1 MPa_A.
[II] Not included in Fig. 5.4 (inexact value).

In Fig. 5.4 we also included the methane ν_1 value for a natural gas sample from Nybro contained in the sapphire tube cell at 8.0 MPa_A. By comparing this value with the ν_1 values it is seen that it is slightly higher (~0.3 cm^{-1}), i.e. the methane ν_1 vibration is affected by its environments. This observation gave rise to the studies described in the following Chap. 5.5.

5.5. ν_1 Wavenumber Shifts as a Function of Pressure in Methane Mixtures

5.5.1 Methane ν_1 Wavenumber Shifts as a Function of Pressure in Methane / Ethane Mixtures

The dependency of the methane ν_1 vibration on environments has also been studied in the literature for CH_4 / N_2 mixtures[9,10], CH_4 / CO_2 mixtures[10,11], equimolar mixtures of CH_4 with H_2, Ar and CO_2[10] and an equimolar mixture of CH_4 with N_2[12]. For a mixture containing methane at low pressure, i.e. when the molecules are quite apart from each other, the methane ν_1 band positions almost fit the curve shown in Fig. 5.4. As the pressure is increased however the deviation between the curve for the mixture and the curve for pure methane becomes clear. With increasing pressure the molecules approach each other on the average, i.e. the way the methane molecule vibrates depend more and more on the surroundings. The methane content of the natural gas sample from Nybro was 88.77 mol% and the ethane content was 6.45 mol% measured by gas chromatography. Since ethane generally is the component in natural gas in the next largest amount it was decided to investigate the influence of the presence of ethane on the methane ν_1 vibration.

Two methane / ethane mixtures were prepared with mole fractions of $X(CH_4) = 0.85$, $X(C_2H_6) = 0.15$ and $X(CH_4) = 0.49$, $X(C_2H_6) = 0.51$, respectively (methane of purity N45, ethane of purity N35, both from Hede Nielsen A/S). Both mixtures were successively contained in the sapphire tube cell during the Raman measurements, the former starting at a pressure of 13.1 MPa_A and the latter starting at a pressure of 9.0 MPa_A. A Raman spectrum of each of the mixtures will be presented in Chap. 5.5.2. The methane ν_1 band positions were measured and calibrated in spectra at all pressures as described previously. The results are presented in Fig. 5.5 as a function of the total pressure, Plot I, and partial pressure, Plot II. In the figure we included the methane ν_1 values for the pure methane sample that were determined in Chap. 5.4. Tendency lines have been calculated by regression analysis to guide the eyes. In the Fig. 5.5 we also included values from the literature, like in Fig. 5.4. Data points are listed in Table 5.3, Chap. 5.5.2.

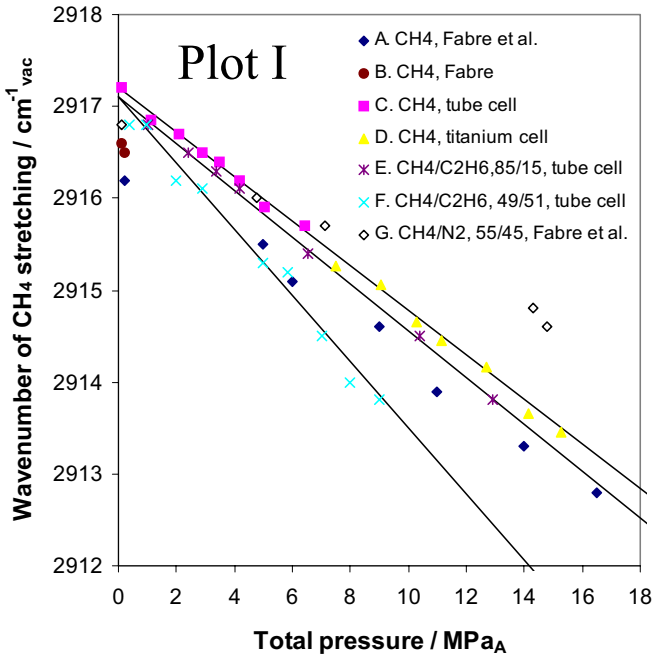

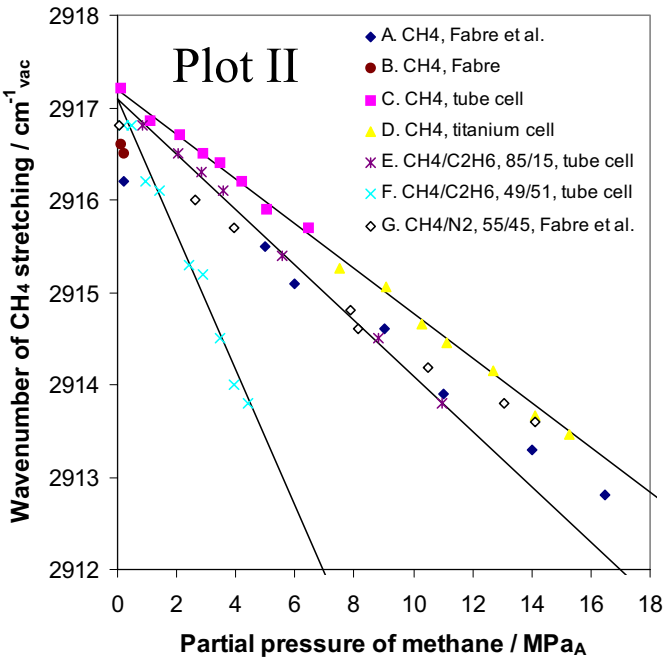

Fig. 5.5. The methane ν_1 band position as a function of pressure, Plot I total pressure, and Plot II partial pressure of methane. A, B, C and D: see Fig. 5.4. E: methane / ethane mixture, $X(CH_4)=0.85$, $X(C_2H_6)=0.15$, obtained in the sapphire tube cell, F: methane / ethane mixture, $X(CH_4)=0.49$, $X(C_2H_6)=0.51$, obtained in the sapphire tube cell and G: ref. 9, methane / nitrogen mixture, $X(CH_4)=0.55$ and $X(N_2)=0.45$.

In both Plot I and Plot II in Fig. 5.5 it is seen that the tendency line for the mixture with high methane content ($X(CH_4)=0.85$) is lower than the tendency line for the pure methane sample. The tendency line combining the values for the nearly equimolar mixture are even lower. This means that the decreasing effect on the methane ν_1 band position with increasing pressure is enhanced if ethane molecules surround the methane molecules. In Fig. 5.5 some methane ν_1 band position points for the CH_4 / N_2 system ($X(CH_4)=0.55$) taken from ref. 9 are also included. In this ref. exact data points were not given, so the data were determined by measuring the coordinates for each point to our best ability. By looking at Plot I it is seen that the opposite effect is observed for nitrogen compared to ethane. The data points fall above the data points from the pure methane sample; i.e. nitrogen does not have the same lowering effect on the methane ν_1 vibration as methane itself. In Plot II nitrogen have a little lowering effect, but when taking a closer look at the points measured by D. Fabre et al., they seem to fall above the literature points for the pure methane sample found by D. Fabre et al.[5].

In the following we present a qualitative explanation for the red shift (lowering in wavenumer) of the methane ν_1 band position on pressure. (The explanation is in accordance with the discussion in ref. 13. In this ref. the wavenumber shifts as a function of pressure in H_2, H_2 / He and H_2 / Ar systems are studied). Since an ethane molecule is larger than a methane molecule it will better accept electronic charge and thereby can lead to a weakening of the C-H bonds in neighbouring methane. This effect will strengthen the intermolecular forces between methane and ethane (van der Waals attraction) compared to the intermolecular forces between two methane molecules. Since the nitrogen molecule is smaller than the methane molecule this acceptance is smaller and the intermolecular force between nitrogen and methane is thereby weaker. An illustration is shown in Fig. 5.6. At high pressures under which condition each CH_4 molecule is near another molecule, the C-H bond will weaken because some charge fraction (δ-) might be delocalised, forming the van der Waals interaction. The effect is considered to be strong for methane interacting with methane (Fig. 5.6, I), even stronger with ethane (Fig. 5.6, II) and not so strong with nitrogen (Fig. 5.6, III). If this explanation is true the C-H bond strength weakening effect in methane should go up from methane interacting with nitrogen to methane to ethane. This should be reflected in the methane ν_1 band position, which should be less shifted for weaker van der Waals bonds. This is exactly what is seen in Fig. 5.5.

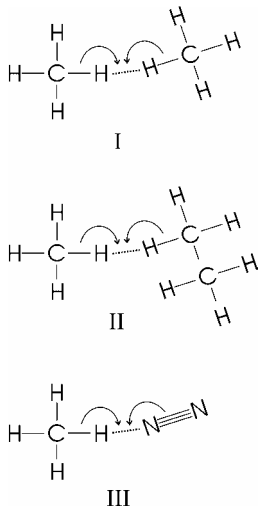

Fig. 5.6. Illustration of the qualitative electron acceptance explanation of the pressure dependence of the methane ν_1 wavenumber shifts. Interaction between methane and I) methane, II) ethane and III) nitrogen.

The above described effect should also be observed for the vibrations of ethane and nitrogen molecules in the mixtures. It was considered to be of interest to investigate the ethane ν_1 band position as a function of pressure in the two methane / ethane mixtures.

5.5.2 Ethane ν_1 Wavenumber Shifts as a Function of Pressure in Methane / Ethane Mixtures

The Raman spectra of the two methane / ethane mixtures obtained for the studies described in Chap. 5.5.1 were the same spectra used in this chapter. The Raman spectrum of the mixture of composition $X(C_2H_6) = 0.15$ obtained at a pressure of 12.9 MPa_A is shown in Fig. 5.7, as a dashed line curve. In Fig. 5.7 the Raman spectrum of the mixture with composition $X(C_2H_6) = 0.51$ is also included obtained at 9.0 MPa_A (continous curve). The band at 2954 cm^{-1} was assigned to the overtone of one of the CH_3 deformation vibrations (probably the ν_{11} ~1460 cm^{-1})[14] and the band at 2896 cm^{-1} was assigned to the ethane ν_1 band. These observed ethane bands probably also are coupled by Fermi resonance, somewhat similar to the case of CO_2 described in Chap. 4.3.

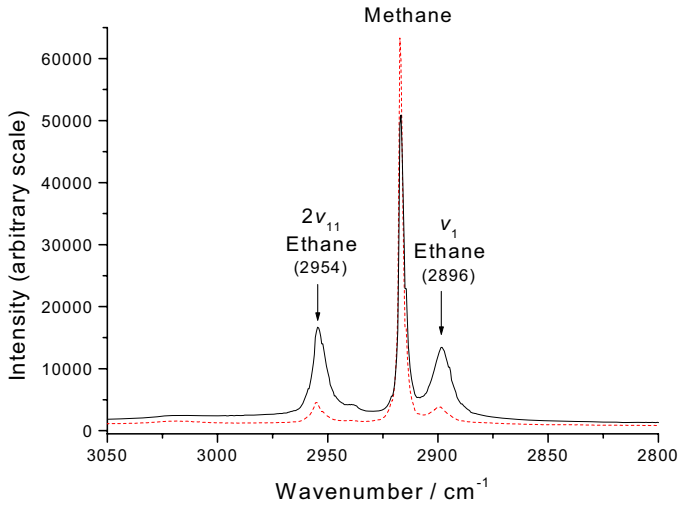

Fig. 5.7. The Raman spectra of the two methane / ethane mixtures in the C-H stretching region obtained in the sapphire tube cell. Dash line curve: $X(C_2H_6) = 0.15$ at a pressure of 12.9 MPa_A. Solid line curve: $X(C_2H_6) = 0.51$ at a pressure of 9.0 MPa_A. Methane: N45, 99.995% and ethane: N35, 99.95%, Hede Nielsen A/S. Further experimental details are given in legend to Fig. 5.1. The wavenumbers in parentheses are from the literature[15].

The ethane ν_1 band positions were measured and calibrated in all of the obtained Raman spectra. These ν_1 wavenumber positions were plotted as a function of total pressure. This work is presented in Fig. 5.8 and data points are listed in Table 5.3.

Table 5.3. Measured ν_1 wavenumber position for two methane / ethane mixtures as a function of total pressure.

	⟵ ν_1 methane[1] ⟶		⟵ ν_1 ethane ⟶	
P_{total}	$X(CH_4)$: 0.85	$X(CH_4)$: 0.49%	$X(C_2H_6)$:0.15	$X(C_2H_6)$:0.51
MPa_A	$cm^{-1}{}_{vac}$	$cm^{-1}{}_{vac}$	$cm^{-1}{}_{vac}$	$cm^{-1}{}_{vac}$
0.4		2916.8		
1.0	2916.8	2916.8		2898.5
2.0		2916.2		2898.4
2.4	2916.5		2898.8	
2.9		2916.1		2898.2
3.4	2916.3		2898.7	
4.2	2916.1		2898.4	
5.0		2915.3		2897.2
5.9		2915.2		2896.8
6.5	2915.4		2897.7	
7.0		2914.5		2896.2
8.0		2914.0		2895.6
9.0		2913.8		2895.0
10.4	2914.5		2896.5	
13.0	2913.8		2895.7	

[1] Methane ν_1 wavenumber positions discussed in previous chapter, Chap. 5.5.1. Plots of the data were shown in Fig. 5.6.

In Fig. 5.8 tendency lines were not included because it seems like the points follow a nonlinear curve. It is however clearly seen from Fig. 5.8 that the curve for the mixture with high ethane content, $X(C_2H_6) = 0.51$, lies lower than the curve for the mixture with low ethane content, $X(C_2H_6) = 0.15$. This observation is in accordance with the electron acceptance explanation discussed in Chap. 5.5.1. Further support comes from the data on N_2 / CH_4 mixture presented in ref. 7.

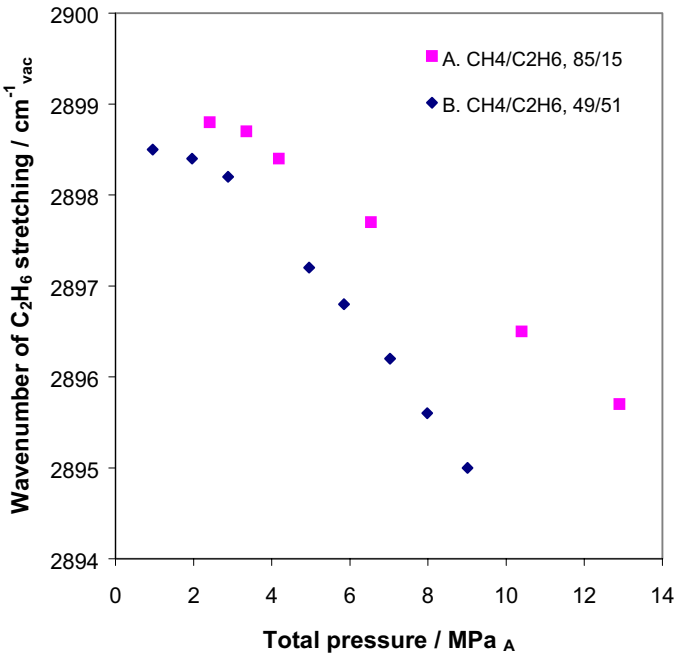

Fig. 5.8. The ethane ν_1 wavenumber position as a function of total pressure in the two methane / ethane mixtures. A: $X(CH_4) = 0.85$, $X(C_2H_6) = 0.15$ and B: $X(CH_4) = 0.49$, $X(C_2H_6) = 0.51$.

5.6 Conclusions

The ν_1 wavenumber positions have been studied as a function of pressure in pure methane and in two methane / ethane mixtures. The methane ν_1 band positions for pure methane as a function of pressure showed to be a little higher than what has been reported in the literature. Agreement was obtained with respect to the slope of the tendency line. The methane ν_1 band position for the two methane / ethane mixtures were measured and compared to results from the pure methane sample. It was observed that the decreasing effect on the methane ν_1 band position with increasing pressure is *enhanced*, if ethane molecules surround the vibrating methane molecules. This observation, and the literature on related systems have lead us to propose, a qualitative explanation model based on electron accepting properties. The wavenumber of the ethane ν_1 band position as a function of total pressure was also measured. A decreasing effect on the ν_1 wavenumber position was observed as expected by our model. Furthermore, it was seen that the decreasing effect on the ethane ν_1 band position with increasing pressure is *weakened* if methane molecules

surround the vibrating ethane molecules, which is in accordance with the electron accepting explanation.

The "methane ν_1 wavenumber shift"-method can without doubt be used to determine the total pressure in methane mixtures. Because of the decrease in wavenumber position with increasing pressure is affected both with an overall lowering effect on pressure and an enhancement effect depending on which kind of molecules surround methane, it is very important to know the composition of the mixture qualitatively and quantitatively. To make the method useful in practice it is important to obtain data from much more methane systems both with respect to kind of components (including multi component systems) and composition.

5.7 References

1. S. Brunsgaard Hansen, R. W. Berg and E. H. Stenby, ”Raman spectroscopic studies of methane-ethane mixtures as a function of pressure”, appear in Appl. Spectrosc.
2. H. Hamaguchi, “Calibrating multichannel Raman spectrometers”, Appl. Spectrosc. Rev. **24**, 137 (1988).
3. C.-H. Tseng, J. Ford, C. K. Mann and T. J. Vickers, “Wavelength calibration of a multichannel spectrometer”, Appl. Spectrosc. **47**, 1808 (1993).
4. N. C. Craig and I. W. Levin, “Calibrating Raman spectrometers with plasma lines from the Argon ion laser”, Appl. Spectrosc. **33**, 475 (1979).
5. D. Fabre and R. Couty, C. R. Acad. Sci. Paris **303**, série II, 1305 (1986).
6. Ph. Marteau and D. Fabre, private communication (1999).
7. B. P. Stoicheff, J. Molecul. Spectr. **10**, 448 (1963).
8. A. D. May, J. C. Stryland and H. L. Welch, “Raman spectra of H_2 and CH_4 at high pressures”, J. Chem. Phys. **30**, 1099 (1959).
9. D. Fabre and B. Oksengorn, “Pressure and density of the CH_4 and N_2 Raman lines in an equimolar CH_4/N_2 gas mixture”, Appl. Spectrosc. **46**, 468 (1992).
10. J. C. Seitz, J. D. Pasteris and I.-M. Chou, “Raman spectroscopic characterization of gas mixtures. I. Quantitative composition and pressure determination of CH_4, N_2 and their mixtures”, Am. J. Sci. **293**, 297 (1993).
11. J. C. Seitz, J. D. Pasteris and I.-M. Chou, “Raman spectroscopic characterization of gas mixtures. II. Quantitative composition and pressure determination of the CO_2-CH_4 system”, Am. J. Sci. **296**, 577 (1996).
12. I.-M. Chou, J. D. Pasteris and J. C. Seitz, “High-density volatiles in the system C-O-H-N for the calibration of a laser Raman microprobe”, Geochim. Cosmochim. Acta. **54**, 535 (1990).
13. A. D. May, V. Degen, J. C. Stryland and H. L. Welsh, “The Raman effect in gaseous hydrogen at high pressures”, Can. J. Phys. **39**, 1769 (1961).
14. G. Hertzberg, *Molecular Spectra and Molecular Structure* (D. Van Nostrand, New York, 1964), II, Chap. 3, p. 345.
15. *Raman / IR Atlas of Organic Compounds*, B. Schrader and W. Meier (Verlag Chemie, Weinheim, 1974), A 1-26.

6. Intensity Ratio between two Methane Bands (ν_3, $2\nu_2$) as a Function of Pressure in Pure Methane and Methane Mixtures

6.1. Introduction

The studies described in the previous chapter are concerned with the issue "how to determine the pressure in a methane mixture by means of its Raman spectrum". It is, as it was shown in chapter 5, possible to determine the pressure if the composition is known and if methane ν_1 wavenumber shift data are available. Many more methane mixtures in different concentrations have however to be investigated, before the ν_1 wavenumber shift method in a realistic way can be used for a determination of the pressure in methane mixtures which cannot be otherwise studied e.g. fluid inclusions in rocks. Other methods to determine total pressures in methane mixtures with known compositions have been investigated in the literature, e.g. based on the line width broadening of the methane ν_1 band as a function of pressure in CH_4 / N_2 mixtures[1,2]. (The line width broadening was incidentally shown in Chap. 5.2, Fig. 5.2). A method to determine total pressure in CH_4 / CO_2 mixtures, based on the area ratio between the methane ν_1 band and the CO_2 $2\nu_2$ band as a function of pressure, has also been described[3]. The above mentioned methods have in common that they all are based on the study of the methane ν_1 band. This is not surprising since the methane ν_1 band is by far the most intense one in spectra of methane mixtures as seen several times previously.

In our work dealing with analysis of the natural gas samples, Chap. 4.4, it was necessary to blow up the Raman spectra to be able to see other bands in the spectra than the intense methane ν_1 band. In the expanded spectra (C-H stretching region, 3150-2850 cm^{-1}, shown in Fig. 4.13a), a clear pressure dependency between two of the bands is obvious. An extract of Fig. 4.13a is presented in Fig. 6.1 to illustrate this effect. In Fig. 6.1 it seems like the methane ν_3 band (at ~3020 cm^{-1}) is lowered relatively to the methane $2\nu_2$ band (at ~3070 cm^{-1}) as the pressure is raised. The purpose of the present work was to investigate this observation further. The intensity ratio between these two methane bands as a function of

pressure has been investigated for a pure methane sample, Chap. 6.2, two methane / ethane mixtures, Chap. 6.3, and a methane / N_2 mixture, Chap. 6.4. The investigations were successful in that way that the intensity ratio Iv_3 / $I2v_2$ as a function of pressure showed to be independent of the composition of the methane mixture. This means that it should be possible to use the method to determine directly the total pressure in methane mixtures, i.e. natural gas and fluid inclusions in rocks, in which the composition is not known. The present results have never been reported elsewhere and the finding is our own.

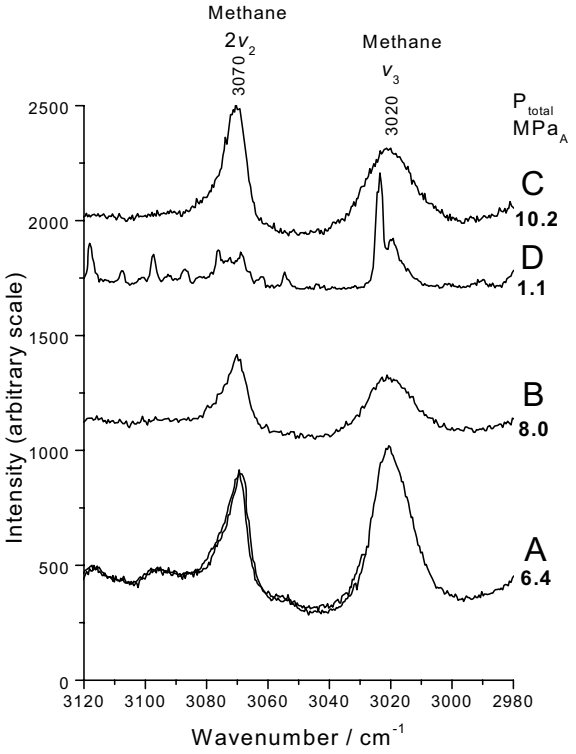

Fig. 6.1. The methane ν_3 and $2\nu_2$ region of the natural gas Raman spectra, which were shown in Chap. 4.4, Fig. 4.13.a. A: Ll. Torup (6.4 MPa_A); B: Nybro, downstream of pressure regulation and filtration (8.0 MPa_A); C: Nybro, raw (10.2 MPa_A); and D: same as C, but at a lower pressure (1.1 MPa_A). For experimental details see the legend to Fig. 4.13.a.

6.2. Raman Spectroscopic Studies of the two Methane Bands, ν_3 and $2\nu_2$, as a Function of Pressure in Pure Methane

The sapphire tube cell was once again filled with pure methane at a pressure of 7.9 MPa_A (N45, 99.995%, Hede Nielsen A/S). Several Raman spectra were obtained at different pressures. The different pressures were obtained by letting gas out of a valve (2b) as mentioned previously. The Raman spectra are shown in Fig. 6.2. A vertical line has been drawn at the $2\nu_2$ wavenumber position to guide the eyes. It is clearly seen in Fig. 6.2 that the ν_3 band increases relatively to the $2\nu_2$ band as the pressure is lowered. It is also seen that the ν_3 wavenumber position decreases with increasing pressure. The $2\nu_2$ band position however seems to be constant at ~3070 cm^{-1}. Before the band ratios were determined some considerations had to be done.

In addition to the vibrational transition ν_3 and the overtone $2\nu_2$ it is also possible to observe rotational vibrational transitions in the Raman spectra shown in Fig. 6.2. This was also the case in the Raman spectra of the natural gas samples. A curious peak observed at ~3019 cm^{-1} (indicated with an arrow in the Fig. 6.2, the 0.2 MPa_A spectrum) does not look like belonging to this class of transitions. It could be (although the author is in doubt) that the peak is a part of the structure of the rotational wing (Q branch wing, i.e. $\Delta J = 0$ transitions). The wing is clearly seen in the Raman spectrum of methane obtained by Brodersen *et al.*[4,5]. The wing was also seen in the Raman spectra of H_2S and N_2, shown in Chap. 4.4, Fig. 4.16, but in the N_2 wing no peaks were observable. Due to the wavenumber of the fundamental vitrational transition, the curious peak at ~3019 cm^{-1} can neither be an overtone band nor a combination band. Interpreted or not, the band is incorporated in the ν_3 band at higher pressures and it is impossible to sort it out. Finally, with respect to the methane $2\nu_2$ band it is very difficult to determine where the band starts, especially at lower pressures.

When considering how to get the most real ratio between the ν_3 band and the $2\nu_2$ band, the area ratio method was chosen not to be used for the above mentioned reasons. In stead the band intensity was in all of the spectra measured with a ruler as the hight over an estimated background level. The calculated intensity ratios $I\nu_3$ / $I2\nu_2$ were plotted as a function of pressure. This plot is shown in Fig. 6.3 and the data points are listed in Appendix D.

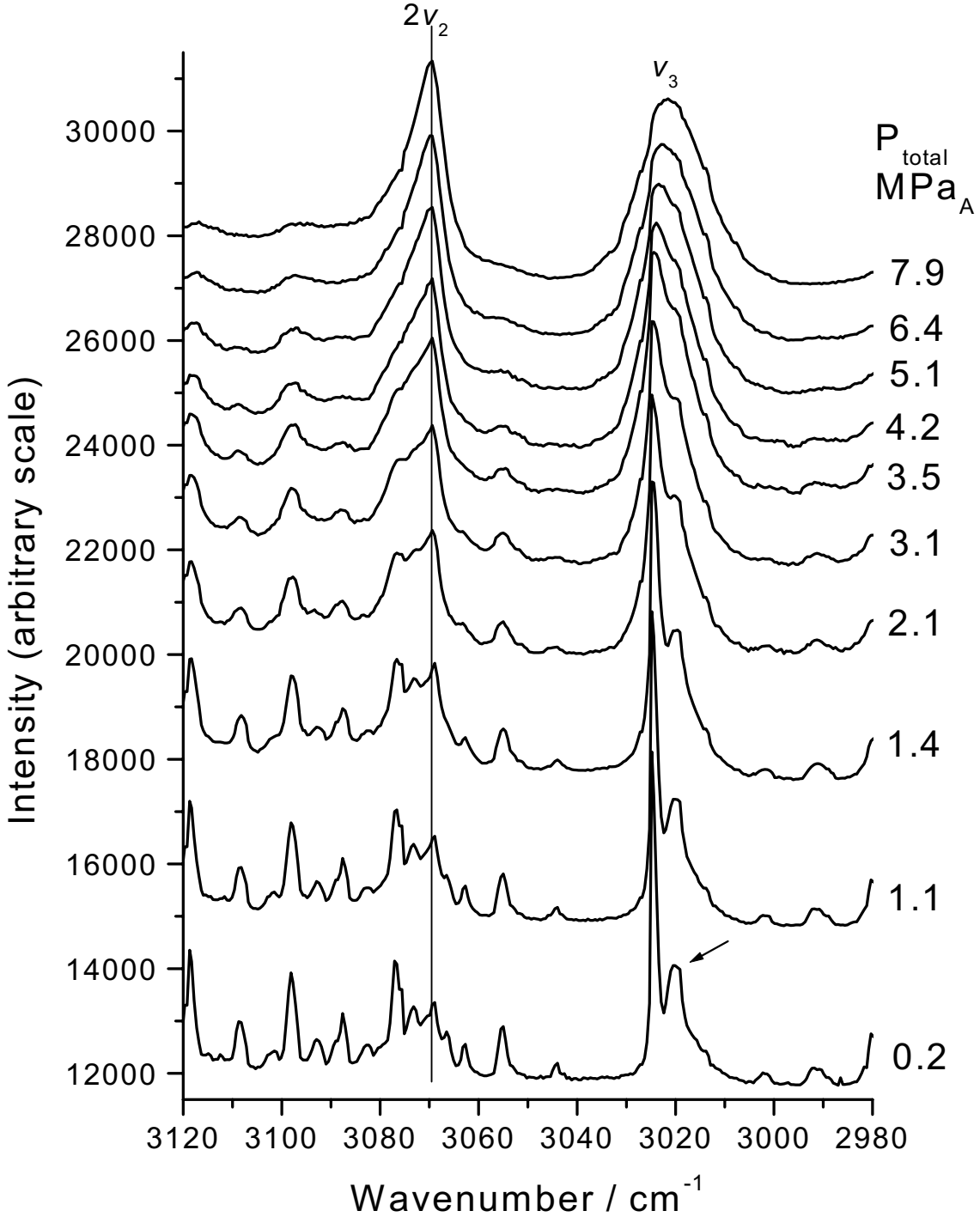

Fig. 6.2. Raman spectra of the pure methane sample (contained in the sapphire tube cell) at different pressures (7.9 – 0.2 MPa_A). The spectra were acquired by use of the 1st spectrograph and the excitation source was the 514.53 nm_{air} laser line of the Ar-ion laser (~200 mW). The collection geometry was 90°. Arrow: see discussion in the text.

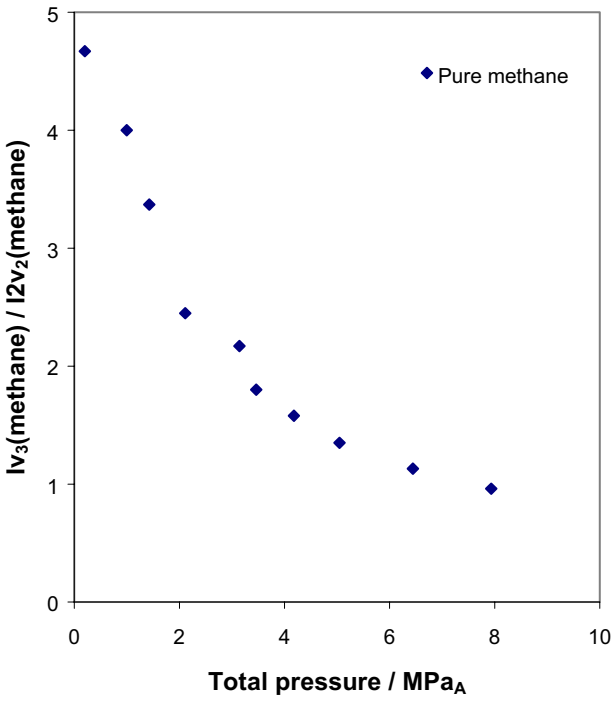

Fig. 6.3. Intensity ratio, Iv_3 / $I2v_2$, as a function of total pressure for the pure methane sample (pressure range: 7.9 – 0.2 MPa_A). Data points are listed in Appendix D.

It is seen from the plot shown in Fig. 6.3 that the intensity ratio, Iv_3 / $I2v_2$, is indeed decreasing with increasing pressure. The slope of the curve is increasing towards lower pressures. Thus it was concluded that it is important to include the intensity ratio also at pressures below 0.2 MPa_A.

6.3. The Intensity Ratio, Iv_3 / $I2v_2$, as a Function of Pressure for two Methane / Ethane Mixtures

Raman spectra of two methane / ethane mixtures with mole fractions of $X(CH_4)$ = 0.85, $X(C_2H_6)$ = 0.15 and $X(CH_4)$ = 0.49, $X(C_2H_6)$ = 0.51 were obtained. Actually it was the same two mixtures treated in Chap. 5.5. The spectra obtained in Chap. 5.5 and the spectra presented in this chapter are not the same however. In Fig. 6.4 is shown the Raman spectra of the methane / ethane mixture with highest methane content and at a pressure of 2.4 MPa_A obtained with different integration time, 150 seconds and 6 seconds and with the same laser power (~200 mW). The longer the integration time, the better sensitivity. Since the two methane bands, ν_3 and $2\nu_2$, were weak relatively long integration times were chosen for the spectra treated in this chapter. With a long integration time saturation of some of the bands occurred (about 64.000 counts), as it is seen for the methane ν_1 band in the upper spectrum shown in Fig. 6.4. Because of this saturation it is not possible to read the precise ν_1 wavenumber position, for which reason relatively short integration times were used in the Raman spectra in Chap. 5.

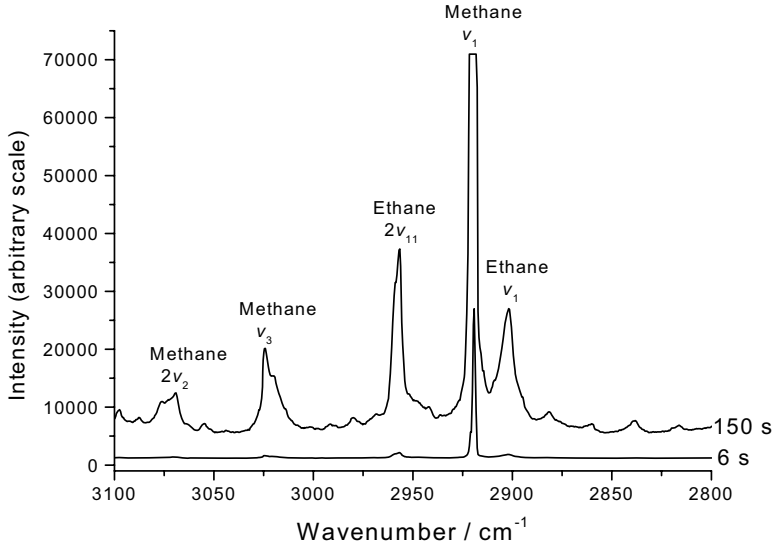

Fig. 6.4. The Raman spectra of the methane / ethane mixture ($X(CH_4)$ = 0.85), contained in the sapphire tube cell at a pressure of 2.4 MPa_A, obtained with different integration times, 150 seconds and 6 seconds. (Same laser power were used, ~200mW). Experimental details are given in Fig. 5.1.

The Raman spectra of the methane / ethane mixture with high methane content ($X(CH_4)$ = 0.85) are shown in Fig. 6.5, in the pressure range 12.0 – 0.1 MPa_A. The intensity (heights) of the methane ν_3 bands and the methane $2\nu_2$ bands shown in Fig. 6.5 were measured as described in Chap. 6.2 without any difficulties. The intensity ratios $I\nu_3$ / $I2\nu_2$ were plotted as a function of pressure. The plot is shown later (the squares in Fig. 6.8) and data points are listed in Appendix D.

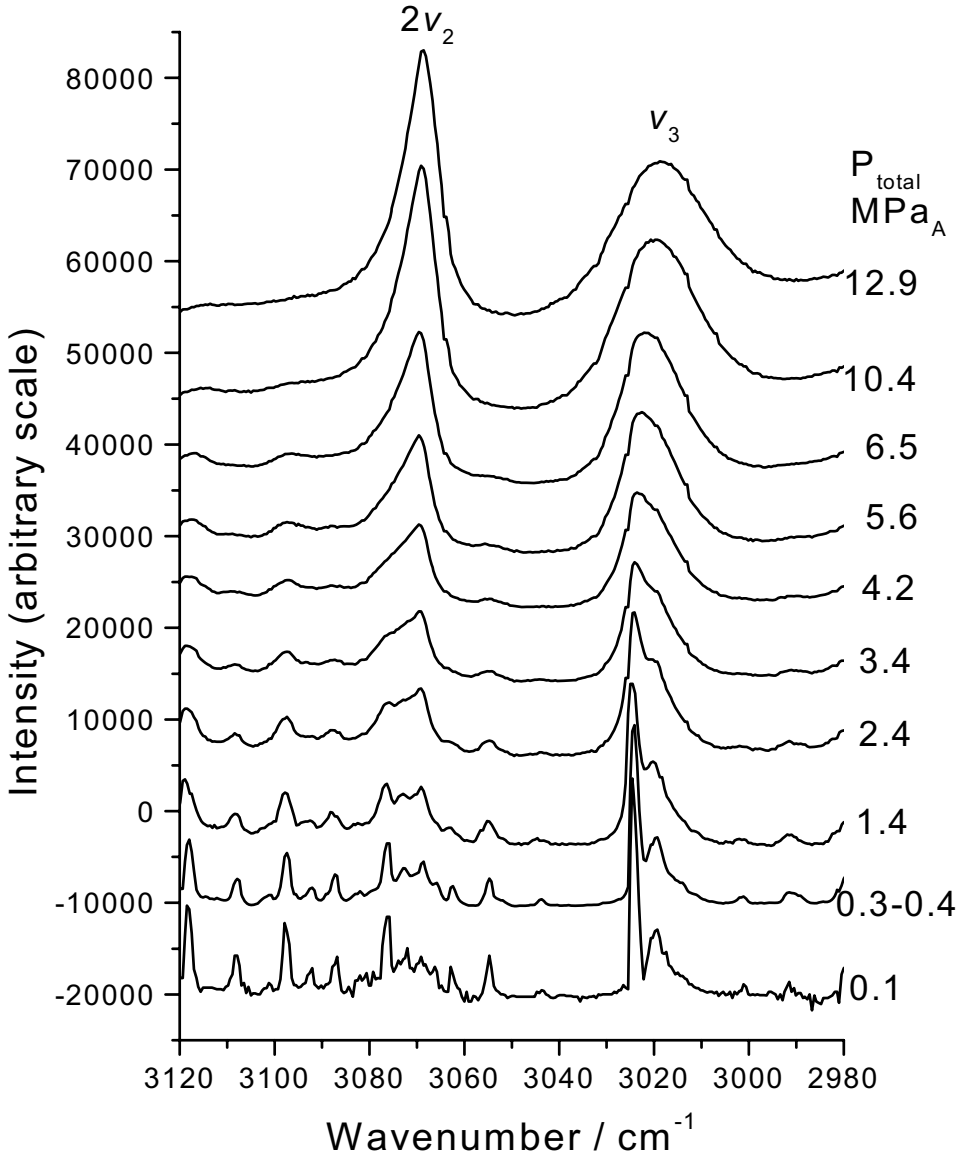

Fig. 6.5. Raman spectra of the methane / ethane mixture with high methane content ($X(CH_4)$ = 0.85) at different pressures. For experimental details see legend to Fig. 6.2.

The Raman spectra of the nearly equimolar methane / ethane mixture ($X(CH_4)$ = 0.49), obtained in the pressure range 9.0 – 0.1 MPa_A, gave rise to some considerations, because at higher pressures it was difficult to determine the real intensity (height) of the methane ν_3 band with precision. Fig. 6.6 shows the Raman spectrum of the mixture obtained at a pressure of 7.0 MPa_A in the 3150-2800 cm^{-1} region. As seen the ethane $2\nu_{11}$ band is very intense (and saturated) compared to the methane ν_3 band and the methane $2\nu_2$ band because the high ethane content in the mixture. As was seen in Chap. 5, Fig. 5.2, the line width of the methane ν_1 band increased as the pressure was raised. The same effect was observed for the ethane $2\nu_{11}$ bands, resulting in an increasing overlap between the methane ν_3 and the ethane $2\nu_{11}$ as the pressure was raised. Because of the saturation of the ethane $2\nu_{11}$ it was not possible to resolve the bands with the Microcal Origin Peak Fitting Module. All the obtained Raman spectra of the nearly equimolar methane / ethane mixture are shown in Fig. 6.7. The intensity ratios, $I\nu_3$ / $I2\nu_2$, were measured for spectra obtained at lower pressures (0.1-2.0 MPa_A) and plotted as a function of pressure. The plot is shown in Fig. 6.8 (the triangles) and data points are listed in Appendix D.

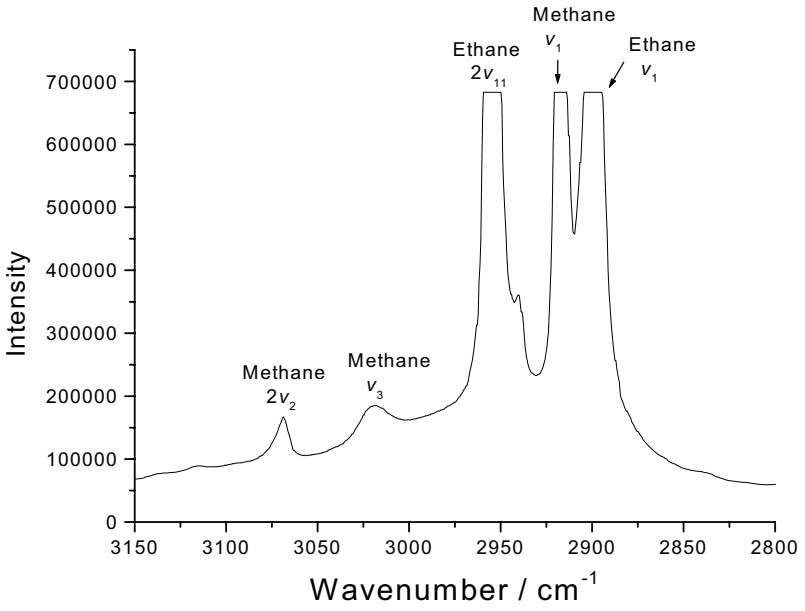

Fig. 6.6. Raman spectrum of the equimolar methane / ethane mixture ($X(CH_4)$ = 0.49) obtained at 7.0 MPa_A. The spectrum illustrates the overlapping of the methane ν_3 band. Experimental details as described in the legend to Fig. 6.2.

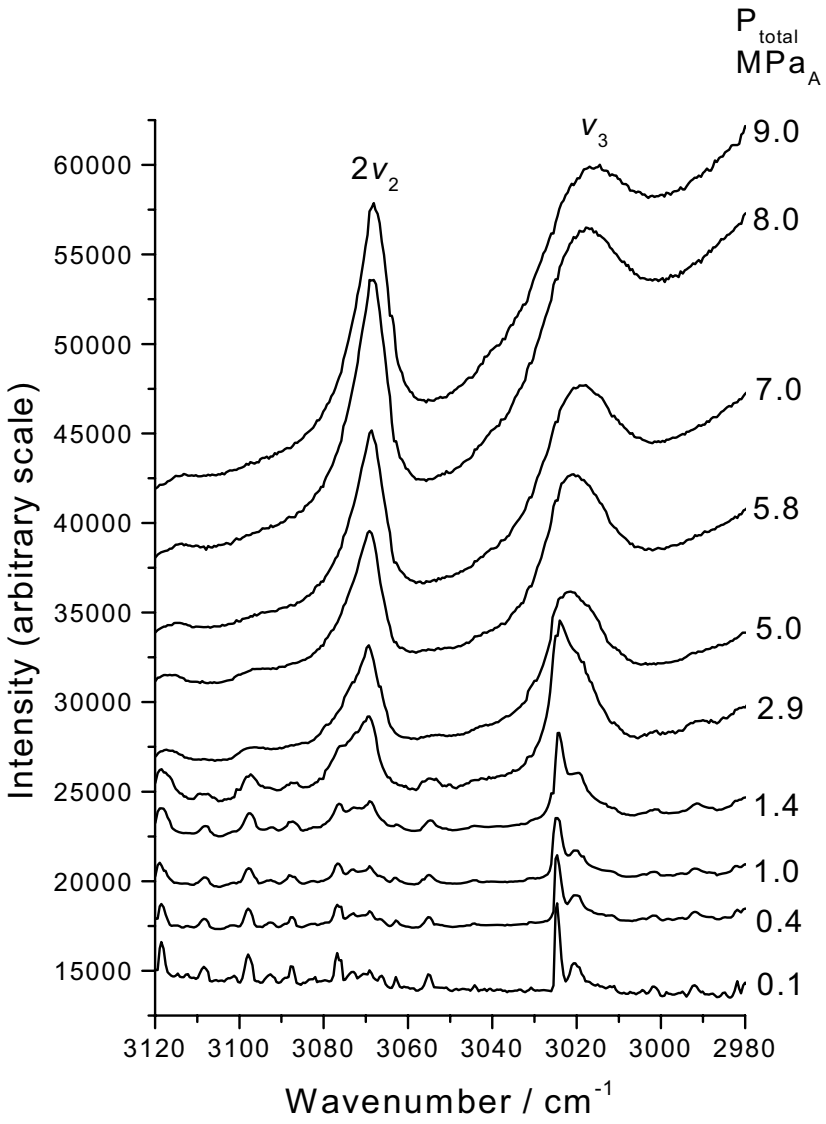

Fig. 6.7. Raman spectra of the nearly equimolar methane / ethane mixture ($X(CH_4) = 0.49$) in the pressure range (9.0 – 0.1 MPa_A). Experimental details as described in the legend to Fig. 6.2.

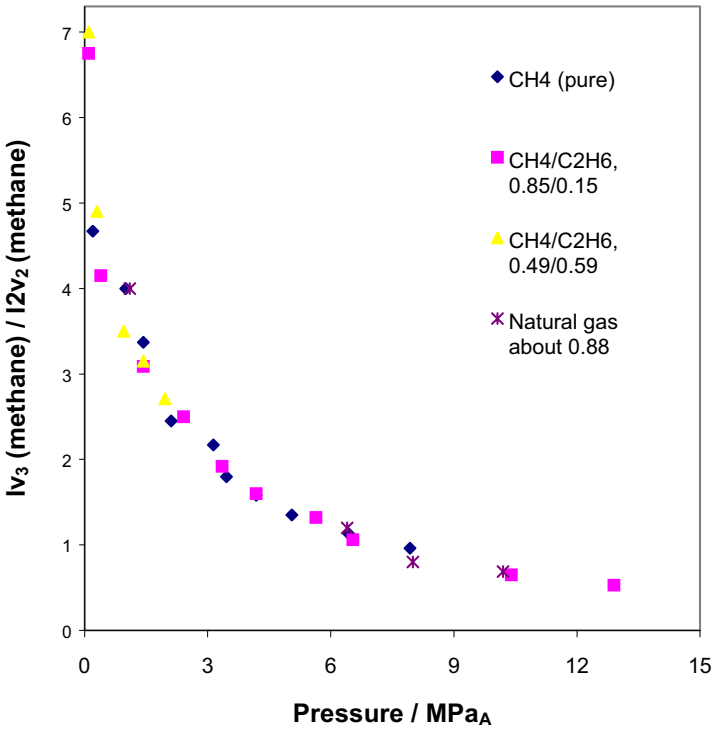

Fig. 6.8. Intensity ratio, $I\nu_3$ / $I2\nu_2$, as a function of the total pressure for two methane / ethane mixtures. In the plot are also shown the results from the natural gas samples (Fig. 6.1) and the pure methane sample, also shown in Fig. 6.3. Data points are listed in Appendix D.

It is seen from the Fig. 6.8 that the points from the two different methane / ethane mixtures follow the same curve, and even better they also follow the points obtained from the Raman spectra of the pure methane sample. Intensity ratios between the methane ν_3 band and the methane $2\nu_2$ band were also measured in the Raman spectra of the natural gas samples shown in Fig. 6.1 (because of noise in the spectra the ratios are somewhat uncertain). These results were all plotted in Fig. 6.8 and a rather nice fit is seen. It is therefore concluded that the intensity ratio between the two methane band, ν_3 and $2\nu_2$ seem to be of use in determining the total pressure in methane containing mixtures in which the composition is not known (so far with some limitations if the ethane content is high). To investigate this further it was decided to determine the intensity ratio as a function of pressure for a methane / nitrogen mixture.

6.4. The Intensity Ratio, $I\nu_3$ / $I2\nu_2$, as a Function of Pressure for a Methane / Nitrogen Mixture

A methane / nitrogen mixture was prepared with mole fractions $X(CH_4) = 0.47$ and $X(N_2) = 0.53$ (both gases were of purity N45, Hede Nielsen A/S). The mixture was filled in the sapphire tube cell and the starting pressure was 15.9 MPa_A. This high pressure was achieved by using a pump, ISCO Syringe Pump model 260D. In fact the achieved pressure was higher than the cell was leak tested for, but the cell showed to be perfectly tight also at 15.9 MPa_A. The Raman spectra of this mixture are presented in Fig. 6.9 in the pressure range 15.9 – 0.6 MPa_A. As seen from Fig. 6.9 all of the spectra nicely show the same pattern as for the pure methane sample and the two methane / ethane mixtures. The intensities of the methane ν_3 band and the methane $2\nu_2$ band were measured without difficulties. The intensity ratio was plotted as a function of total pressure as shown in Fig. 6.10, Plot I. In the figure the points shown in Fig. 6.8 are also included. It is concluded from the Fig. 6.10 (Plot I) that the points, arising from four different series, follow the same curve, i.e. the intensity ratio, $I\nu_3$ / $I2\nu_2$, is independent of "in which surroundings the methane molecules are vibrating".

The slope of the curve is highest at lower pressures and levels off at higher pressures. It was investigated if the curve was an exponential one by making the same plot with a logarithmic scale. This plot is shown in Fig. 6.10, Plot II. As it is seen the data points do not follow a straight line and it is concluded that the curve is not an exponential one. The curve seems to reach a constant value, intensity ratio ~0.5, at higher pressures. It was therefore decided to investigate if the intensity ratio remains at this constant value at even higher pressures. A Raman spectrum of a pure methane sample (N45, Hede Nielsen A/S) contained in the titanium cell at a pressure of 39.6 MPa_A was obtained. This spectrum is shown in Fig. 6.11. The spectrum was very intense even though the integration time was short (15 seconds) because of the high pressure (i.e. high gas concentration). A fluorescence background was observed in the left end of the spectrum probably due to the sapphire windows. A baseline can be estimated but because of the broadness of the methane ν_3 band (due to the high pressure), it was not possible to measure the intensity precisely. The plot in Fig. 6.12 shows the same plot as shown in Fig. 6.10, included the intensity ratio,

Iv_3 / $I2v_2$, at the pressure of 39.6 MPa_A. The tendency is clear – the intensity ratio is lower than 0.5.

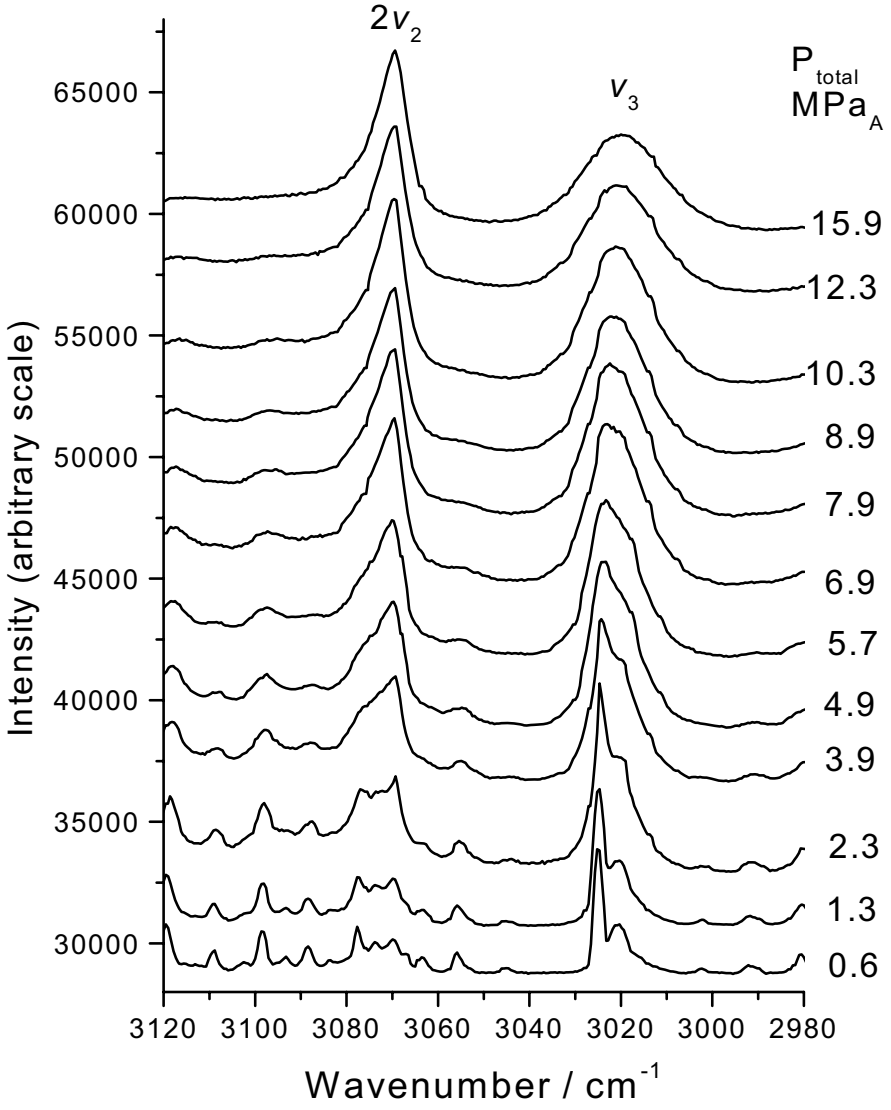

Fig. 6.9. Raman spectra of the methane / nitrogen ($X(CH_4)$ = 0.47) mixture in the pressure range 0.6 – 15.9 MPa_A. Experimental details as described in legends to Fig. 6.2.

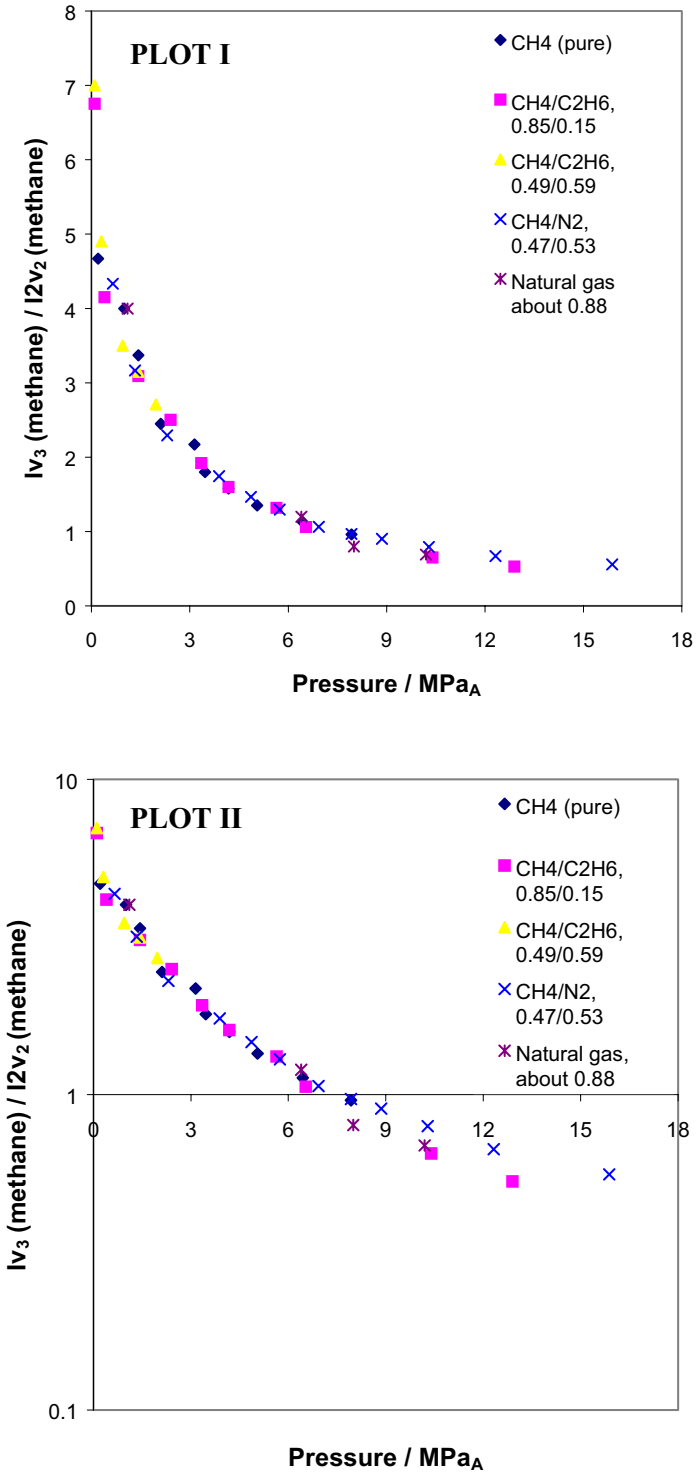

Fig. 6.10. Intensity ratio, Iv_3 / $I2v_2$, as a function of pressure for the pure methane sample and the methane mixtures. Plot I: normal scale and Plot II: logarithmic scale.

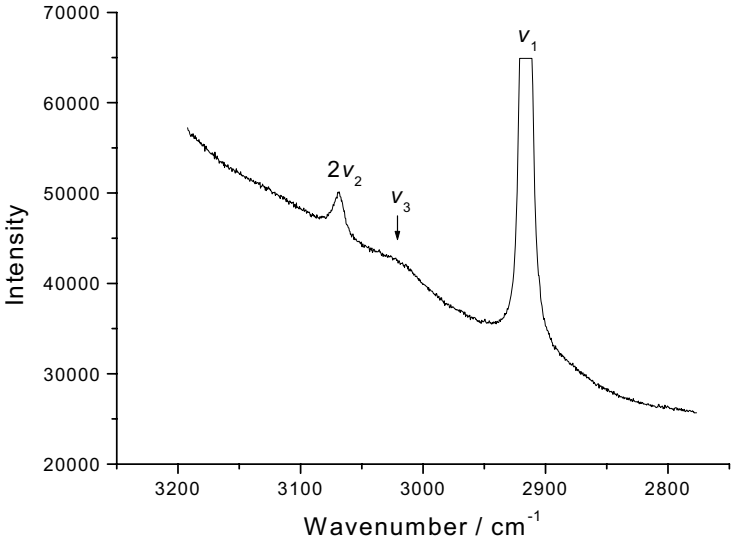

Fig. 6.11. The Raman spectrum of a pure methane sample contained in the titanium cell at a pressure of 39.6 MPa_A. The spectrum was acquired by use of the 1st spectrograph and the 514.53 nm_{air} excitation line from the Ar-ion laser (~200 mW). The collection geometry was 180° (back scattering).

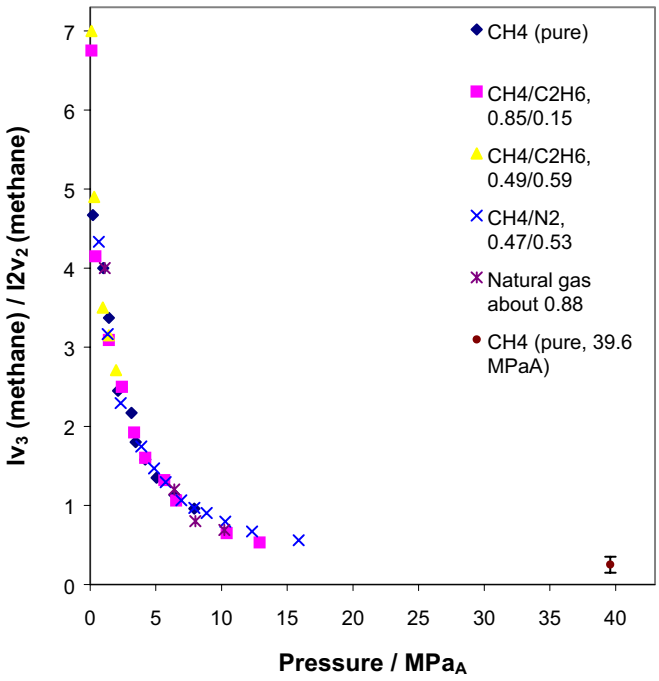

Fig. 6.12. Intensity ratio, Iv_3 / $I2v_2$, as a function of total pressure for the pure methane sample and the methane mixtures (also shown in Fig. 6.10). In the plot is included the intensity ratio calculated from the Raman spectrum of the high pressure methane sample (39.6 MPa_A).

6.5. Conclusion

The intensity ratio between two methane bands, $I\nu_3$ / $I2\nu_2$, has been studied as a function of total pressure in a pure methane sample, in two methane / ethane mixtures, in natural gas and in a methane / nitrogen mixture. The results were surprising in that way that the intensity ratio showed to be independent of the composition and thereby of the surroundings in which the methane molecules are vibrating. It is therefore concluded that by means of these to bands it is possible to determine pressures in methane mixtures. The composition needs not to be known nor determined. The plot of the intensity ratio as a function of total pressure was shown not to be an exponential curve. It is a future goal to investigate how the curves would look like if the intensity ratios were plotted as a function of gas density instead of pressure. In the equimolar methane / ethane mixture a problem occurred due to partial overlap of important bands at higher pressure. The overlap arose because of a broadening of the ethane $2\nu_{11}$ band with increasing pressure reaching the methane ν_3 band. If the intensity method should be used to determine the pressure in methane / ethane mixtures with *high* ethane contents, then methods to resolve the two bands (methane ν_3 and ethane $2\nu_{11}$) have to be developed. So far the method should be useful to determine the pressure e.g. in natural gas and fluid inclusions in rocks.

6.6. References

1. D. Fabre and B. Oksengorn, "Pressure and density dependence of the CH_4 and N_2 Raman lines in an equimolar CH_4/N_2 gas mixture", Appl. Spectrosc. **46**, 468 (1992).
2. J. C. Seitz, J. D. Paseris and I.-M. Chou, " Raman spectroscopic characteriszation of gas mixtures. I. Quantitative composition and pressure determination of CH_4, N_2 and their mixtures", Am. J. Sci. **293**, 297 (1993).
3. J. C. Seitz, J. D. Paseris and I.-M. Chou, "Raman spectroscopic characterization of gas mixtures. II. Quantitative composition and pressure determination of the CO_2-CH_4 system", Am. J. Sci. **296**, 577 (1996).
4. S. Brodersen, D. L. Gray and A. G. Robiette, Mol. Phys. **34**, 617 (1977).
5. S. Brodersen, "High-Resolution Rotation-Vibrational Raman Spectroscopy" in *Topics in Current Physics, Raman Spectroscopy of Gases and Liquids*, A. Weber, Ed. (Springer-Verlag, New York, 1979), Chap. 2, p. 7.

7. Raman Spectroscopic Studies of Gasoline

7.1. Introduction

Gasoline taken directly from the refinery is not useable in an internal combusting engine. It would make the engine knock, especially at low temperatures. The gasoline octane number is an experimentally determined value, which defines the antiknock quality. To increase this number TEP (tetraethyl lead) was added for many years to the gasoline. Oxygenates, e.g. methanol, ethanol and MTBE, also exhibit the effect to increase the octane number. MTBE was chosen as a substitute for the very toxic and polluting TEP, among other things because it is cheap to produce. In the recent years there has been a public interest about MTBE, primarily because American investigations have shown that MTBE is able to penetrate the soil and thus pollute the underground water reserves. On January 1st 2000 a new legislation was introduced in Denmark with respect to aromatics in gasoline: the maximum allowed benzene content was fixed to be 1 % and the maximum total aromatic content was 42 %[1]. Before this date there was no restrictions with respect to total aromatic content. Since aromatics also act as octane boosters the legislation caused that more MTBE had to be added to the gasoline.

Danish gasoline is analysed in many different ways. For instance the total aromatic content is determined by a PIONA analyser, which is based on a gas chromatographic method. The parafines (alkanes), iso parafines, olefines (alkenes), naphthenes and aromatics in the gasoline are separated and analysed. The benzene and MTBE contents are also traditionally determined by gas chromatographic methods[1]. Raman spectroscopic studies of gasoline have occasionally been described in the literature, e.g. with respect to octane number and Reid vapour pressure[2,3,4], percent content of oxygen[5] and aromatics[6,7]. It was found of interest in the Ph.D. project to investigate the feasibility of the Raman technique to analyse gasoline by univariate data treatment. The present Chap. 7.2 is concerned with Raman spectroscopic studies of MTBE content in gasoline. The chapter summarises some of the work presented in our publication “Determination of methyl tertiary butyl ether (MTBE) in gasoline by Raman spectroscopy” (Appendix F). In Chap. 7.2 is also included some considerations about determination of MTBE in water, Chap. 7.2.4. Chap. 7.3 concerns

further Raman spectroscopic studies of gasoline, primarily with respect to aromatics, and some considerations on the contents of sulphur compounds are also included, Chap. 7.3.1.

7.2 Determination of Methyl Tertiary Butyl Ether (MTBE) in Gasoline by Raman Spectroscopy

7.2.1 The Raman Spectrum of Pure MTBE

A pure MTBE[i] sample (>99.9 % by vol., Fischer) stored in a 0.2 ml injection glass sealed with an Al stopper was placed under the microscope for Raman measurement. The FT-IR spectrum of the sample was also obtained. These spectra are presented in Fig. 7.1.

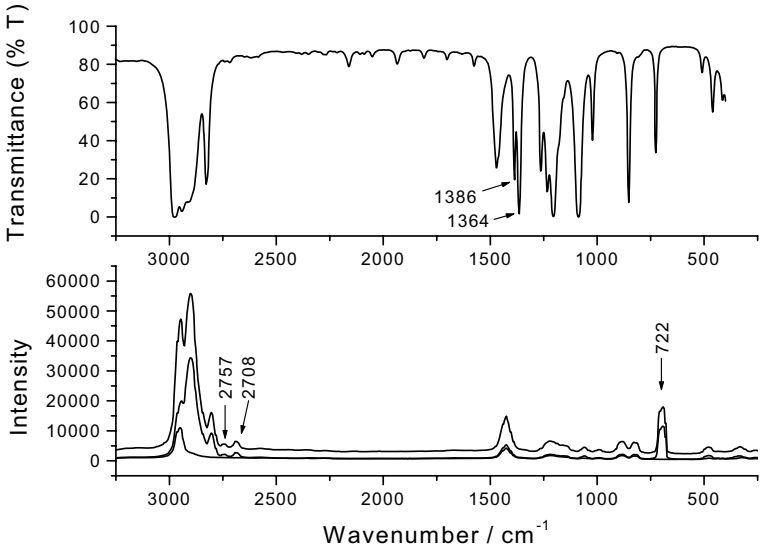

Fig. 7.1. FT-IR spectrum and Raman spectra of the MTBE sample. The FT-IR spectrum was acquired by use of a Fourier transform infrared spectrometer (Perkin Elmer FT-IR 1760X). The spectrum consisted of 4 scans at 4 cm^{-1} resolution. The cell used was a 0.0125 mm liquid cell with KBr windows. The Raman spectra were acquired by use of the 2nd monochromator and the 514.53 nm_{air} line of the Ar-ion laser as the excitation source. The upper Raman spectrum was obtained with no polarizer and the lower Raman spectra were obtained by use of a polarizer in the scattered beam. The sample was placed in the microscopic position.

The IR active symmetric CH_3 "umbrella" deformation at ~1375 cm^{-1} splits up in two bands in tert- butyl compounds, ~1391-1381 cm^{-1} and ~1368-1366 cm^{-1}, and the one with lowest

[i] MTBE (methyl tertiary butyl ether): $CH_3OC(CH_I)_3$

wavenumber is the most intense[8a]. This point was also mentioned in Chap. 4.3.2, in the study of the Oppanol compound. The splitting is clearly seen (indicated with arrows) in the FT-IR spectrum shown above. The two Raman active overtones (2ν) of the splitting are also observed, but they are relatively weak (indicated with arrows at ~2757 cm^{-1} and ~2708 cm^{-1}). The band at ~722 cm^{-1} is due to the C-C symmetric stretching involving the tertiary carbon in the tert-butyl group[5,9]. Thus it can be concluded that the two overtone bands and the band at ~722 cm^{-1} might candidate to be used to search for MTBE in the Raman spectra of gasoline. The two overtone bands however were so weak that they were not expected to be detected.

7.2.2 The Raman Spectra of Octane 98 Gasoline Samples

Several unleaded octane 98 gasoline samples were collected from different local gasoline stations (North Zealand) during the spring / summer 1998. Raman spectra of the gasoline samples were at first obtained by visible light excitation (514.53 nm_{air} line of the Ar-ion laser). All of the gasoline samples were fluorescing resulting in a broad background in the Raman spectra. An example of such a fluorescent gasoline Raman spectrum will be presented in Chap. 7.3 (Fig. 7.3). Attempts to correct for the fluorescence backgrounds were done by means of mathematical data manipulation (first, second and third order polynomials were introduced to make a smooth background curve that could be subtracted from the spectra). Even though this correction resulted in remarkably better spectra, it was not at all possible to detect the two overtone bands at ~2757 cm^{-1} and ~2708 cm^{-1}, and neither the band at ~722 cm^{-1} was observed. Thus it was decided to investigate how large the MTBE content should be to make the bands visible in a Raman spectrum of such a home-made "artificial" gasoline mixture.

7.2.3 The Raman Spectra of Artificial Gasoline Samples

"Artificial" gasoline samples were prepared by mixing heptane with MTBE in different concentrations, 30-100 vol.% MTBE. (Heptane: >99.5 %, Fischer). The mixtures were made volumetrically and contained in 0.2 ml injection glasses sealed with an Al-stopper. Heptane was chosen because it gave little fluorescence. Surprisingly high fluorescence backgrounds were however observed in the Raman spectra. The fluorescence arose from the liquids themselves when mixed. This observation was seen repeatedly.

The characteristic MTBE band at ~722 cm^{-1} was observed in all of the spectra, but only weakly in the spectrum of the 30 vol.% MTBE mixture extensively covered by the fluorescence. It was observed that the more dilute the mixture the weaker became the band at ~722 cm^{-1}, in comparison to the C-H stretching bands. The correlation between the C-H stretching band areas and the MTBE ~722 cm^{-1} butyl band areas was found by the area ratio method. The total integral under the C-H stretching and the ~722 cm^{-1} bands were found by using the software associated with the Raman instrument[10] (the fluorescence backgrounds were left out by user-guided experimentation). The area ratio, A(722 cm^{-1})/A(C-H stretching bands), was plotted versus the vol.% of MTBE. A clear tendency was observed; The points followed a straight line but scattered with some uncertainty (linear regression forced through the origin gave R^2 of 0.944). It was concluded that the area ratio plots might be used to determine the volumetric MTBE percentage in an unknown binary sample provided the fluorescence was not too strong.

7.2.4 Determination of the Detection Limit of MTBE in Drinking Water

MTBE dissolves in water and is able to penetrate soil and thus pollute the underground drinking water reserves. If that happen it can cause the water to be undrinkable due to poor taste and odour. We thus found it of interest to investigate if it should be possible to detect MTBE in drinking water down to very low concentrations. MTBE / water mixtures were prepared and the Raman spectra of the samples were obtained. Some of these spectra are presented in Fig. 7.2.

In Fig. 7.2 it is seen that it was possible to detect a level of MTBE content in water down to 0.50 vol.% by means of the butyl band at ~720 cm^{-1} without any problems. With respect to the sample containing 0.33 vol.% MTBE the band was faintly seen, and at lower concentrations it was not possible within a reasonable time to detect the band at all. It is therefore concluded that the detection limit of MTBE in water by means of our Raman instrument is on the order of 0.3-0.4 vol.%.

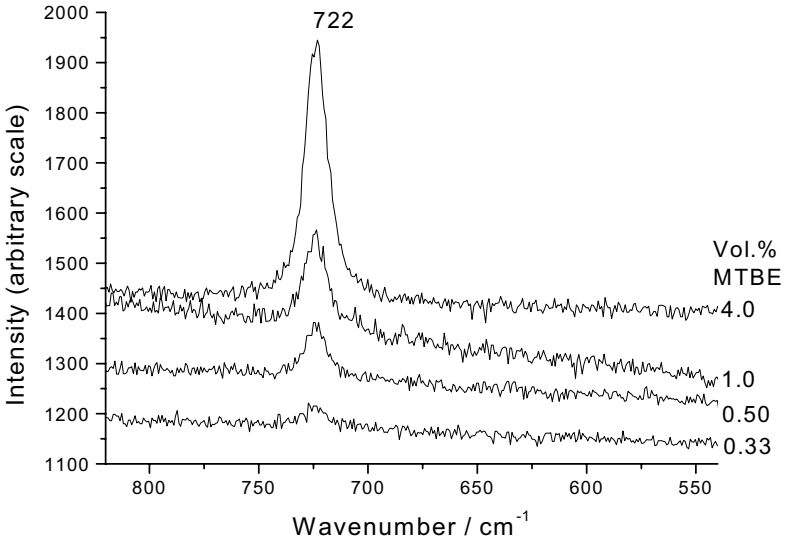

Fig. 7.2. The Raman spectra (820-540 cm^{-1}) of MTBE / water mixtures (0.33, 0.50, 1.0 and 4.0 vol.% MTBE) acquired by use of the 1st spectrograph (1800 grooves per mm) and the 514.53 nm_{air} line of the Ar-ion laser as the excitation source (~200 mW, vertically polarized). The samples were contained in glass ampoules and placed in the macroscopic position (90° collection geometry).

7.3. Further Raman Spectroscopic Studies of Gasoline

7.3.1 Introduction

From the work dealing with determination of MTBE content in gasoline it was concluded that Raman excitation by visible light detection causes a broad fluorescence background in the spectra. Attempts to subtract the fluorescence background were done, but still it was difficult to detect small amounts of MTBE. Thus it was decided to try using the NIR-FT Raman technique (cf. Chap. 2.1) in the studies on gasoline with respect to aromatics. The technique has also been used previously to determine the content of aromatic in gasoline by use of partial least square regression models[7]. The present study was primarily focused on the benzene content in gasoline. The FT-Raman spectrum of a Danish unleaded octane 98 gasoline sample is shown in Fig. 7.3. In the figure the fluorescence Raman spectrum of the same gasoline sample is also included excited with green laser light.

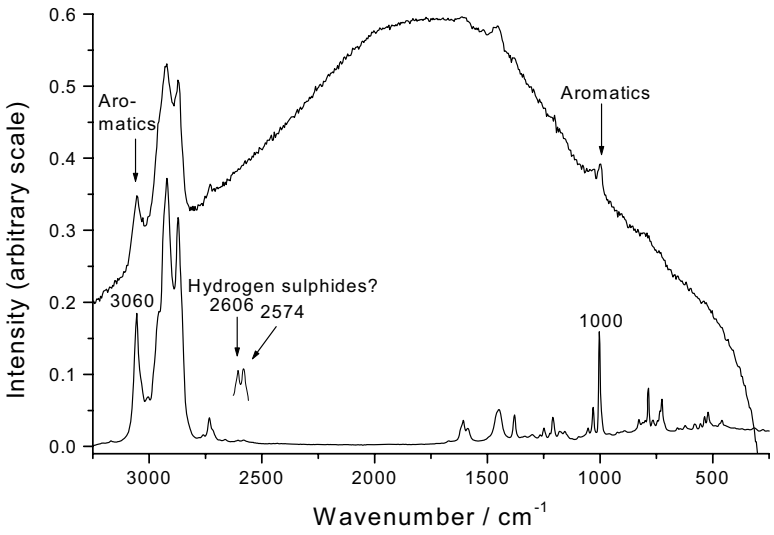

Fig. 7.3. Upper curve: The Raman spectrum of an unleaded octane 98 gasoline sample (from the area of Copenhagen), acquired by use of the 2nd monochromator (grating: 600 grooves/mm). The sample was placed in the microscopic position (10 x objective), i.e. 180 ° scattering. The 514.53 nm_{air} line from the Ar-ion laser was used as the excitation source (~200 mW). The obtained spectrum was divided by a factor of hundreds. Lower curve: The FT-Raman spectrum of the same gasoline sample. The sample was placed in a little tube of quartz. A small part of the spectrum (2625-2560 cm^{-1}) was blown up by a factor 20.

Aromatics were detected in both of the spectra at ~3060 cm^{-1} and ~1000 cm^{-1}. Before working further with this issue (in Chap. 7.3.3) we need to make some considerations about the two weak bands at (~2606 cm^{-1} and ~2574 cm^{-1}) clearly seen in the blown up part of the FT-Raman spectrum. The two bands probably are due to sulphur compounds.

7.3.2 Detection of Hydrogen Sulphide and Thiols in Gasoline?

Because of the position in a range where not many other compounds occur the two bands at ~2606 cm^{-1} and ~2574 cm^{-1} were interpreted (tentatively) as S-H stretching bands. H_2S bands were previously observed at ~2585 cm^{-1} in the Raman spectra of natural gas samples at high pressures (1.1 – 10.2 MPa_A) (see Chap. 4.3, Fig. 4.13.a). As discussed it was surprising that it was possible to detect it at all since H_2S is only present in Danish domestic distributed natural gas at very low concentrations. The Raman spectrum of a home-made H_2S gas sample was also obtained and a band at ~2617 cm^{-1} was observed (Chap. 4.3, Fig. 4.15), in close accordance with the value given in the literature for the gas phase, 2611 cm^{-1}. Thus it was obvious to assign the band at ~2606 cm^{-1} as symmetric S-H stretching (in gas phase). According to Danish gasoline companies the level of *total* sulphur content is typically about 50 ppm (maximum value is 150 ppm). Two methods are traditionally used to reveal hydrogen sulphides, a copper strip corrosion method and a "doctor test", ASTM[ii] 4952. It has however not been possible for us to get information on the level of H_2S content, because that it is not measured routinely. According to the gasoline companies however the level is very low, informed guess: <1 ppm[1]. Hydrogen sulphide is absolutely undesirable in gasoline[1]. Not only H_2S molecules but also hydrogen sulphides are present in gasoline as thiols[iii] (mercaptans). A strong polarized band in the S-H stretching region is found in the Raman spectrum for both the R-SH and Ar-SH sort of thiols. In the liquid phase the S-H stretching vibration is observed at 2590-2560 cm^{-1} for R-SH and at 2580-2560 cm^{-1} for Ar-SH[8b]. The same vibration is observed at 2598-2584 cm^{-1} for R-SH in the vapour phase[8b,11]. It is however presumed that the thiols only are present in gasoline in the liquid state. In the view of this, the two bands observed at ~2606 cm^{-1} and ~2574 cm^{-1} in the gasoline sample was interpreted as S-H stretching in hydrogen sulphide and in alkanethiols. It is quite interesting that the Raman method seems to be suited to measure

[ii] ASTM:American Society for Testing and Materials
[iii] R-SH (alkanethiols) and Ar-SH (benzenethiols)

sulphur components in gasoline. When studying Raman spectra obtained of other components present in the gasoline, peaks near the S-H stretching area were observed, arising from overtones and combination bands. In a FT-Raman spectrum of o-xylene obtained recently by the author, a weak polarized band was observed ~2578 cm^{-1}. The same weak band has been observed in the literature ~2580 cm^{-1} (exact value was not given)[12a]. This value is very close to the observed band at ~2574 cm^{-1} in the FT-Raman spectrum of gasoline interpreted as discussed above as S-H stretching in thiols. Thus although the above-discussed interpretation is very tentatively it might be extended to other cases. As concluded previously further Raman studies of hydrogen sulphide and hydrogen sulphide mixtures need to be done.

7.3.3 Detection of Aromatics in Gasoline by FT-Raman Spectroscopy

At first it was decided to focus on the determination of benzene contents in gasoline by use of the area ratio method. Benzene was diluted by mixing it with heptane. Seven mixtures were prepared with different known concentration in the range 0.5 – 20 % by volume. The chemicals at hand were: Benzene from Merck (1782) and heptane (>99.5% by vol.) from Fischer. FT-Raman spectra of pure benzene and heptane samples were obtained. These spectra are presented in Fig. 7.4.

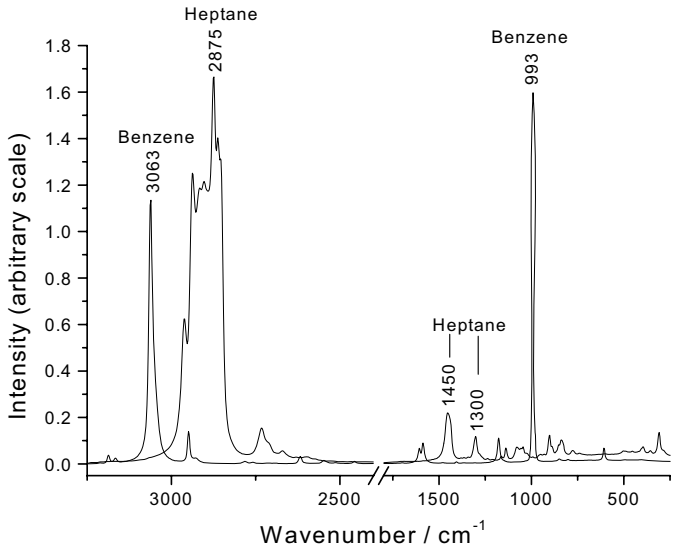

Fig. 7.4. The FT-Raman spectra of a pure benzene sample and a pure heptane sample. The samples were placed in small tube of quartz. Characteristic bands for each sample are indicated with sample name and the wavenumber position.

Suitable bands, i.e. characteristic bands in which the area can be easily determined, were searched for. The choices with respect to benzene were, as indicated in the figure, the ~3063 cm^{-1} (C-H symmetric stretching) and ~993 cm^{-1} (C-C stretching) bands. With respect to heptane the ~1450 cm^{-1} (C-H bending) and ~1300 cm^{-1} (-$(CH_2)_5$- in phase twist)[8a] bands were chosen. Even though the heptane band at ~2875 cm^{-1} is overlapped by several bands, it was decided to include it to get experience with peak fitting by the Microcal Origin[13].
The FT-Raman spectra of all the prepared benzene / heptane mixtures were obtained. These spectra are shown in Fig. 7.5.

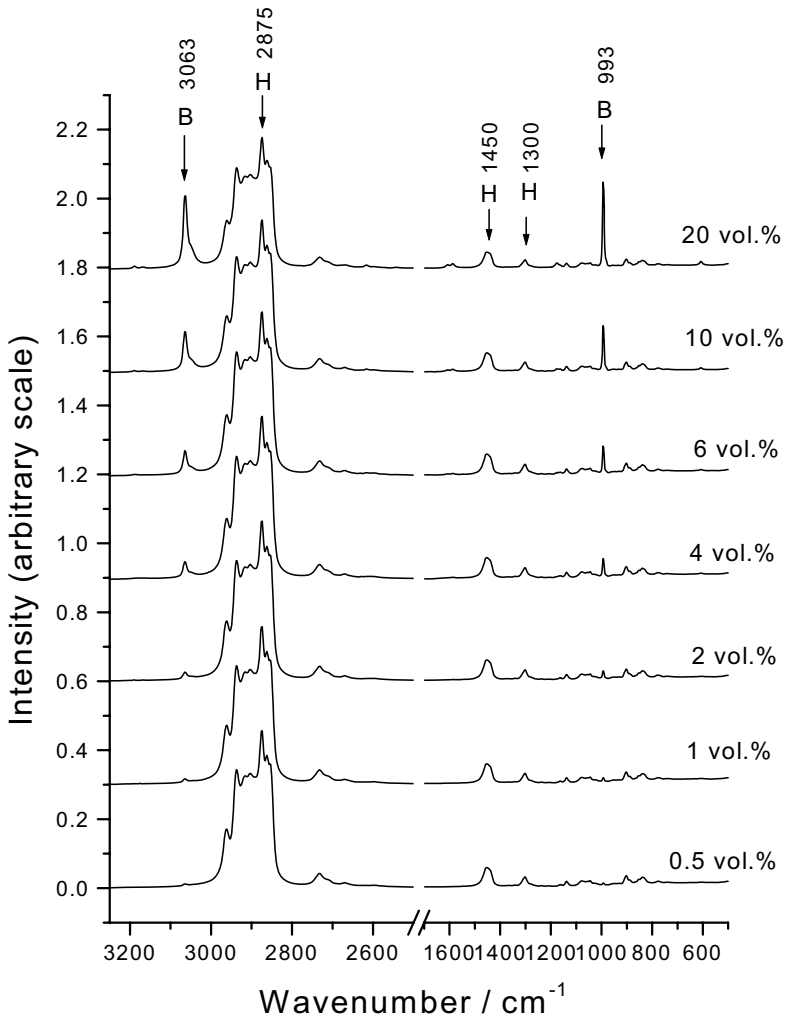

Fig. 7.5. The FT-Raman spectra of the benzene / heptane mixtures as a function of benzene concentration. The letter B indicates benzene bands and the letter H heptane bands.

It is clearly seen in Fig. 7.5 that the intensity of each of the two benzene bands (at ~3063 and ~993 cm^{-1}) increases relatively to the heptane bands as the benzene concentration increases. The intensity relations between the benzene bands and the heptane bands as a function of the benzene concentration in the mixtures were investigated. At first, areas of selected bands (indicated with arrows in the Figure) were determined by means of the Microcal Origin peak fitting module (PFM)[13]. The areas of the bands at ~3063 cm^{-1}, ~1450 cm^{-1}, ~1300 cm^{-1} and ~993 cm^{-1} could be determined without any complications. Because of the overlap of several bands in the C-H stretching region however some care must be applied, when resolving the band at ~2875 cm^{-1}. In Fig. 7.6 we present seven overlapping heptane C-H stretching bands from the upper FT-Raman spectrum shown in Fig. 7.5 (i.e. the 20 vol. % benzene mixture). The bands were resolved by the PFM and this result is also presented in Fig. 7.6. The Lorentz function was used as the fitting function.

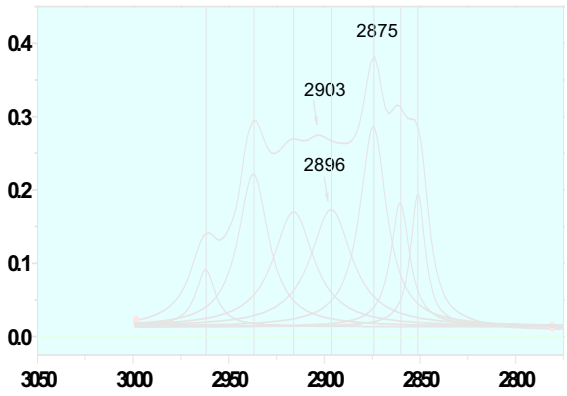

Fig. 7.6. Upper curve: The FT-Raman spectrum of a benzene / heptane mixture (20 vol.% benzene) in the aliphatic C-H stretching region (3000-2550 cm^{-1}). Lower curves: The resolved heptane bands (fitting function: Lorentz). Correlation coefficient: 0.99673.

It is seen that the bands can be well resolved. According to the horizontal lines included in the figure it is obvious that the wavenumber position for each band is the same before and after it has been resolved, except for one band. The band seemed to be at a wavenumber position of ~2903 cm^{-1} before it was resolved and at ~2896 cm^{-1} after it was resolved. This tendency was reproducible in all of the obtained FT-Raman spectra of the methane / heptane mixture presented in Fig. 7.5.

The areas of the bands at ~3063 cm^{-1}, ~2875 cm^{-1}, ~1450 cm^{-1}, ~1300 cm^{-1} and ~993 cm^{-1} were all determined. The baselines were all estimated by "free form". All the determined areas are listed in Appendix E. The area ratio, A(benzene band) / A(heptane band), was plotted as a function of the benzene concentration. This work is presented in Fig. 7.7. As it is seen there is an obvious linear correlation between area ratio and the benzene concentration. Thus it was concluded that the presented curves can be used for a determination of the benzene contents in benzene / heptane mixtures. It was furthermore concluded that it should be possible by the same area ratio method to determine the benzene contents in gasoline. Before we go further, into this issue however some considerations had to be done.

Besides benzene there are other aromatics present in gasoline, that is methylbenzene (toluene), ethylbenzene and dimethylbenzene (xylene) isomers (ortho-, meta- and para-xylene) to mention the simplest. Benzene and these simple aromatics are often given as the acronym BTEX in the literature. The FT-Raman spectrum of a pure benzene sample was shown in Fig. 7.4. It was decided to obtain FT-Raman spectra of the "TEX" too. The chemicals were provided: toluene (PA, Ferak 01548), ethylbenzene (PA, Fluca 03030), o-xylene (S, Merc 808697), m-xylene (PA, Fluca 95672) and p-xylene (PA, Fluca 96682). The FT-Raman spectra were obtained of all of the samples. The C-H stretching parts of the spectra (3100–2800 cm^{-1}) are presented in Fig. 7.8. In the figure are also included the FT-Raman spectrum of an octane 98 gasoline sample (shown in Fig. 7.3) and the FT-Raman spectrum of benzene (shown in Fig. 7.4). The gasoline spectrum is presented as a dashed curve and the benzene spectrum as a dotted curve.

The above discussed area method to determine benzene content in heptane (or gasoline) was e.g. based on the aromatic C-H stretching band at ~3063 cm^{-1}. As it is seen in the Fig. 7.8 each of the aromatics has a band near this wavenumber position. In fact the bands are so close to each other that it (so far) not has been possible to resolve them. It is therefore concluded that the band at ~3063 cm^{-1} is useless, when determining the *benzene* content in gasoline by the discussed area ratio method. But the possibility remains that the band could be used in a determination of the total aromatic content.

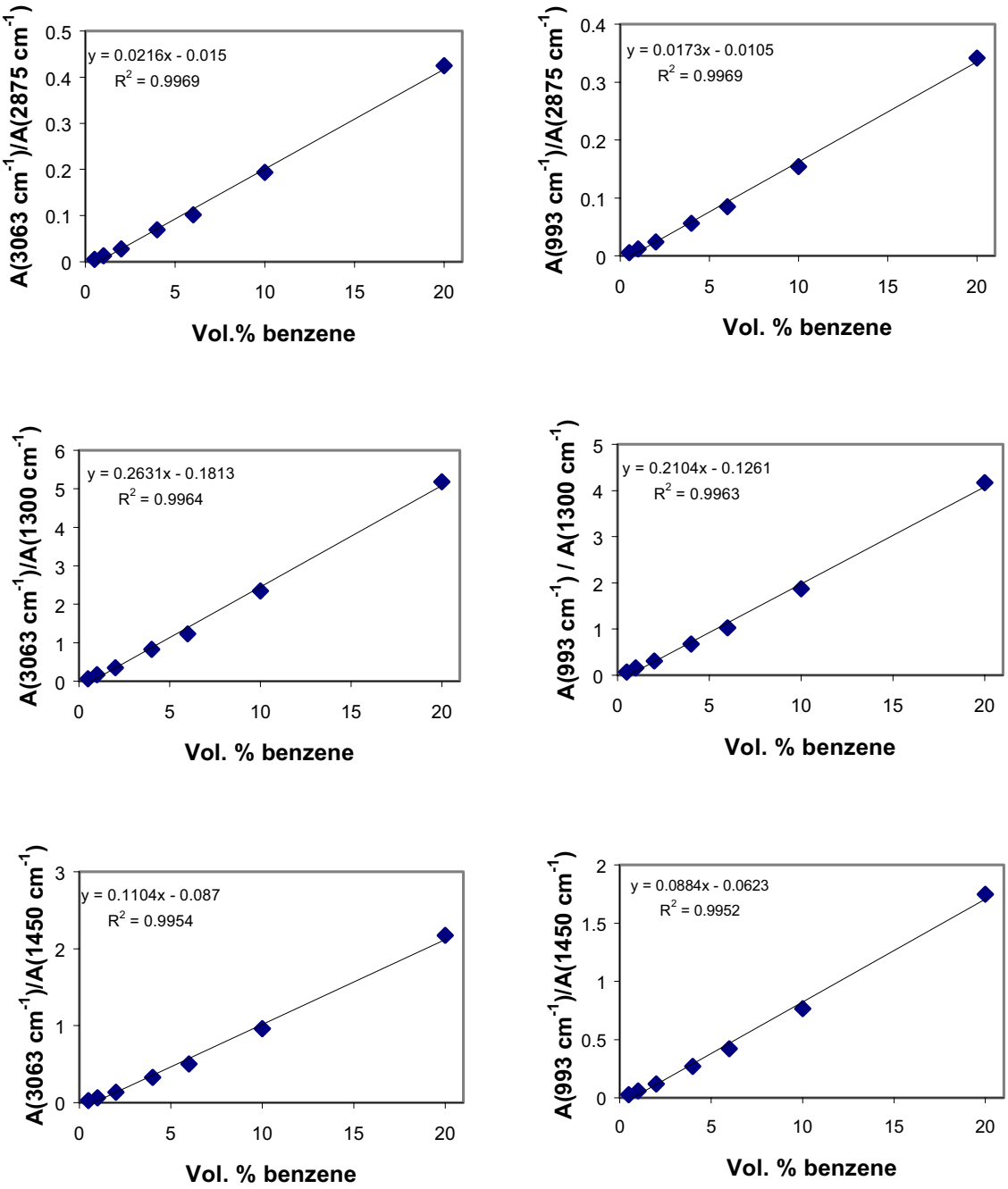

Fig. 7.7 The area ratio A(benzene) / A(heptane) as a function of benzene concentration by volume.

The CH_3 symmetric stretching vibration band occurs near 2882-2862 cm^{-1} (and the antisymmetric near 2972-2952 cm^{-1})[8a]. In the FT-Raman spectrum of the octane 98 gasoline sample the symmetric stretching band was observed at ~2875 cm^{-1}, as seen in Fig. 7.8. With respect to the toluene and xylene isomers however the CH_3 symmetric stretching bands were observed at a lower wavenumber position ~2863 cm^{-1}. For molecules with one or more CH_3 groups attached directly to a benzene ring, two bands are regularly observed in the Raman spectra, at positions near 2925 cm^{-1} and 2865 cm^{-1}. These two bands are assigned as the overtone (2ν) of the CH_3 bending vibration at ~1450 cm^{-1} in Fermi resonance with the CH_3 symmetric stretching vibration[14]. This phenomenon is clearly seen in the FT-Raman spectra of toluene and the xylene isomers shown in Fig. 7.8 (the overtone at ~2920 cm^{-1} and the CH_3 symmetric stretching at ~2863 cm^{-1}). Because of the Fermi resonance the overtone bands occur with a relatively high intensity and the CH_3 symmetric stretching bands with relatively low intensities. Thus it was decided that the band at ~2875 cm^{-1} should be used in the area ratio method, but some uncertainty might arise due to the CH_3 symmetric stretching bands belonging to the aromatics.

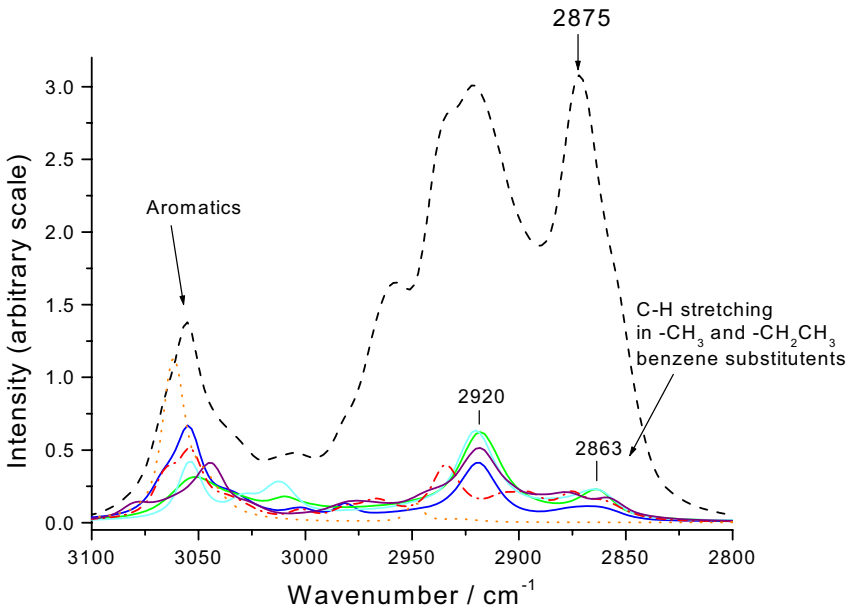

Fig. 7.8. The FT-Raman spectra (3100-2800 cm^{-1}) of toluene, ortho-, meta- and para-xylene (lower curves), ethylbenzene (dashed dotted curve), benzene (dotted curve) and an octane 98 gasoline sample (dashed curve).

The FT-Raman spectra of the BTEX and the octane gasoline spectrum are presented in Fig. 7.9 in the wavenumber ranges of 1080-960 cm^{-1} (A) and 860-700 cm^{-1} (B).

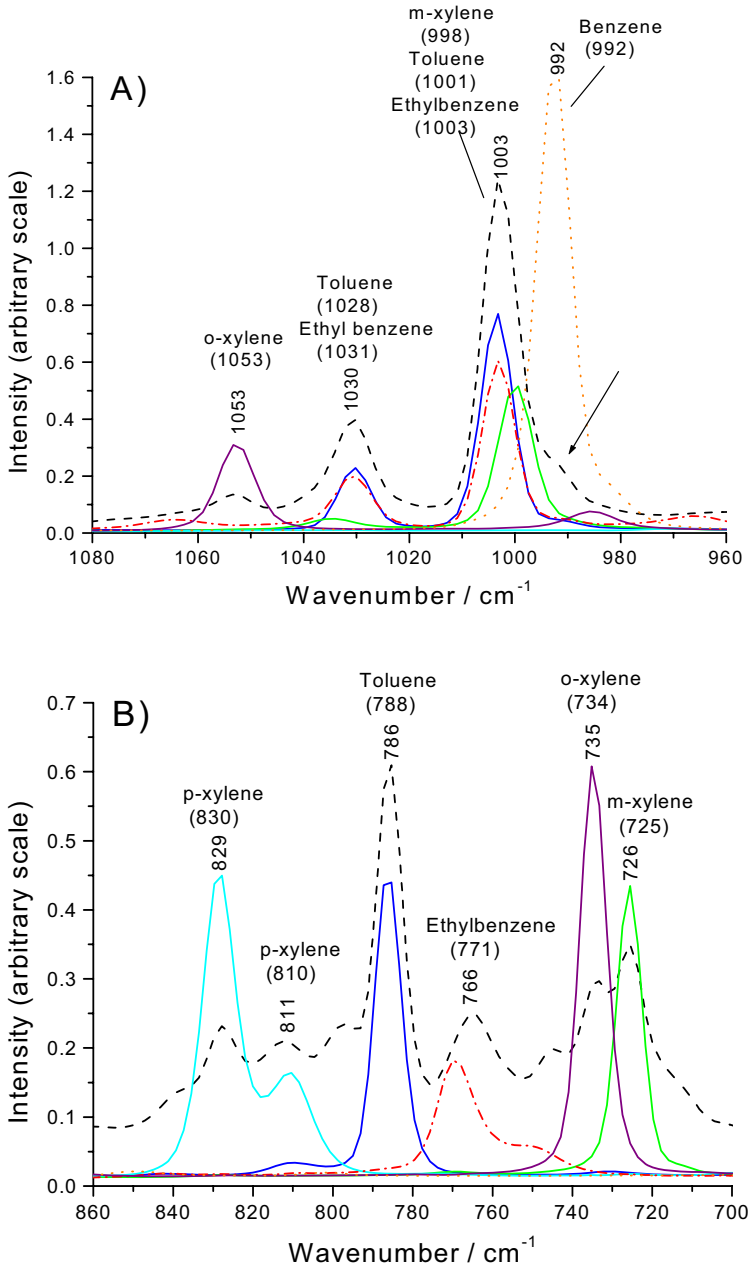

Fig. 7.9. The FT-Raman spectra of toluene, ortho-, meta- and para-xylene (solid curves), ethylbenzene (dashed doted curve), benzene (dotted curve) and the octane 98 gasoline sample (dashed curve). Wavenumbers in parentheses are values given in the literature[12a,b]. A) 1080-960 cm^{-1}, and B) 860-700 cm^{-1}.

At first it was investigated if the benzene C-C stretching band at ~993 cm^{-1} could be used as a suitable band in the area ratio method. The bands due to aromatics are clearly seen in the FT-Raman spectrum of the gasoline sample, shown in Fig. 7.9.A. The most intense one in the spectrum is the band at ~1003 cm^{-1} arising from vibrations in m-xylene, toluene and ethylbenzene. Very close to this band the benzene C-C stretching vibration is observed at ~993 cm^{-1} as a shoulder. Attempts to resolve the two bands, in the same way as described previously, were done successfully as shown in Fig. 7.10.A. The area of the band at ~993 cm^{-1} was determined to 0.09931 cm^{-1}·counts. Even though the band at ~2875 cm^{-1} in FT-Raman spectrum of the gasoline sample is not a "pure" heptane band, it was decided to try to use it in the are ratio method to see if the magnitude of the content in the gasoline as determined comes out well.

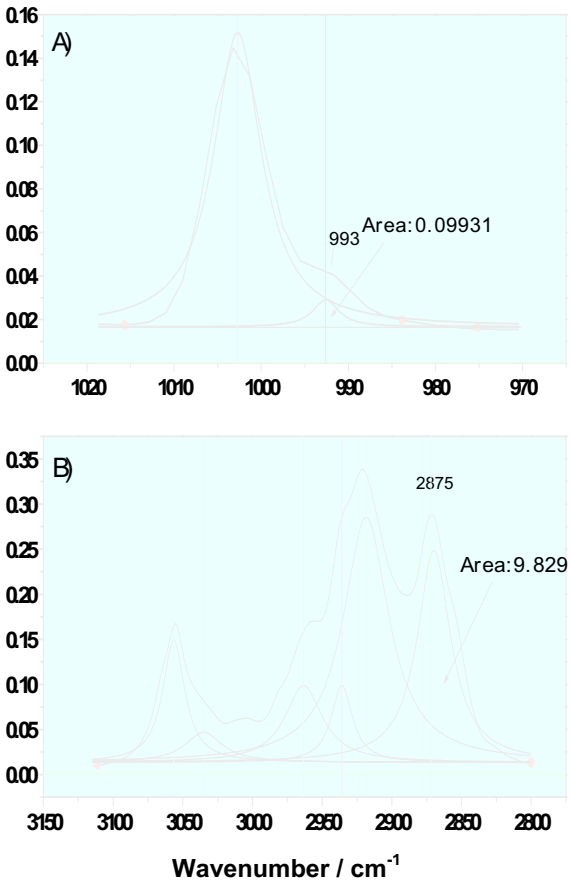

Fig. 7.10. FT-Raman spectrum of the octane 98 gasoline sample. A) The resolved benzene band at ~993 cm^{-1}. Correlation coefficient: 0.98738. B) The resolved CH_3 symmetric stretching band ~2875 cm^{-1}. Correlation coefficient: 0.99444.

At first the gasoline band at ~2875 cm^{-1} was resolved from the other C-H stretching bands in the wavenumber range 3120-2600 cm^{-1}, as shown in Fig. 7.10.B. The area of the band was determined to 9.829 cm^{-1}·count. Thus the area ratio between the two bands were determined to 0.0101.

$$\frac{A(993cm^{-1})}{A(2875cm^{-1})} = \frac{0.09931}{9.829} = 0.0101$$

By using the equation indicated in the Fig. 7.7.b (y = 0.0173x – 0.0105, found by linear regression) the vol.% benzene (x) was calculated to be 1.2 %. The magnitude of the value seems reasonable, but the value is probably lower. It was however included in this chapter for illustrative reasons.

Then it was decided to turn the attention to the FT-Raman spectra of toluene, ethylbenzene and the xylene isomers. There was, as it can be seen in Fig. 7.8 and 7.9.A, a high degree of band overlap in the spectra of toluene and ethylbenzene. The same was the case for the xylene isomers as also concluded in the literature[15]. Characteristic bands for each compound were searched for in the FT-Raman spectra. In the wavenumber range of 860-700 cm^{-1} it was observed that toluene has a characteristic band at ~786 cm^{-1} and ethylbenzene one at ~766 cm^{-1}. Furthermore para-, orto- and meta-xylene have characteristic bands at ~829 cm^{-1}, ~735 cm^{-1} and ~726 cm^{-1} respectively. Unfortunately one cannot be sure that the octane 98 gasoline band at ~726 only arises due to vibrations in meta-xylene. As described in the previous chapter, MTBE shows a band at ~722 cm^{-1} due to symmetric C-C stretching vibrations involving the tertiary carbon in the tert-butyl group. It seems probable that the band at ~726 cm^{-1} in the FT-Raman spectrum of the gasoline sample could be a combination of vibrations in both meta-xylene molecules and MTBE molecules. Moreover another characteristic m-xylene band, which can be easily resolved, was found at ~278 cm^{-1}, as shown in Fig. 7.11. Even though there is a high degree of spectral overlap between the aromatic compounds, it ought to be possible (by means of the above given characteristic bands) to determine the content of each compound by means of the area method.

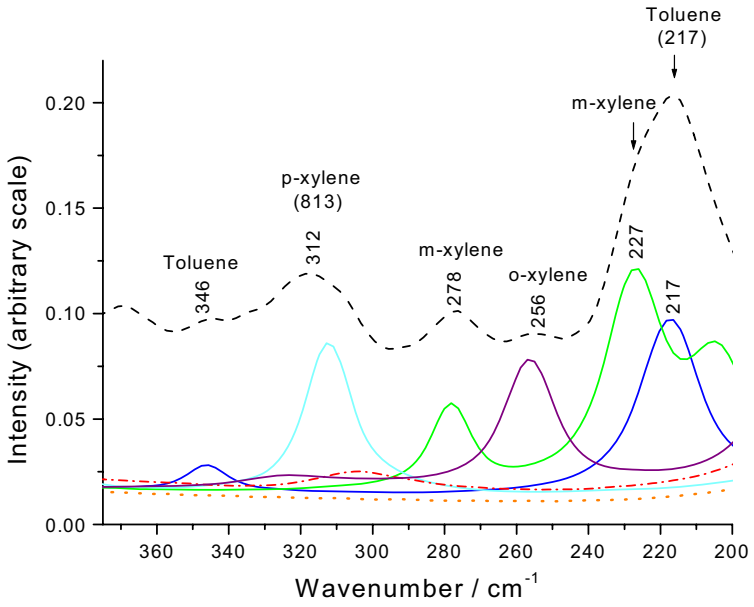

Fig. 7.11. FT-Raman spectra (375-200 cm^{-1}) of toluene, ortho-, meta- and para-xylene (solid curve), ethylbenzene (dashed dotted curve), benzene (dotted curve) and the octane 98 gasoline sample (dashed curve). Wavenumbers in parentheses are values given in the literature[12a,b], (parentheses indicate that an exact value is given in the literature).

7.4. Conclusions

The Raman spectroscopic studies of gasoline were found to be very interesting and informative. One aim was to investigate whether Raman spectroscopy using visible light excitation could be used to determine the MTBE contents in gasoline samples. Two overtone bands (from the symmetric CH_3 umbrella deformation) at ~2757 cm^{-1} and ~2708 cm^{-1}, plus a band at ~722 cm^{-1} arising from vibrations in the tert-butyl group, were characteristic for the Raman spectrum of MTBE. The two overtone bands were too weak to be detected in the Raman spectrum of the examined gasoline sample. The band at ~722 cm^{-1} however was so intense that it ought to be observed if MTBE was present, even at low concentrations. Because of the broad fluorescence backgrounds in the spectra it was concluded that the sensitivity of the Raman method in the present version is not particularly high. The MTBE was not detected at all in any of the obtained Raman spectra of several gasoline samples. The Raman spectra of the "artificial" gasoline samples (prepared by mixing heptane with MTBE) were also influenced by a fluorescence background but to a

lesser degree. The detection limit of the band at ~722 cm^{-1} in these mixtures was in our experimental setup determined to be around 30 vol.% MTBE. The ratio between the area of the band at ~722 cm^{-1} and all of the C-H stretching bands were plotted as a function of the MTBE content. A clear linear correlation was found, but with some uncertainty (R square was 0.944). Finally the detection limit of MTBE in drinking water was determined to 0.3-0.4 vol.% MTBE.

In our spectroscopic studies of gasoline samples with respect to aromatics, the FT-Raman technique was chosen because of the fluorescence under visible light excitation. Two weak bands were observed at ~2606 cm^{-1} and ~2574 cm^{-1} in the Raman spectra of the gasoline samples. It was concluded that such bands might arise from S-H symmetric stretching in hydrogen sulphide and thiols, respectively. "Artificial" gasoline samples were prepared by mixing heptane with benzene. FT-Raman spectra of these samples were acquired. It was obvious that two benzene bands at ~3063 cm^{-1} and ~993 cm^{-1} increased in intensity relatively to three chosen heptane bands at ~2875 cm^{-1}, ~1450 cm^{-1} and ~1300 cm^{-1}, as the benzene content in the mixture was increased. The bands (i.e. the two mentioned benzene bands and the three heptane bands) were resolved and areas determined. The area ratio, A(benzen band) / A(heptane band), was plotted as a function of the benzene content and clear linear correlations were found in all six plots (tendency lines determined by regression gave R square of order 0.996).

In addition to the FT-Raman spectra of an octane 98 gasoline sample and a benzene sample, FT-Raman spectra of toluene, ethylbenzene and the xylene isomers were also obtained. All these spectra were compared. It was with success possible to resolve the benzene band at ~992 cm^{-1} in the FT-Raman spectrum of the gasoline sample. The area of this band was determined and so was the CH_3 symmetric stretching band in the same spectrum. The area ratio was determined and an estimate of the benzene content was given (probably below 1.2 vol. benzene). Finally characteristic bands for toluene, ethylbenzene and the xylene isomers were found. With that in mind it should be interesting to determine the contents of these compounds in gasoline, also by Raman spectroscopy. In further work with Raman spectroscopic studies of gasoline it should be very interesting to remeasure a series of gasoline samples with exactly known composition.

7.5. References

1. Private communications with technical co-ordinators in the product service departments of Station, Shell, Q8 and the refinery in Kalundborg, Denmark.
2. C. J. de Bakker and P. M. Fredericks, "Determination of petroleum properties by fiber-optic Fourier transform Raman spectrometry and partial least-squares analysis", Appl. Spectrosc. **49**, 1766 (1995).
3. J. B. Cooper, K. L. Wise, J. Groves and W. T. Welch, "Determination of octane numbers and Reid Vapor pressure of commercial petroleum fuels using FT-Raman spectroscopy and partial least-squares regression analysis", Anal. Chem. **67**, 4096 (1995).
4. P. E. Flecher, W. T. Welch, S. Albin and J. B. Cooper, "Determination of octane numbers and Reid vapor pressure in commercial gasoline using disperse fiber-optic Raman spectroscopy", Spectrochim. Acta **53A**, 199 (1997).
5. J. B. Cooper, K. L. Wise, W. T. Welch, R. R. Bledsoe and M. B. Sumner, "Determination of weight percent oxygen in commercial gasoline: A comparison between FT-Raman, FT-IR and dispersive near-IR spectroscopies", Appl. Spectrosc. **50**, 917 (1996).
6. R. H. Clarke, W. M. Chung, Q. Wang, D. DeJesus and U. Sezerman, "Determination of aromatic composition of fuels by laser Raman spectroscopy", J. Raman Spectrosc. **22**, 79 (1991).
7. J. B. Cooper, K. L. Wise, W. T. Welch, M. B. Sumner, B. K. Wilt and R. R. Bledsoe, "Comparison of near-IR, Raman and mid-IR spectroscopies for the determination of BTEX in petroleum fuels", Appl. Spectrosc. **51**, 1613 (1997).
8. D. Lien-Vien, N. B. Cholthup, W. G. Fately and J. G. Grasselli, *The Handbook of Infrared and Raman Frequencies of Organic Molecules* (Academic Press, Boston, 1991), a) chap. 2, b) chap. 14.
9. J. A. Dean, *Handbook of Organic Chemistry*, (McGraw-Hill, New York, 1987).
10. Speclab version 2.01 (Dilor SA, 1996).
11. R. A. Nyquist, "The interpretation of vapor phase infrared spectra, group frequency data", Sadtler Research Laboratories **1**, (1984).
12. *Raman / IR Atlas of Organic Compounds*, B. Schrader and W. Meier (Verlag Chemie, Weinheim, 1974), group F, a) F3-07, b) F1-01,08,23; F4-05; F5-02).

13. Microcal Origin version 6 and The Peak Fitting Module version 6 (Microcal Software Inc., 1999).
14. A. B. Dempster, D. B. Powell and N. Sheppard, "Vibrational spectroscopic studies of internal rotation of symmetrical groups. III. Toluene and some deuterated derivatives in the condensed state", Spectrochim. Acta **28A**, 373 (1972).
15. C. A. Gresham, D. A. Gilmore and M. B. Denton, "Direct comparison of near-infrared absorbance spectroscopy with Raman scattering spectroscopy for the quantitative analysis of xylene isomer mixtures", Appl. Spectrosc. **10**, 1177 (1999).

8. Raman Spectroscopic Studies of the Ternary system Water-Methanol-Oil

8.1. Introduction

The main goal of the present work was to investigate if it would be possible to provide experimental data of the ternary system water-methanol-oil by means of Raman Spectroscopy. Data of such systems are useful as models for property modification of use in oil recovery. In the recovery e.g. methanol can be added to the water in oil in order to prevent the formation of gas hydrates. Experimental tie-line data (liquid-liquid equilibrium compositions) can be found for some systems in the literature, but most of them are given at 0.1 MPa_A (ambient pressure, see e.g. ref. 1). In this work the purpose was to obtain experimental tie-line data for the water-methanol-oil system as a function of pressure. The different pressures can be achieved simply by using the titanium cell as a container for the mixture and increase the pressure in the same way as described previously for the gas measurements. As a beginning it was decided to investigate the water-methanol-oil system at ambient conditions. As a model oil decane was chosen. The work described in the following is preliminary and is mostly a report of the difficulties so far, especially due to fluorescence. It is, however, concluded that there are some promising prospects in the use of Raman spectroscopy to obtain data in multiphase systems.

Chap. 8.2 concerns the Raman spectroscopic studies of the water-methanol-decane system. It was possible to obtain Raman spectra with success of pure methanol without fluorescence. But especially when mixing methanol with decane a broad fluorescence background occurred in spectra of the methanol phases, but not in the spectra of the decane phases. Thus, it was decided to use the FT-Raman technique instead. In this technique however problems also arose due to backgrounds in the methanol phases and surprisingly also in the decane phases, as will be described in Chap. 8.3. Finally in Chap. 8.4 some considerations are given on the titanium cell, with respect to its suitability as a container for ternary systems.

8.2. Raman Spectroscopic Studies of the Water-Methanol-Decane System

As a beginning Raman spectra of the pure components, water (distilled), methanol (analytical reagent, May & Baker) and decane (>95 %, Merck), were obtained to investigate if there were any fluorescence problems. These spectra are presented in Fig. 8.1. As it is seen there was very little fluorescence at all.

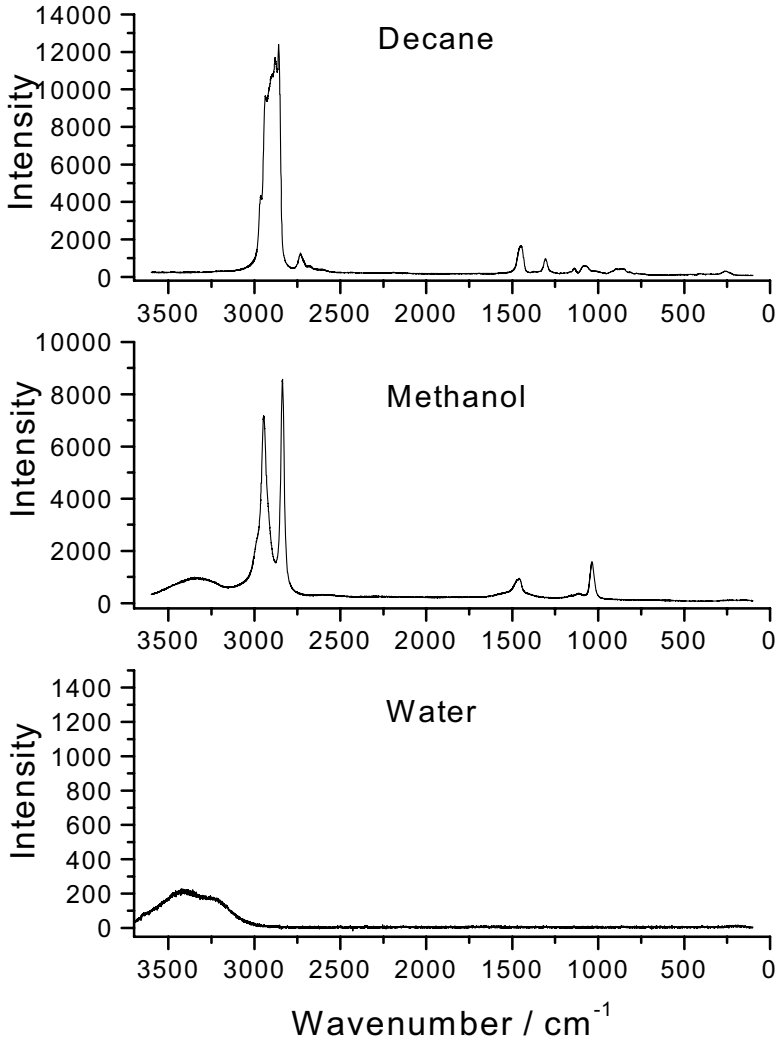

Fig. 8.1. The Raman spectra of pure decane, methanol and water. The spectra were acquired by use of the 1st spectrograph (1800 grooves per mm). The 514.53 nm_{air} line of the Ar-ion laser was used as the excitation source (~200 mW). The samples were contained in test tubes and placed in the macroscopic sampling position (90 ° collection geometry).

Thus it was decided to prepare a series of binary and ternary mixtures of the three components. The compositions of the mixtures were chosen as shown in the triangular diagram in Fig. 8.2. A square and a letter indicate each mixture. The concentrations are given in mole percent and each vertex represents one of the pure components.

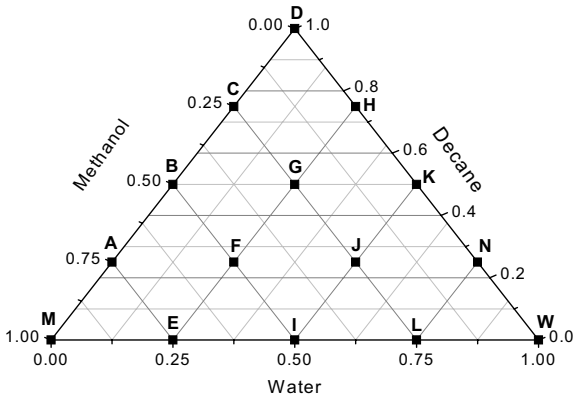

Fig. 8.2. Triangle illustrating the mixtures, which were prepared for Raman measurements.

The mixtures were prepared by weighing the components into test tubes closed with rubber stoppers. Each mixture was shaken well and lift for some time to make sure that an equilibrium had been achieved prior to measurements. The Raman spectrum of the binary mixture A (cf. Fig. 8.2, $X_{decane} = 0.25$ and $X_{methanol} = 0.75$) lower phase, i.e. a phase of mostly methanol, is shown in Fig. 8.3. As it is seen there is a broad fluorescence background. A similar phenomenon was not observed in any of the Raman spectra obtained for the decane phases. The fluorescence background was however reproducible for all of the methanol phases when making new mixtures from non-fluorescing components. It was considered if the fluorescence might arise from impurities due to the rubber stoppers. A new mixture was prepared in a clean test tube equipped with a rubber stopper covered by cleaned aluminium foil. The same fluorescence background remained to be observed in the spectrum. To avoid any contact with suspect material it was decided to prepare a new series of mixtures and let them be contained in sealed glass ampoules. These could be left standing for ageing to let the fluorescence perhaps die out and to avoid having changes in composition due to evaporation. The volumes of the water phases were relatively smaller than the decane phases (especially for the mixture H). The use of sealed glass ampoules had

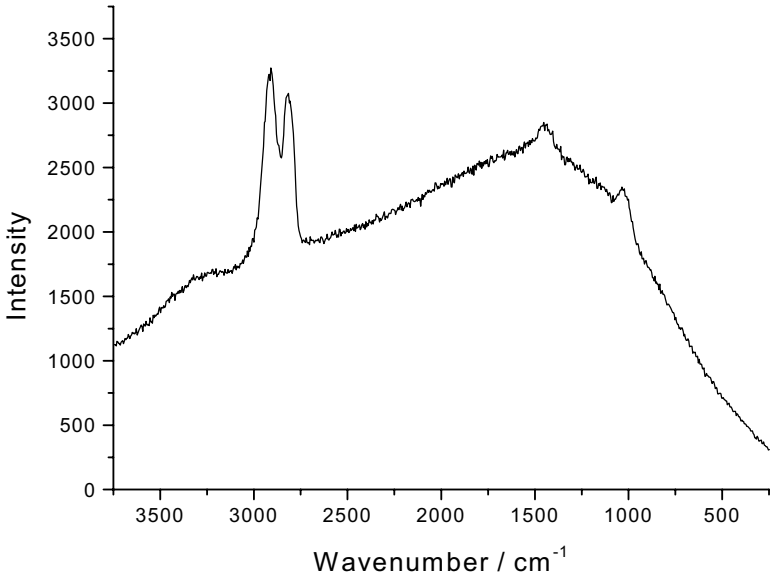

Fig. 8. 3. The Raman spectrum of mixture A (X_{decane} = 0.25, $X_{methanol}$ = 0.75), lower phase contained in a test tube equipped with a rubber bung. The spectrum was acquired by use of the 2nd monochromator (with a grating of 600 grooves per mm) and the 514.53 nm_{air} line of the Ar-ion laser (~200 mW). The sample was placed in the macroscopic position (90 ° collection geometry).

the advantage, that they could be turned upside down, allowing the liquids to run to the thin end of the ampoule and thus making it much easier to focus the laser light into the lower phase (a disadvantage is however that more glass volume are close to the sample volume).

Raman spectra of all the mixtures were finally obtained and these spectra are presented in the following pages. Fig. 8.4 the spectra are shown of the decane / methanol mixtures, Fig. 8.5 of the decane / water mixtures, in Fig. 8.6 of the decane / methanol / water mixtures and Fig. 8.7 of the methanol / water mixtures (one phase system only). From the presented figures it is seen that there was no fluorescence problem with respect to the decane phases. The water phases in the case of decane / water systems also gave quite nice Raman spectra, except for some noise in two of the spectra (Fig. 8.5). Fluorescence backgrounds were however to be observed in all of the Raman spectra obtained from phases containing methanol, especially when mixed with decane (Fig. 8.4 and Fig. 8.6) and to a lower degree when mixed with water (Fig. 8.7).

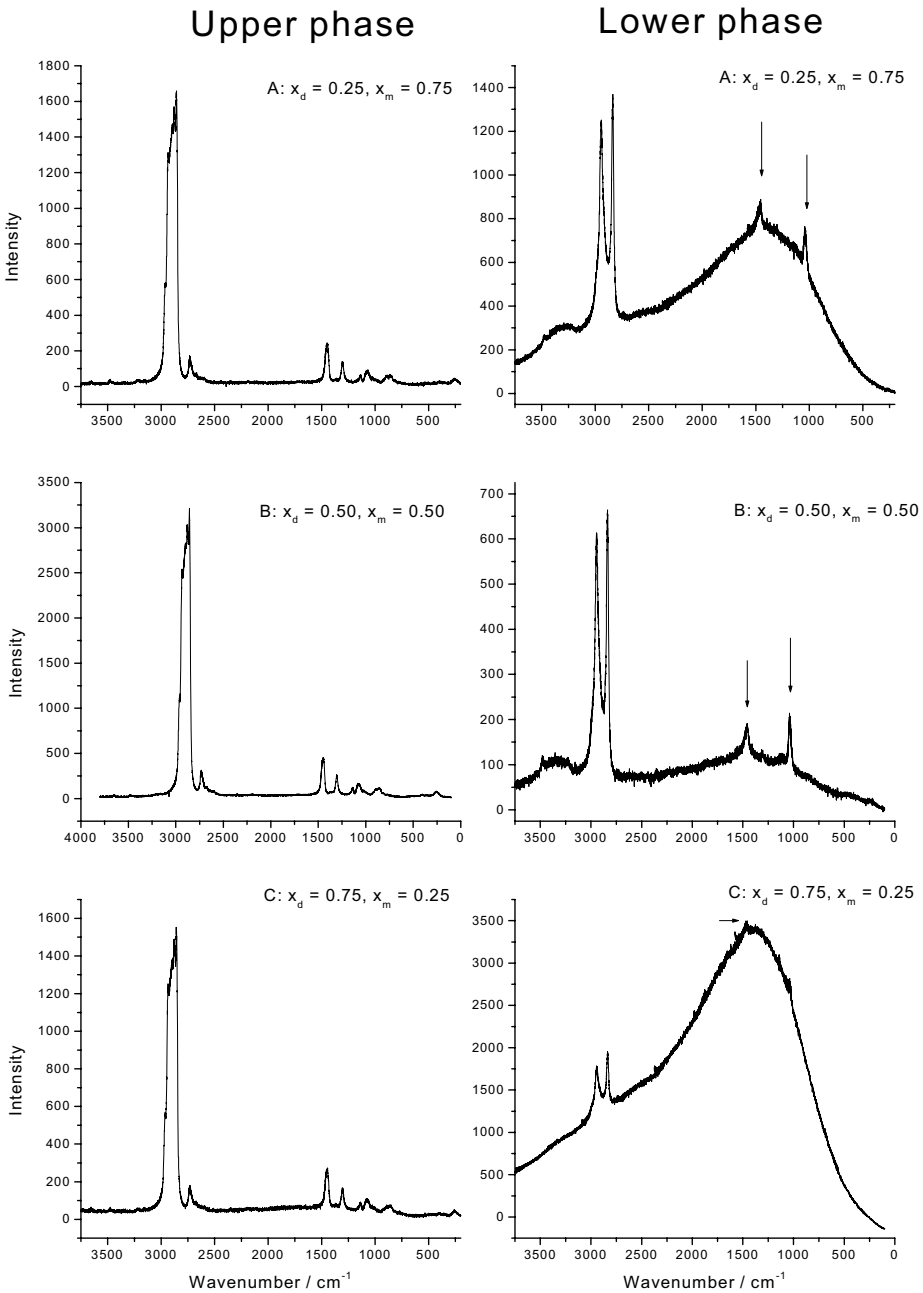

Fig. 8.4. Raman spectra of decane / methanol mixtures contained in sealed glass ampoules. Upper phase spectra are presented to the left and lower phase spectra to the right. The spectra were acquired by use of the 1st spectrograph (1800 grooves per mm) and the 514.53 nm_{air} line of the Ar-ion laser was used as the excitation source (~200 mW). The ampoules were placed in the macroscopic sampling position (collection geometry 90°).

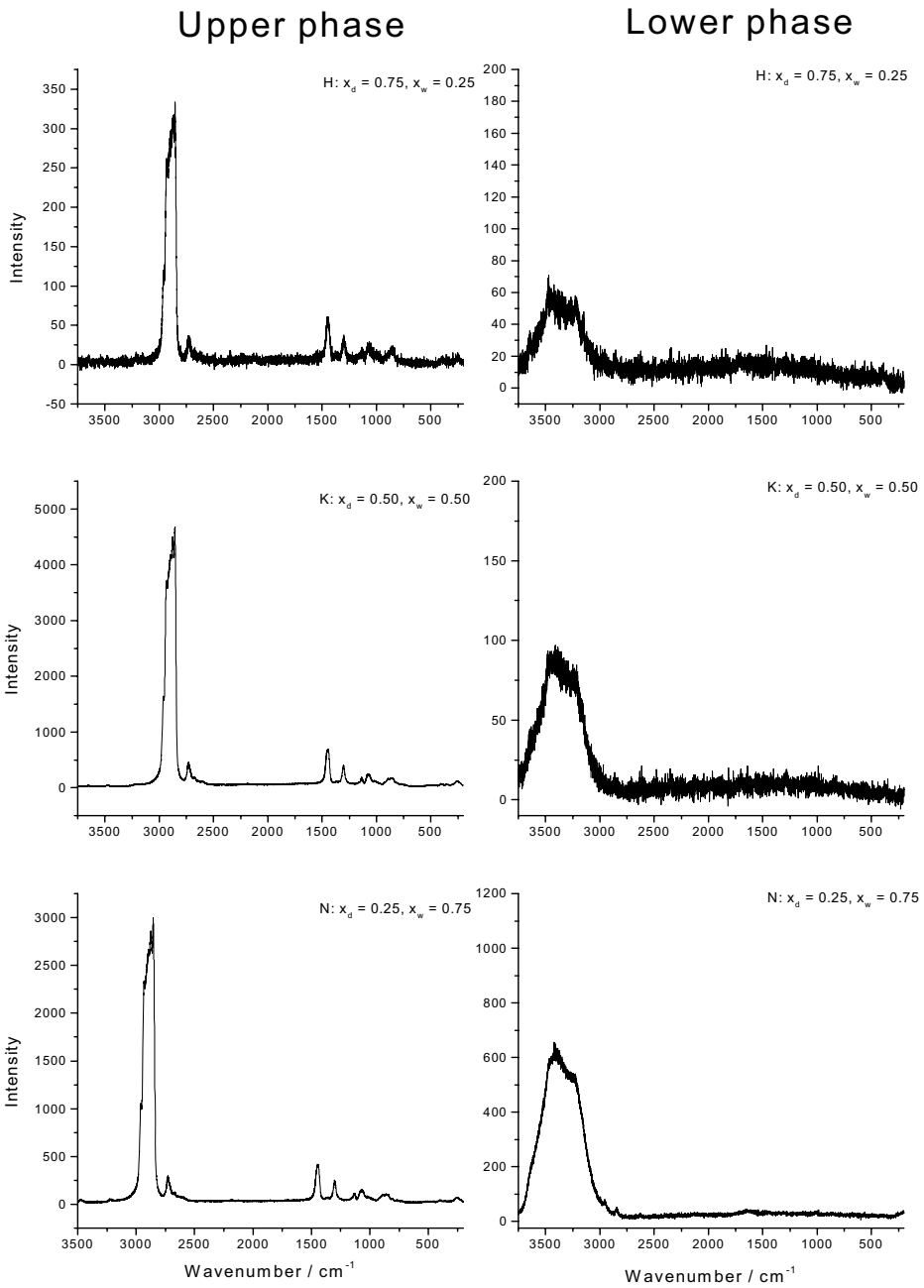

Fig. 8.5. Raman spectra of decane / water mixtures. For further details see the legend to Fig. 8.4.

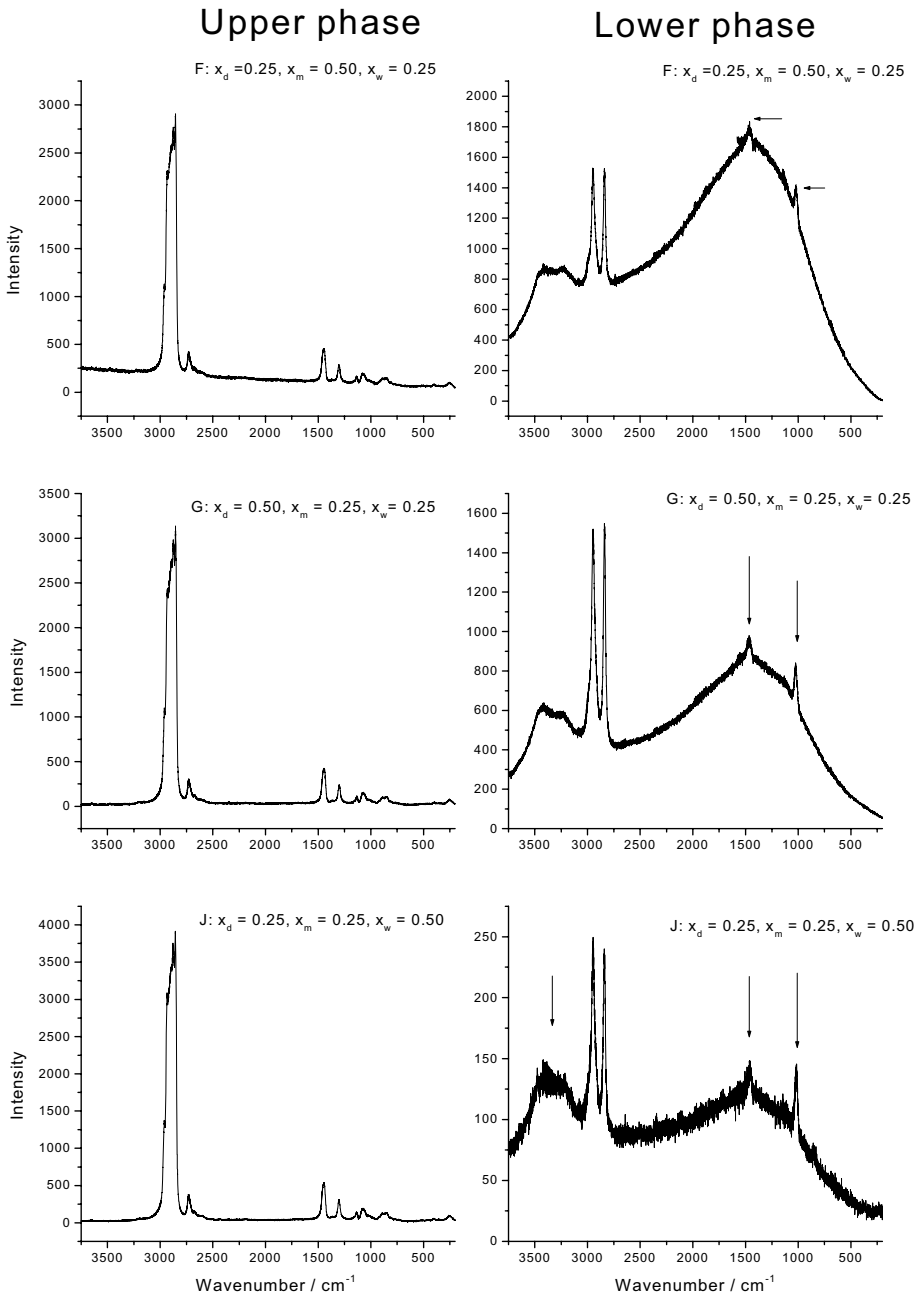

Fig. 8.6. Raman spectra of water / methanol / decane mixtures. For further details see the legend to Fig. 8.4.

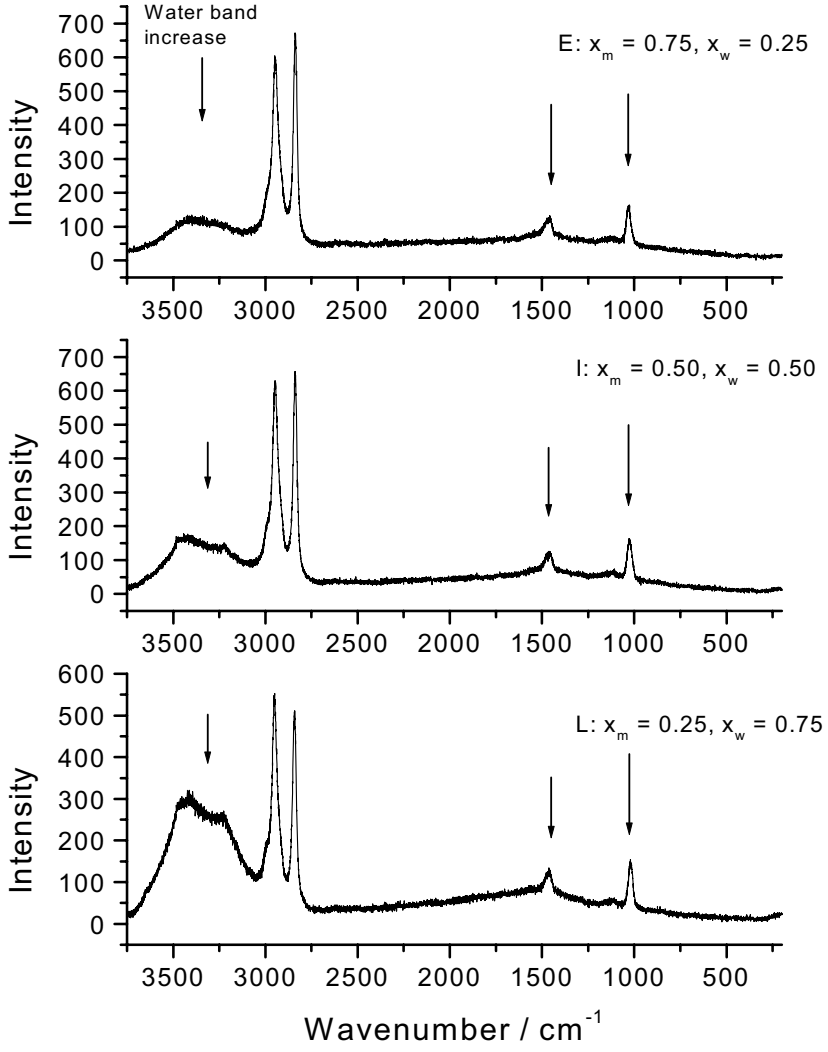

Fig. 8.7. Raman spectra of water / methanol mixtures. For further details see the legend to Fig. 8.4.

It was clearly seen in the FT-Raman spectra of the water / methanol mixtures, Fig. 8.7, that the water bands at ~3400 cm^{-1} (O-H stretching vibrations) increased relatively to the methanol band, as the water content in the mixture was increased (indicated with arrows in the figure). This may be used to determine the water content in water / methanol mixtures. The fluorescence background had a maximum intensity of ~1500 cm^{-1} in all the obtained

spectra of the methanol phases. The two methanol bands at ~1450 cm^{-1} and ~1034 cm^{-1}, arising from CH_3 asymmetric deformation and C-O stretching respectively, are somewhat distorted by the intense background. As seen in Fig. 8.4, 8.6 and 8.7 these bands are however faintly seen in most of the spectra (indicated with arrows).

Because of the broad and intense background in the methanol phase spectra it was decided to try if the FT-Raman technique could give some better spectra.

8.3. FT-Raman Spectroscopic Studies of the Water-Methanol-Decane System

The same mixtures, contained in the sealed glass ampoules, were transported to the H. C. Ørsted Institute in Copenhagen for the FT-Raman measurements. Because of the fact that the glass ampoules were relatively larger than sample tubes normally used it was necessary to realign the FT-Raman instrument set-up. A glass ampoule was buckled to a rack and placed in front of the Nd-YAG laser beam. By means of an infrared viewing instrument it was possible to focus the "invisible" laser beam in the middle of the ampoule. The collection geometry was 180°.

FT-Raman spectra of the upper and lower phases of mixture J's (X_{water} = 0.50, $X_{methanol}$ = 0.25 and X_{decane} = 0.25) are presented in Fig. 8.8 (lower spectra). In Figure 8.8 are included the corresponding dispersive Raman spectra for comparison. As seen there was a background in the FT-Raman spectra of the methanol phase. This background however did not look like the fluorescence background observed in the dispersive Raman spectrum (upper spectrum). Surprisingly a background was also to be observed in the FT-Raman spectrum of the decane phase and this background looked very similar to the background observed in the methanol phase. It was considered if the background could arise from the glass material. A FT-Raman spectrum of a pure distilled water sample contained in a sealed glass ampoule was obtained, shown in Fig. 8.9. Exactly the same kind of background was observed. It was therefore concluded that at least a major part of the backgrounds in the FT-Raman spectra must be due to the glass material.

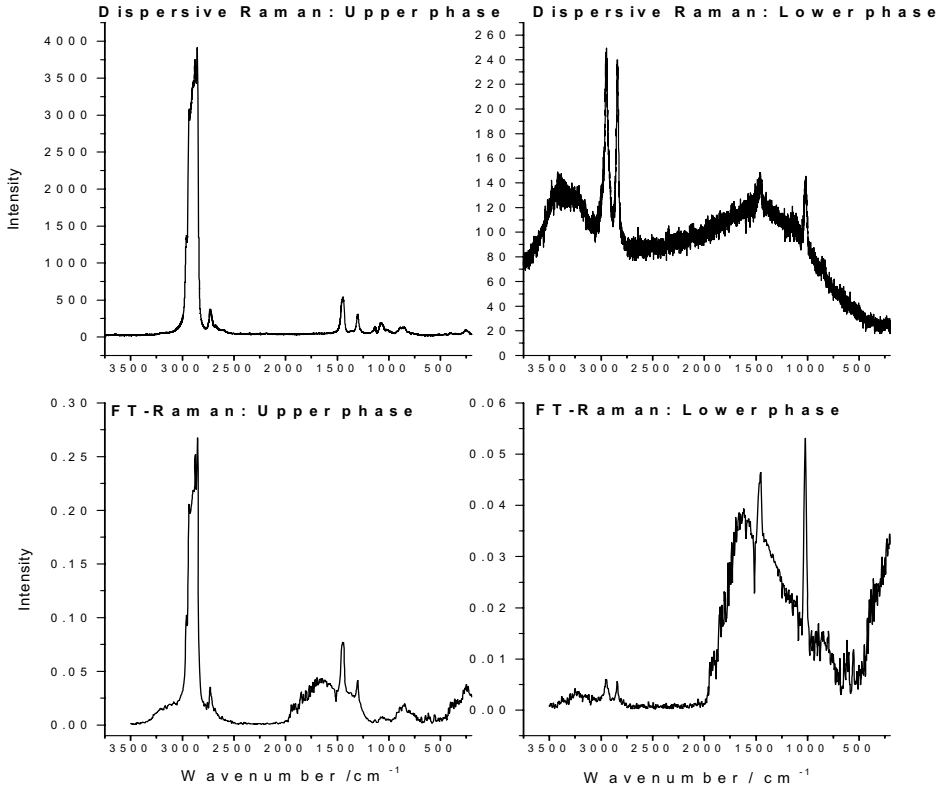

Fig. 8.8. Raman spectra of a water / methanol / decane mixture (J: X_{water} = 0.50, $X_{methanol}$ = 0.25 and X_{decane} = 0.25) contained in glass ampoule. Upper spectra: Raman spectra also shown in Fig. 8.6. Lower spectra: The FT-Raman spectra of the same mixture; the upper phase and the lower phase.

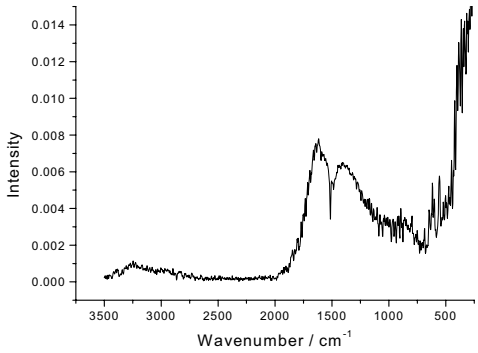

Fig. 8.9. The FT-Raman spectrum of a pure distilled water sample contained in a glass ampoule.

Even though it thus was concluded that a considerable part of the background in the FT-Raman spectra of the methanol phases came from the glass, we were still convinced that a fraction of the background in the spectra of the methanol did not came from glass. This conclusion was first of all based on the fact that no fluorescence was to be observed in the spectra of the pure methanol sample. To understand and explain the observed fluorescence phenomena however one has to consider the so-called quenching effect. A discussion of this will be too long here and we will only mention that the same fluorescence quenching phenomenon was seen in the case of MTBE in heptane as described in Chap. 7.2.3 (and Appendix F).

8.4. Some Considerations about the Titanium Cell with Respect to its Suitability as a High Pressure Mixture Container for Raman Measurements

The titanium cell was described in detail in Chap. 2.2.3. In Chap. 5 and Chap. 6 it was shown that the cell is suitable for high pressure gas measurements, up to at least 40.0 MPa_A. It was one goal in this Ph.D. project to trying the cell for high pressure mixtures too, especially with respect to the above discussed water-methanol-decane system. Many too many problems arose during the Raman measurements on the system. However it is estimated that the cell should be usefull for Raman spectroscopy to study liquid-liquid equilibria systems. Thus, even though the titanium cell was never filled with liquids, some considerations about its suitability as a high pressure mixture cell are presented in the following to help future applications.

The cell can be filled with a mixture of liquids through a hole next to the manometer, as shown in Fig. 2.7, Chap. 2.2. The hole must be closed with a blind plug before the pressure can be raised. In the Raman measurements the laser and Raman light passes through the transparent sapphire windows of the cell. If the cell is filled with a liquid-liquid phase mixture, there is probably only one of the phases to be seen through the windows. Then if

the cell is turned upside down the possibility exists that the other of the phase might be seen through the windows. In that way one has, when applying suitable amounts of the components, the opportunity to obtain spectra of both of the liquid phases.

Because of the fact that decane has a much higher molecular weight and a lower density compared to the methanol and water[i], the volumes of the water phase in some of the mixtures (cf. Fig. 8.2) are much smaller than the volume of the oil (decane) phases. In the light of this, it was found of interest to consider if there were mixture compositions for which it would not be possible to see both of the liquid phases through the sapphire windows.

The dead volume and the total volume in the titanium cell were determined to be 5.2 cm^3 and 11.9 cm^3 respectively as described in Chap. 3.3. The dead volume of the titanium cell before it was equipped with a manometer, was determined to be 2 cm^3 by means of the ISCO pump method also mentioned in Chap. 3.4. Thus it can be concluded that the manometer volume was 3.2 cm^3. For the cell filled with a given mixture of liquids, the manometer volume is probably filled with a gas (air). The dead volume above and below the sapphire window can be estimated to 1.5 cm^3 and 0.5 cm^3 respectively. Three "situations" were considered: i) piston out, ii) piston in and iii) piston in an intermediate position and the piston can be turned in an upside or down orientation. All these "situations" are described in the following. Conclusions are given separately for each case.

[i] Molecular weight and density data:

Decane [M($C_{10}H_8$): 142.29 $gmol^{-1}$, ρ: 0.73 gcm^{-3} (20 °C), Merc]

Methanol [M(CH_3OH): 32.04 $gmol^{-1}$, ρ: 0.79 gcm^{-3} (20 °C), May & Baker]

Water [M(H_2O): 18.02 $gmol^{-1}$, ρ: 1.0 gcm^{-3} (20 °C), fingertip knowledge]

"Piston out" situation (cell filled to mark)

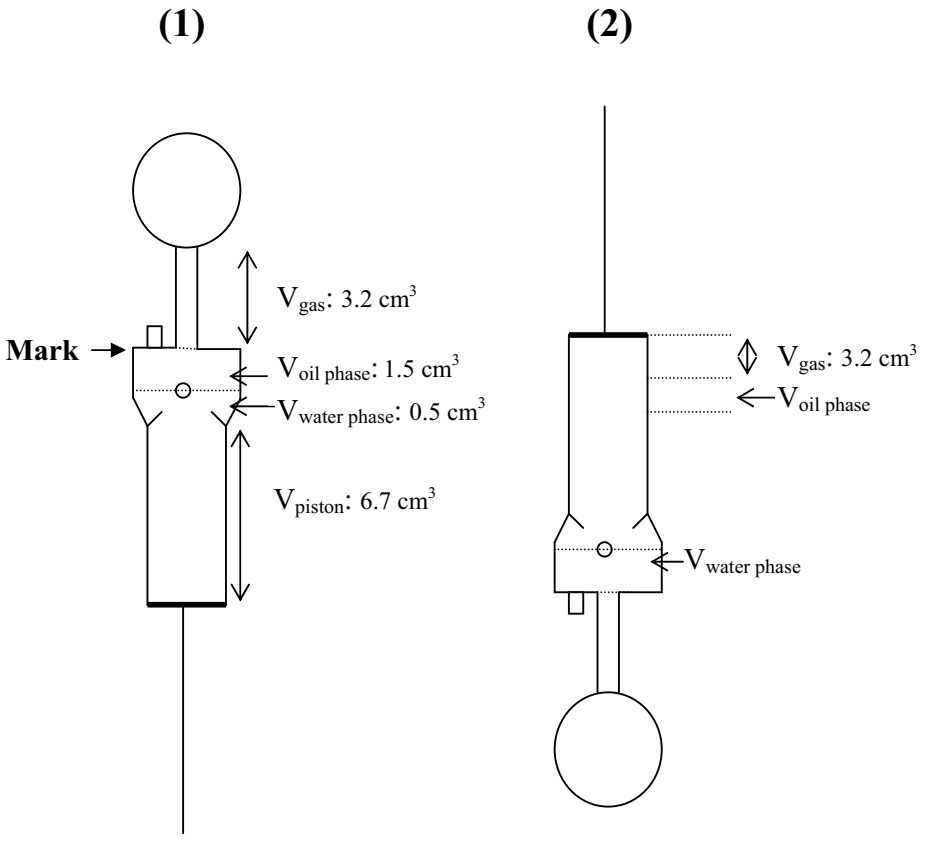

Limiting situation (1): $V_{oil} = 1.5\ cm^3$

$V_{water} = 0.5\ cm^3 + 6.7\ cm^3 = 7.2\ cm^3$

$V_{liquid} = 8.7\ cm^3$

(1): Oil phase is seen when: $V_{oil} > 1.5\ cm^3$ and $V_{water} < 7.2\ cm^3$

(2): (up side down) Water phase is seen when: $V_{water} > 4.7\ cm^3$ ($3.2\ cm^3 + 1.5\ cm^3$)

Conclusion: $4.7\ cm^3 < V_{water} < 7.2\ cm^3$ (the rest of the volume is oil phase).

(1): Water phase is seen if: $V_{water} > 7.2\ cm^3$ and $V_{oil} < 1.5\ cm^3$

(2): (up side down) Oil is seen if: $V_{oil} > 3.7\ cm^3$

Conclusion: $3.7\ cm^3 < V_{oil} < 1.5\ cm^3$ (the rest of the volume is water phase)

"Piston in" situation (cell filled to mark)

(3) **(4)**

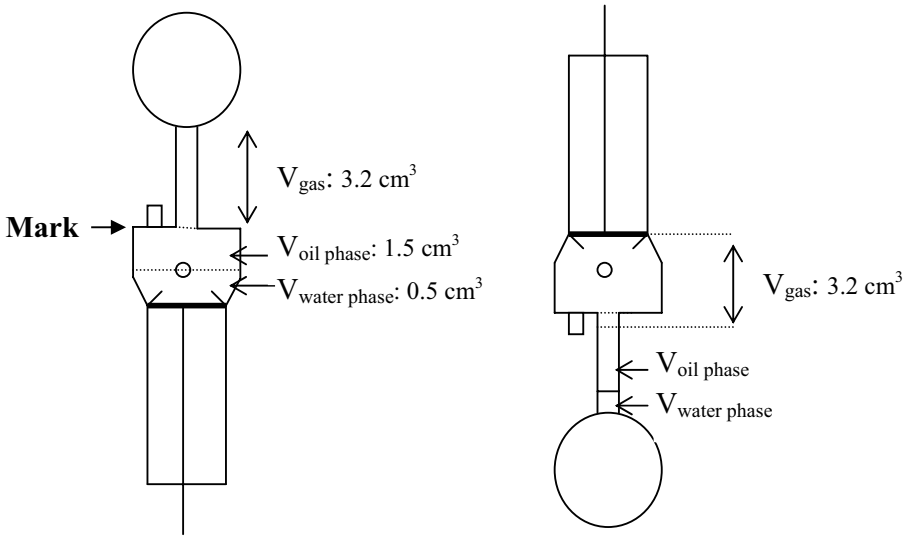

Limiting situation (3): $V_{oil} = 1.5$ cm^3

$V_{water} = 0.5$ cm^3

$V_{liquid} = 2.0$ cm^3

(3): Oil is seen: $V_{oil} > 1.5$ cm^3 and $V_{water} < 0.5$ cm^3

(4): (up side down) Only gas is seen.

Conclusion: If spectra of both of the liquid phases are wanted the piston cannot be totally in.

Considerations with respect to intermediate piston position (cell filled to mark)

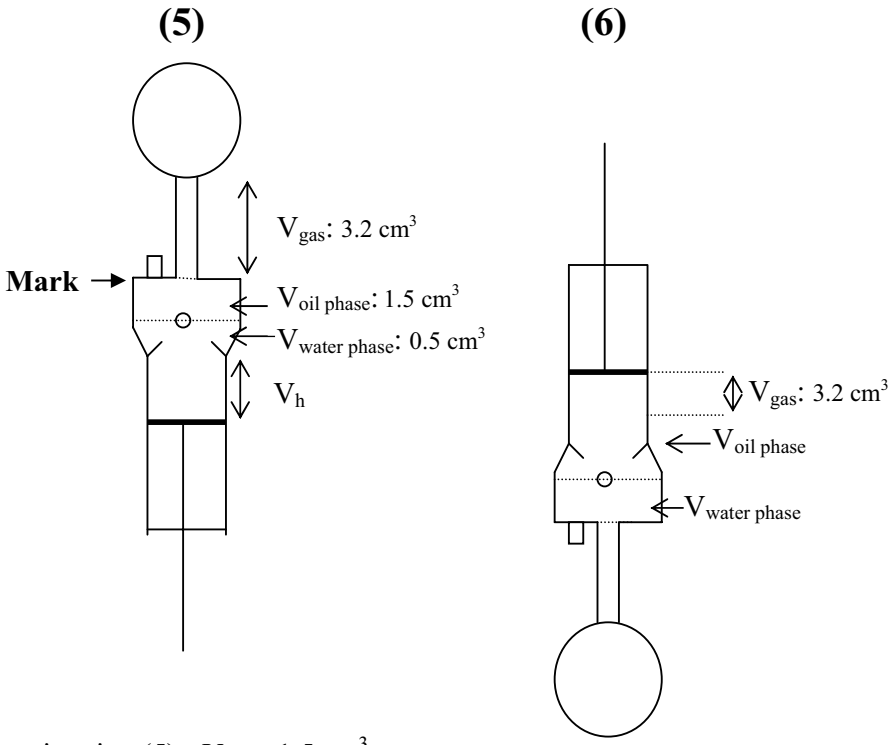

Limiting situation (5): $V_{oil} = 1.5\ cm^3$

$V_{water} = 0.5\ cm^3 + V_h$

$V_{liquid} = 1.5\ cm^3 + 0.5\ cm^3 + V_h$

If not gas but liquid (oil) is to be seen in the up side down position (6) it is required that:

$V_{water} + V_{oil} > 4.7\ cm^3$, if not, only gas is to be seen in the up side down position (6). That is:

$1.5\ cm^3 + 0.5\ cm^3 + V_h > 4.7\ cm^3 \Leftrightarrow V_h > 2.7\ cm^3$

Conclusion: If spectra of both of the liquid phases are wanted, then the piston volume V_h, must be at least 2.7 cm^3.

The manometer connection volume in the present version of the cell is too big; i.e. connection must be replaced. When the manometer volume is lesser it will be 1) easier to obtain both of the liquid phases and 2) easier to achieve a larger pressure range.

8.5. Conclusion

The described work on water-methanol-oil was only preliminary but some conclusions can however be drawn. Both Raman (dispersive) and FT-Raman spectra have been obtained for the water-methanol-decane system. In the Raman spectra no fluorescence background was observed in any of the decane phase spectra and neither for the pure methanol samples. In the phases containing methanol a fluorescence background was observed. In fact it was so broad and intense that it was decided to try the FT-Raman technique. A background also appeared in the FT-Raman spectra of the methanol phases and surprisingly also in the decane phase spectra. It was concluded that the background in the FT-Raman spectra was in part due to the glass container (ampoule) material. The phenomenon observed in the Raman spectra of the methanol phases, namely that two non-fluorescing liquids when mixed start to exhibit fluorescence is probably due to different degree of quenching.

Better ways to obtain fluorescence free Raman spectra are desirable before information about the ternary system could be clearly obtained. It could for instance be interesting to investigate if the FT-Raman of the mixtures sampled in containers of quartz could be obtained without any backgrounds. Improvements of Raman spectra by quenching the fluorescence by radiation have been described in the literature, e.g. ref. 2. A similar experiment could be done to investigate if the same improvement was to be obtained in the Raman spectra of the methanol phases.

Some considerations about the limitations of the titanium cell have been described. The cell is probably suitable for the Raman spectroscopic studies of liquid-liquid phase mixtures up to very high pressures. There are however some limitations with respect to mixture composition if spectra of both phases are wanted. The overall conclusion was that the limitations can be reduced if the volume of the manometer connection is minimised.

8. 6. References

1. A. Skrzecz, D. Shaw and A. Maczynski, “IUPAC-Nist solubility data series 69. Ternary alcohol-hydrocarbon-water systems”, J. Phys. Chem. Ref. Data **28**, 983 (1999).
2. D. Kato, “Improvement of Raman spectroscopy by quenching the fluorescence”, J. Appl. Phys. **45**, 2281 (1974).

APPENDICES

Appendix A: List of components from which the sapphire cell was built up (Chap. 2).

Appendix B: Listed burst pressures for sapphire windows with different sizes (Chap. 2).

Appendix C: Data for determination of the dead volume and total volume of the titanium cell (Chap. 3).

Appendix D: Data on Iv_3 (methane) / $I2v_2$ (methane) (Chap. 6).

Appendix E: Data on band area of benzene and heptane bands (Chap. 8).

Appendix F: Reprint of one of the papers published during the Ph.D. project: S. Brunsgaard Hansen, R. W. Berg and E. H. Stenby, "Determination of Methyl Tertiary Butyl Ether (MTBE) in Gasoline by Raman Spectroscopy", Asian Chemistry Letters **40**, 65 (2000).

Appendix A

List of components from which the sapphire tube cell was built up.

Component numbers refer to numbers in the schematic illustration of the sapphire tube cell, text Fig. 2.3.		Type	Pressure limit MPa
1.	Male connector (NPT) including blind plug	SS-400-1-4[1]	65.4[5]
2.	Packless valve	SS-DSF4-HT[1]	24.1[6]
3.	Male connector	SS-4-WVCO-1-4[1]	65.4[5]
4.	Elbow, including two **O**-rings[8]	S-4-VCO-9[1]	92.3[5]
5.	Socket weld gland	SS-4-VCO-9[1]	44.0[5]
6.	Female nut	SS-4-VCO-4[1]	65.4[5]
7.	Metal disc	-[2]	-
8.	Cajon ultra torr adapter, including two **O**-rings[8]	SS-4-UT-A-4[1]	65.4[5]
9.	Safety metal net	-[2]	-
10.	Sapphire tube	special order[3]	~51[7]
11.	Connector rod	-[2]	-
12.	Tee, including three **O**-rings[8]	SS-4-VCO-T[1]	92.3[5]
13.	Tube adapter gland	SS-4-VCO-3-4TA[1]	72.3[5]
14.	Female connector	SS-400-7-4RG[1]	65.4[5]
15.	WIKA bourdon manometer		-
	¼" RG, pressure range: 0-25.0 MPa_R	Type 233.30.063[4]	25.0[4]
16.	Stabilizing brass plate	-[2]	-
17.	Screw for grounding to earth	-[2]	-
18.	Rack	-[2]	-

[1] Swagelok fittings, catalogue numbers.

[2] Manufactured by the workshop at Department of Chemistry, DTU.

[3] Special order, Sanchez Technology, France.

[4] Purchased at Plesner, Denmark.

[5] Working pressure (excluded safety factor 4).

[6] Pressure rating. Differential back pressure max 10.3 MPa.

[7] Discussed in Chap. 2.2.1.

[8] The original viton **O**-rings were replaced by **O**-rings of nitril.

Appendix B

Burst pressures* given for sapphire windows with different sizes.

Diameter[1] (D) mm	Plate thickness[1] (PT) mm	Ratio D / PT	Burst pressure[1,2] MPa
25	1	25.0	0.5
25	2	12.5	2.5
25	3	8.3	6.9
25	5	5.0	17.7
25	6	4.2	27.7
25	13	1.9	110.8
50	1	50.0	0.1
50	2	25.0	0.6
50	3	16.7	1.8
50	5	10.0	4.6
50	6	8.3	7.1
50	13	3.8	28.6
75	2	37.5	0.3
75	3	25.0	0.8
75	5	15.0	2.0
75	6	12.5	3.2
75	13	5.8	12.7
100	2	50.0	0.2
100	3	33.3	0.4
100	5	20.0	1.1
100	6	16.7	1.8
100	13	7.7	7.1
125	3	41.7	0.3
125	5	25.0	0.7
125	6	20.8	1.1
125	13	9.6	4.6
150	3	50.0	0.2
150	5	30.0	0.5
150	6	25.0	0.8
150	13	11.5	3.2

[1] www.saphikon.com/tubebrst.ht
[2] The approximate safety factor at room temperature is 3 (excluded).

* allowed working pressures

Burst pressure as a function of diameter / plate thickness

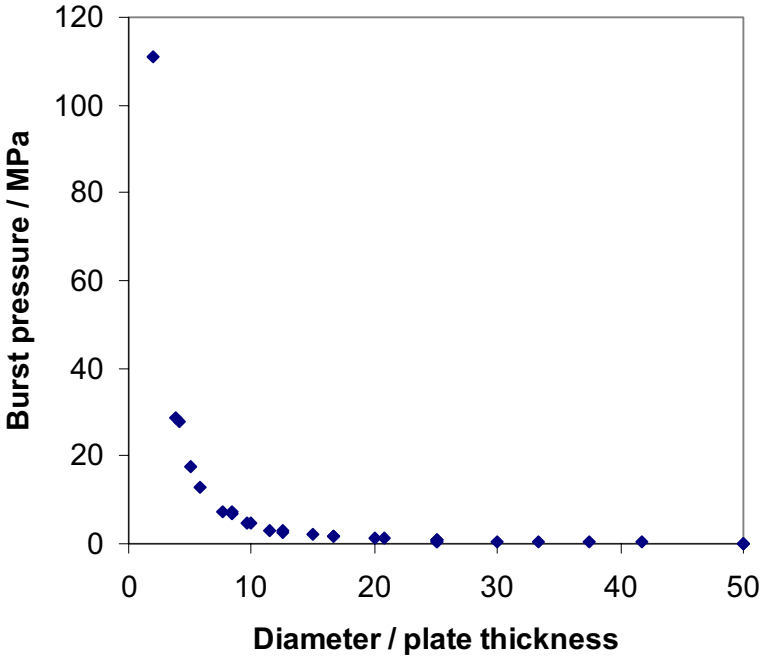

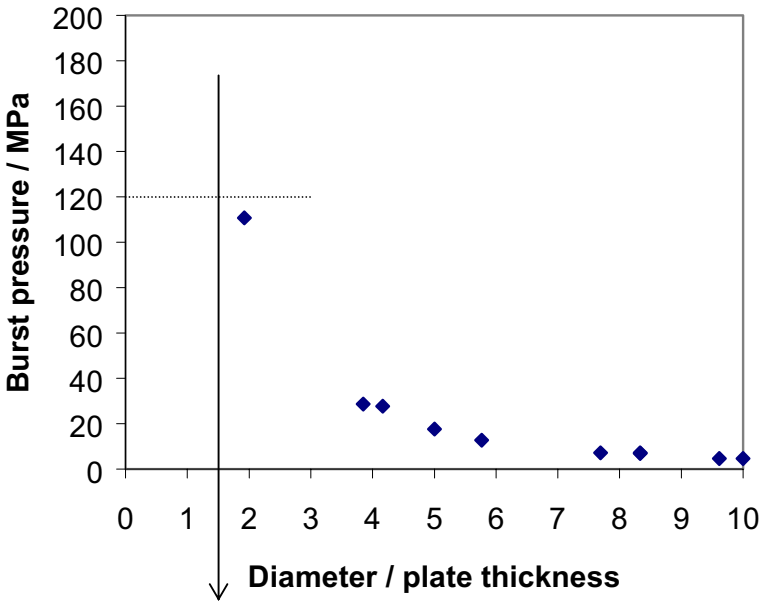

The titanium sapphire cell windows have a D/PT ratio of 10/7=1.4

Appendix C

The plots presented in Chap. 3, Fig. 3.6 were based on the below given data. The plots were used for determination of the dead volume and total volume in the titanium cell.

A) The titanium cell filled with nitrogen (N45, 99.995%, Hede Nielsen A/S) at a starting pressure of 5.7 MPa_A. (t = 24.4 °C).

P	ρ	ρ^{-1}	h	V
MPa_A	cm^3mg^{-1}	$cm^{-3}mg$	cm	cm^3
5.7	64.758	0.015442	3.36	6.71
6.0	68.276	0.014646	3.08	6.15
7.0	79.572	0.012567	2.27	4.53
8.0	90.798	0.011013	1.69	3.38
9.0	101.938	0.009810	1.205	2.41
10.0	112.975	0.008852	0.83	1.66
13.4	147.760	0.006768	0.00	0.00

B) The titanium filled with pure methane (N45, Hede Nielsen A/S) at a starting pressure of 7.0 MPa_A. (t = 25.7 °C).

P	ρ	ρ^{-1}	h	V
MPa_A	cm^3mg^{-1}	$cm^{-3}mg$	cm	cm^3
7.0	51.118	0.019563	3.36	6.71
8.0	59.031	0.016940	2.55	5.09
9.0	67.347	0.014848	1.915	3.83
10.0	75.781	0.013196	1.42	2.84
11.0	84.330	0.011858	1.025	2.05
12.0	92.878	0.010767	0.70	1.40
14.9	117.399	0.008518	0.00	0.00

C) The titanium cell filled with methane (N45, Hede Nielsen A/S) at a starting pressure at 8.2 MPa_A. (t = 26.4 ° C).

P	ρ	ρ^{-1}	h	V
MPa_A	cm^3mg^{-1}	$cm^{-3}mg$	cm	cm^3
8.2	60.618	0.016497	3.36	6.71
9.0	67.069	0.014910	2.805	5.60
10.0	75.452	0.013253	2.20	4.40
11.0	83.950	0.011912	1.705	3.41
12.0	92.447	0.010817	1.33	2.66
13.0	100.895	0.009911	1.00	2.00
14.0	109.342	0.009146	0.73	1.46
17.7	139.083	0.007190	0.00	0.00

Appendix D

The plots presented in Chap. 6 were based on the below given data points.

	← Iv_3 (methane) / $I2v_2$ (methane) →				
P_{total} MPa_A	CH_4 Pure	CH_4/C_2H_6 $X(CH_4)$=0.85	CH_4/C_2H_6 $X(CH_4)$=0.49	CH_4/N_2 $X(CH_4)$=0.47	Natural gas $X(CH_4)$~0.88
7.9	0.96				
6.4	1.13				
5.1	1.35				
4.2	1.58				
3.5	1.8				
3.1	2.17				
2.1	2.45				
1.4	3.37				
1.0	4				
0.2	4.67				
12.9		0.53			
10.4		0.65			
6.5		1.06			
5.6		1.32			
4.2		1.6			
3.4		1.92			
2.4		2.5			
1.4		3.09			
0.3		4.15			
0.1		6.75			
2.0			2.71		
1.4			3.15		
1.0			3.5		
0.4			4.9		
0.1			7		
15.9				0.56	
12.3				0.67	
10.3				0.79	
8.9				0.90	
7.9				0.97	
6.9				1.06	
5.7				1.29	
4.9				1.47	
3.9				1.74	
2.3				2.29	
1.3				3.17	
0.6				4.33	
10.2					0.69
8.0					0.8
6.4					1.2
1.1					4

Appendix E

The plots presented in Chap. 7, Fig. 7.7 were based on the below given data points.

Area of each band was determined by the Origin Microcal peak fitting module.

Vol. % benzene	A(~3063 cm^{-1}) benzene	A(~2875 cm^{-1}) heptane	A(~1450 cm^{-1}) heptane	A(~1300 cm^{-1}) heptane	A(~993 cm^{-1}) benzene
20.0	2.944	6.933	1.355	0.568	2.370
10.0	1.565	8.080	1.626	0.666	1.245
6.0	0.884	8.706	1.752	0.718	0.737
4.0	0.596	8.647	1.808	0.720	0.487
2.0	0.239	8.600	1.749	0.681	0.207
1.0	0.110	8.461	1.715	0.644	0.102
0.5	0.042	8.452	1.643	0.649	0.043

Appendix F